Heavy-Ion Collisions vs. Neutron Star Mergers

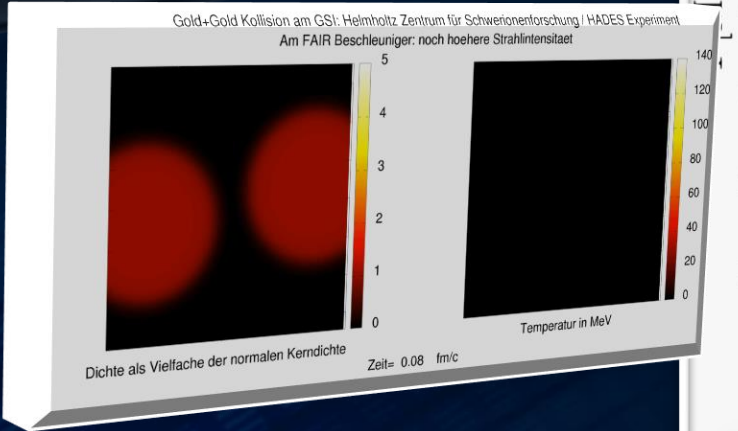

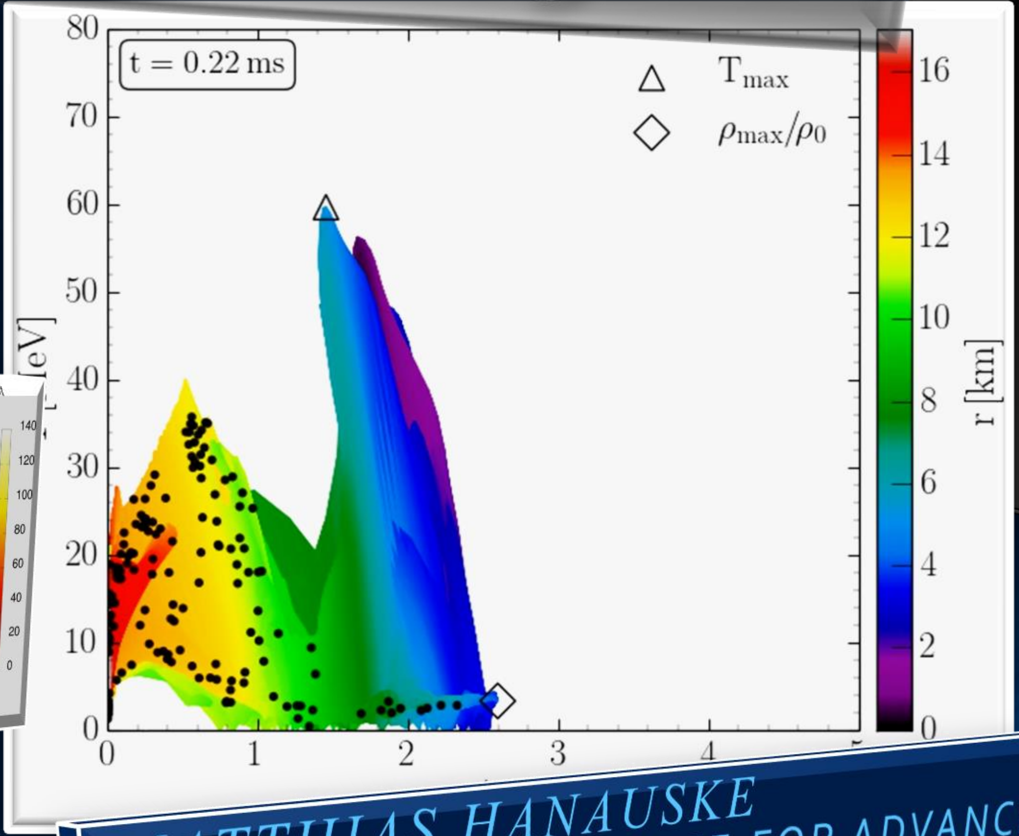

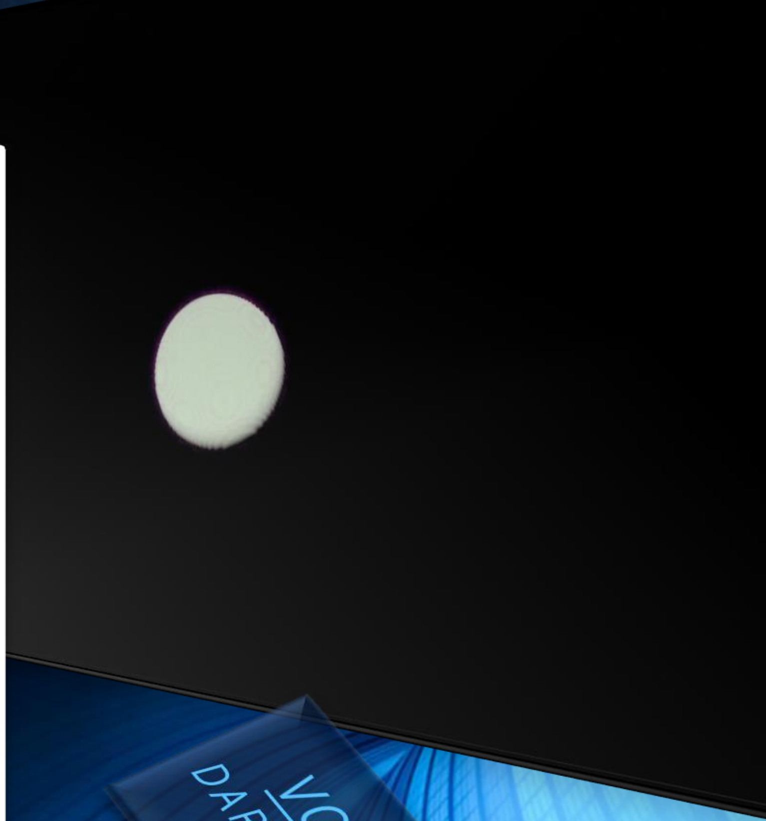

Probing dense baryonic matter with hadrons

Status and Perspective

Comparison between different transport models and similarities to neutron star mergers

MATTHIAS HANAUSKE
FRANKFURT INSTITUTE FOR ADVANCED STUDIES
JOHANN WOLFGANG GOETHE UNIVERSITÄT
INSTITUT FÜR THEORETISCHE PHYSIK
ARBEITSGRUPPE RELATIVISTISCHE ASTROPHYSIK
D-60438 FRANKFURT AM MAIN

VORTRAG AN DER GSI
DARMSTADT, 13 FEBRUARY 2019

The long awaited event GW170817

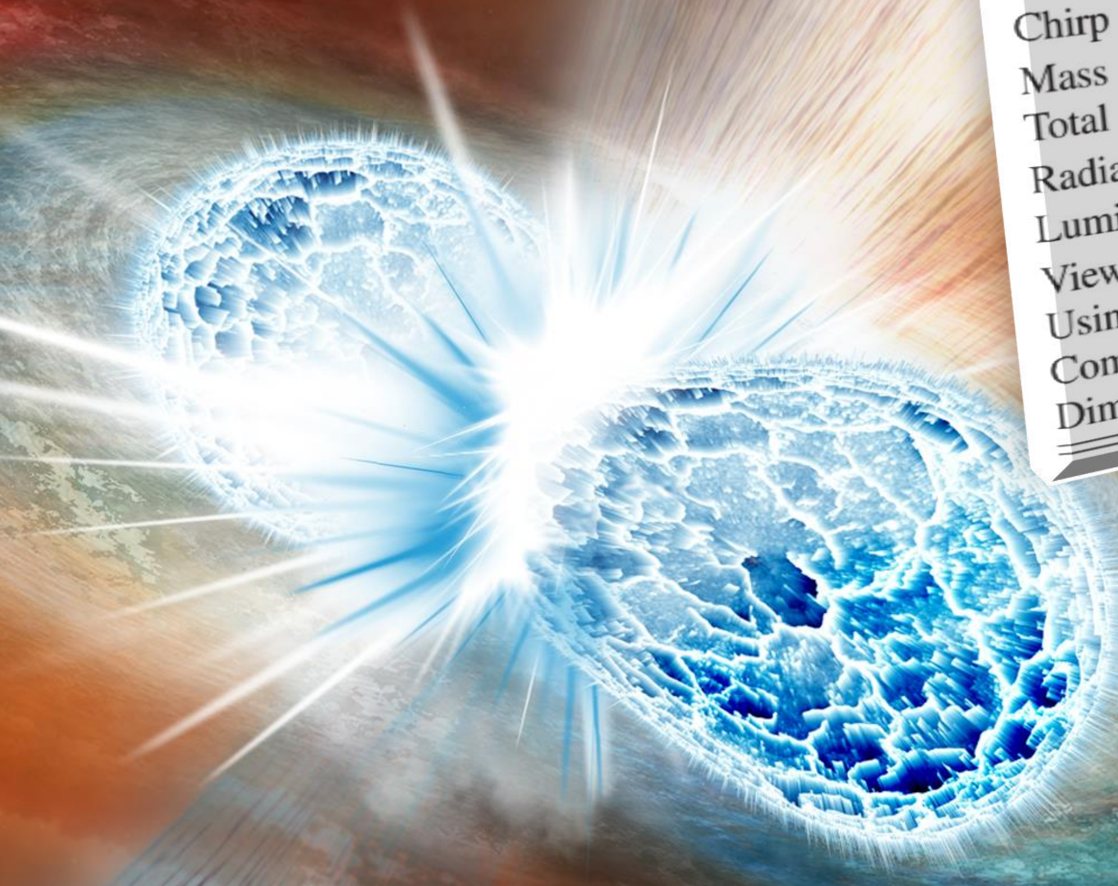

	Low-spin priors ($\|\chi\| \leq 0.05$)	High-spin priors ($\|\chi\| \leq 0.89$)
Primary mass m_1	1.36–$1.60\ M_\odot$	1.36–$2.26\ M_\odot$
Secondary mass m_2	1.17–$1.36\ M_\odot$	0.86–$1.36\ M_\odot$
Chirp mass $\mathcal{M}$	$1.188^{+0.004}_{-0.002} M_\odot$	$1.188^{+0.004}_{-0.002} M_\odot$
Mass ratio m_2/m_1	0.7–1.0	0.4–1.0
Total mass $m_{\rm tot}$	$2.74^{+0.04}_{-0.01} M_\odot$	$2.82^{+0.47}_{-0.09} M_\odot$
Radiated energy $E_{\rm rad}$	$> 0.025 M_\odot c^2$	$> 0.025 M_\odot c^2$
Luminosity distance $D_{\rm L}$	40^{+8}_{-14} Mpc	40^{+8}_{-14} Mpc
Viewing angle Θ	$\lesssim 55°$	$\lesssim 56°$
Using NGC 4993 location	$\lesssim 28°$	$\lesssim 28°$
Combined dimensionless tidal deformability $\tilde{\Lambda}$	$\lesssim 800$	$\lesssim 700$
Dimensionless tidal deformability $\Lambda(1.4 M_\odot)$	$\lesssim 800$	$\lesssim 1400$

17. August 2017

Gravitationswelle einer
Neutronenstern Kollision gemessen!

Die gemessene Gravitationswelle und der darauf folgende hochenergetische Lichtblitz

Der von dem Gammastrahlen Detektor FERMI gemessene Gammastrahlen Ausbruch
(1.7 Sekunden später)

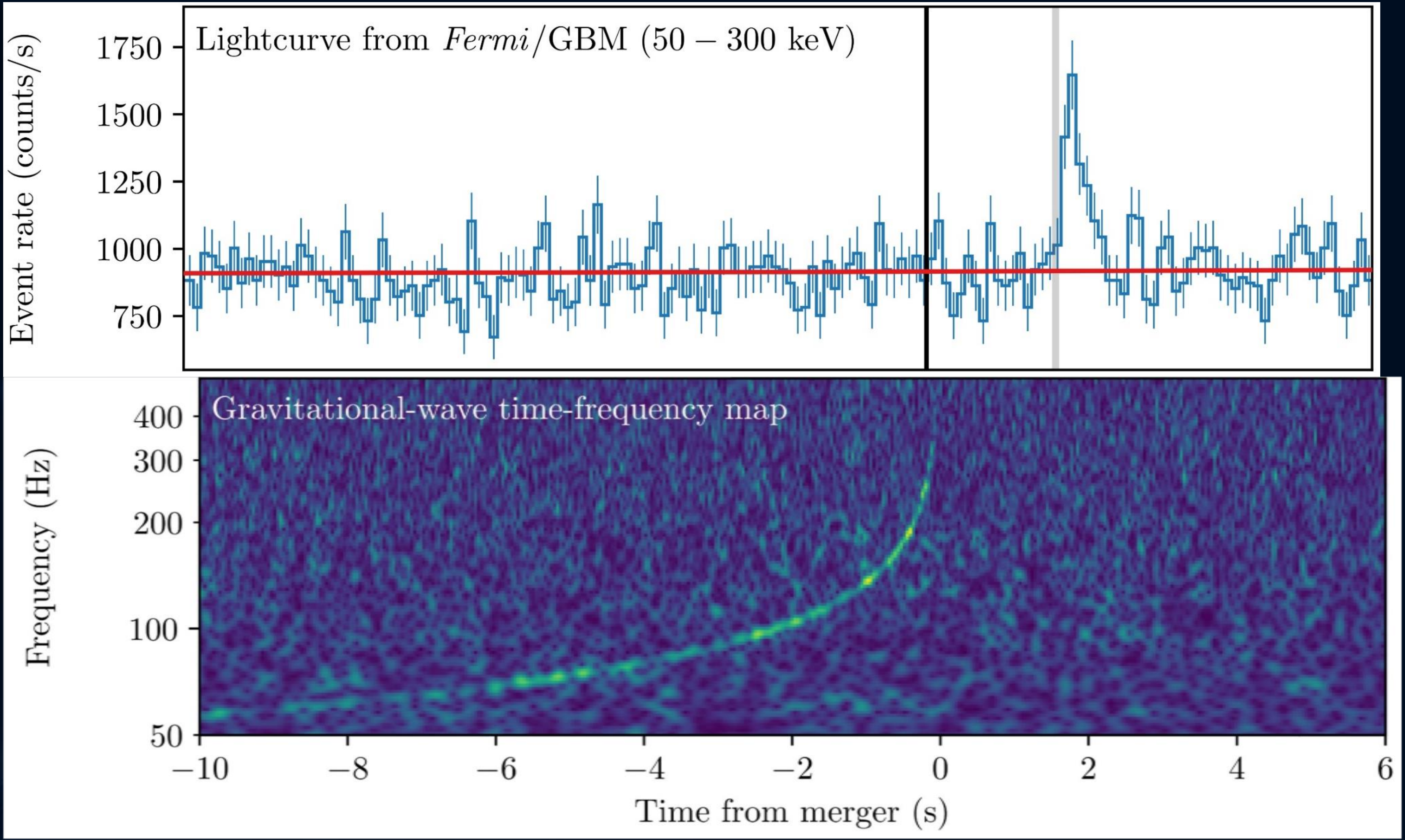

Die von dem Gravitationswellen Detektor LIGO detektierte Frequenz der Gravitationswelle

GW170817: Observation of Gravitational Waves from a Binary Neutron Star Inspiral, LIGO Scientific Collaboration and Virgo Collaboration, Phys. Rev. Lett. 119, 161101 (2017), Gravitational Waves and Gamma-Rays from a Binary Neutron Star Merger: GW170817 and GRB170817A, LIGO, Virgo, Fermi GBM, and INTEGRAL Collaborations, Astrophys. J. Lett. 848, L13 (2017)

GW170817

Tage, Wochen und Monate später detektierten weltweit unterschiedliche Teleskope (radio, infrarot, optische,…) eine Nachstrahlung dieser Neutronenstern Kollision

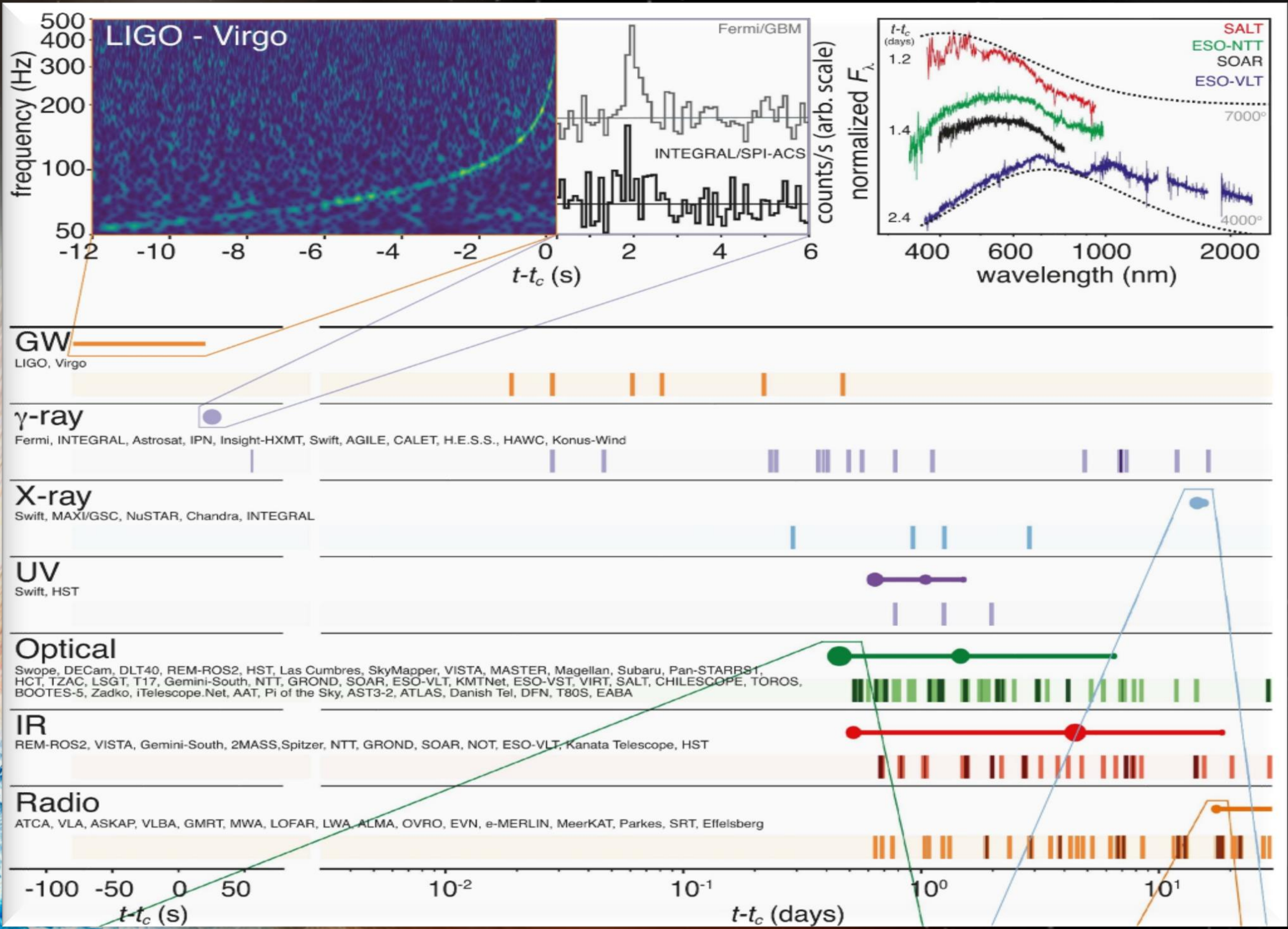

Multi-Messenger Observations of a Binary Neutron Star Merger, LIGO and Virgo Collaborations together with 50 teams of electromagnetic and neutrino astronomers, Astrophys. J. Lett. 848, L12 (2017)

Measured Mass Ratio of GW170817
(for high and low spin assumption)

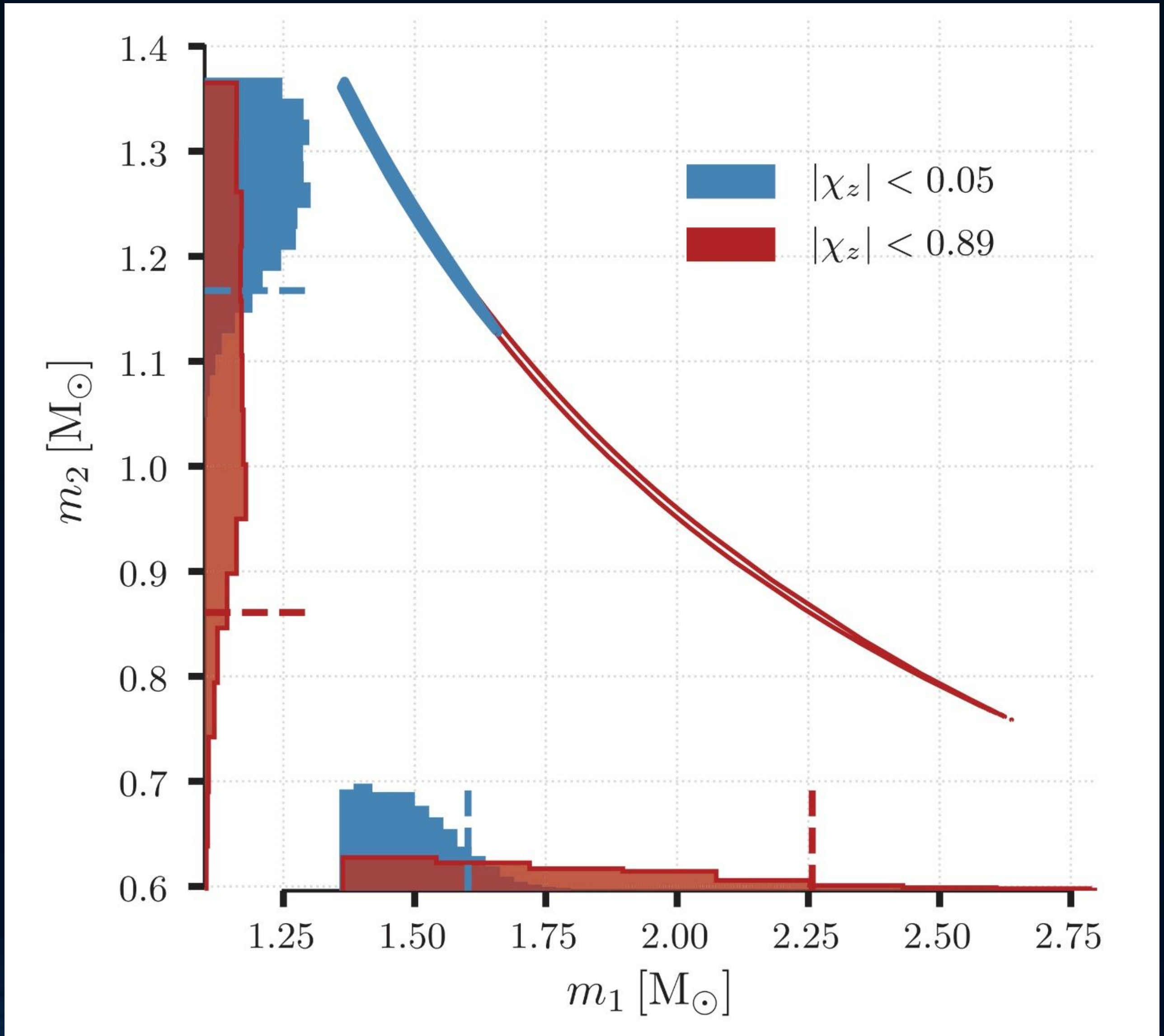

GW170817: Tidal Deformability Restrictions on the Equation of State (EOS) (for high and low spin assumption)

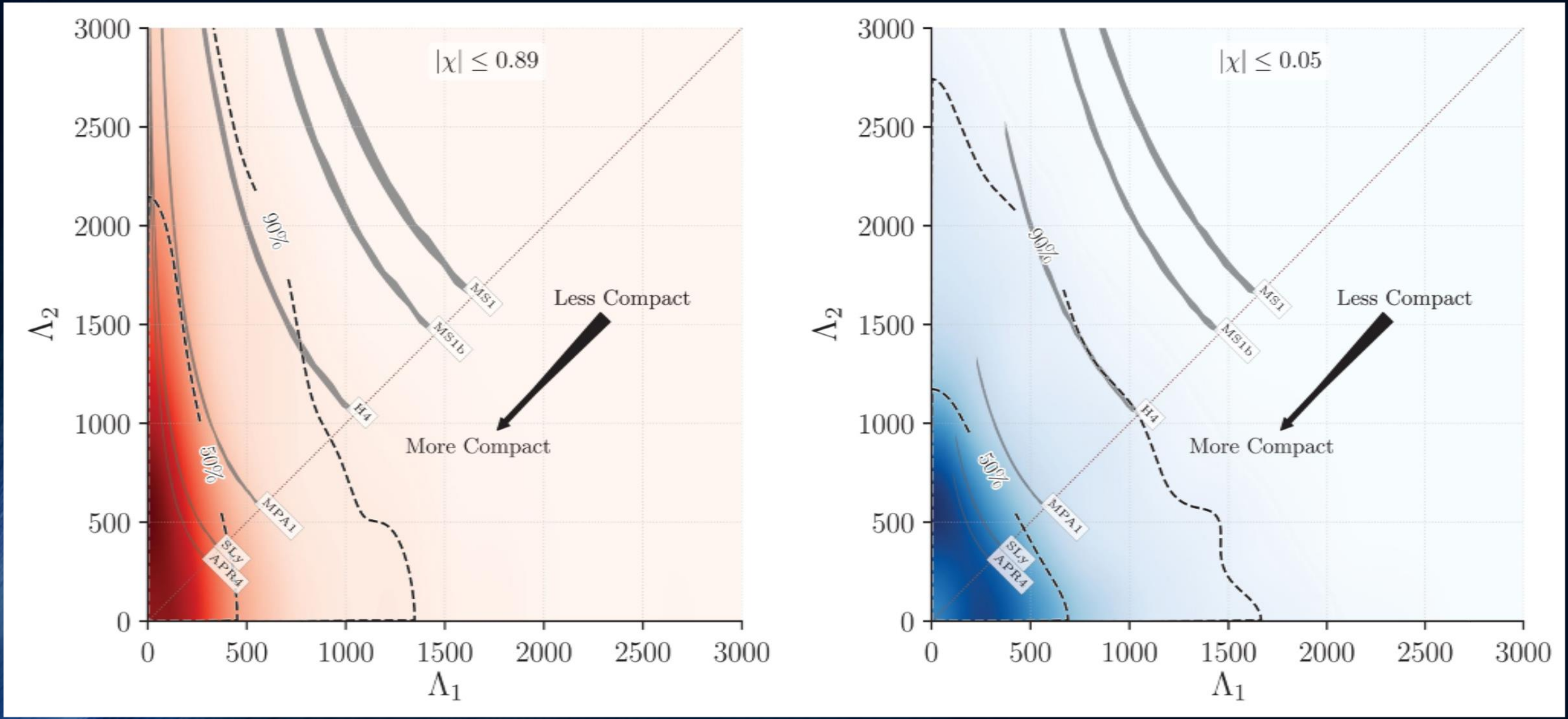

Numerical Relativity and Relativistic Hydrodynamics of Binary Neutron Star Mergers

Einstein's theory of general relativity and the resulting general relativistic conservation laws for energy-momentum in connection with the rest-mass conservation are the theoretical groundings of neutron star binary mergers:

$$R_{\mu\nu} - \frac{1}{2} g_{\mu\nu} R = 8\pi T_{\mu\nu}$$

$$\nabla_\mu (\rho u^\mu) = 0\,,\qquad \nabla_\nu T^{\mu\nu} = 0\,.$$

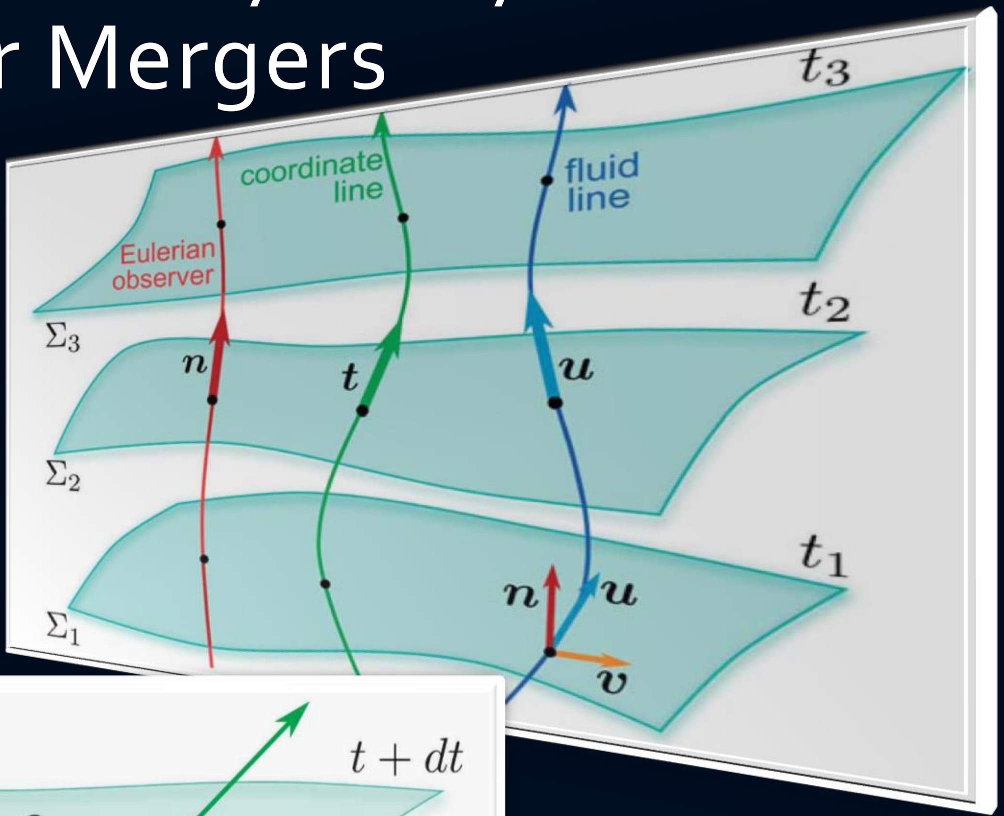

(3+1) decomposition of spacetime

$$g_{\mu\nu} = \begin{pmatrix} -\alpha^2 + \beta_i\beta^i & \beta_i \\ \beta_i & \gamma_{ij} \end{pmatrix}$$

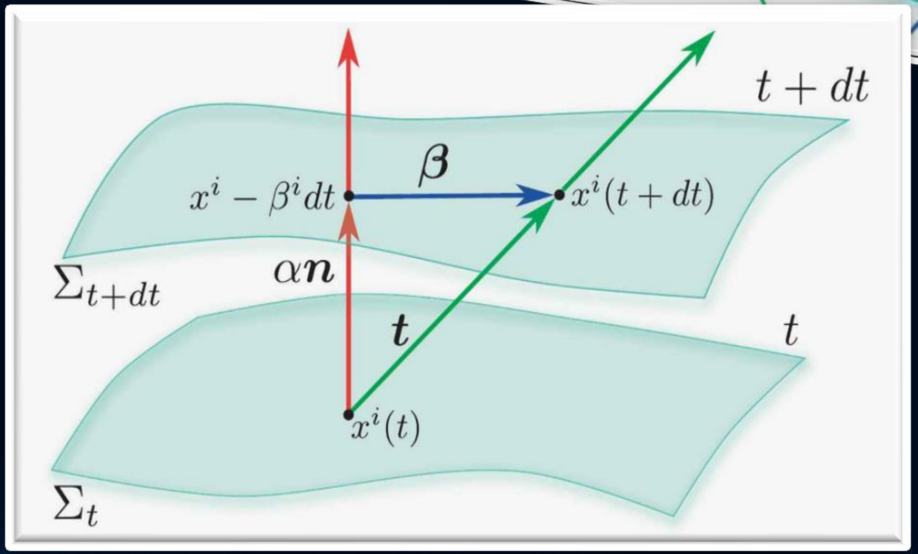

$$d\tau^2 = \alpha^2(t, x^j)dt^2 \qquad x^i_{t+dt} = x^i_t - \beta^i(t, x^j)dt$$

All figures and equations from: Luciano Rezzolla, Olindo Zanotti: Relativistic Hydrodynamics, Oxford Univ. Press, Oxford (2013)

Tidal Deformations in the late Inspiral Phase

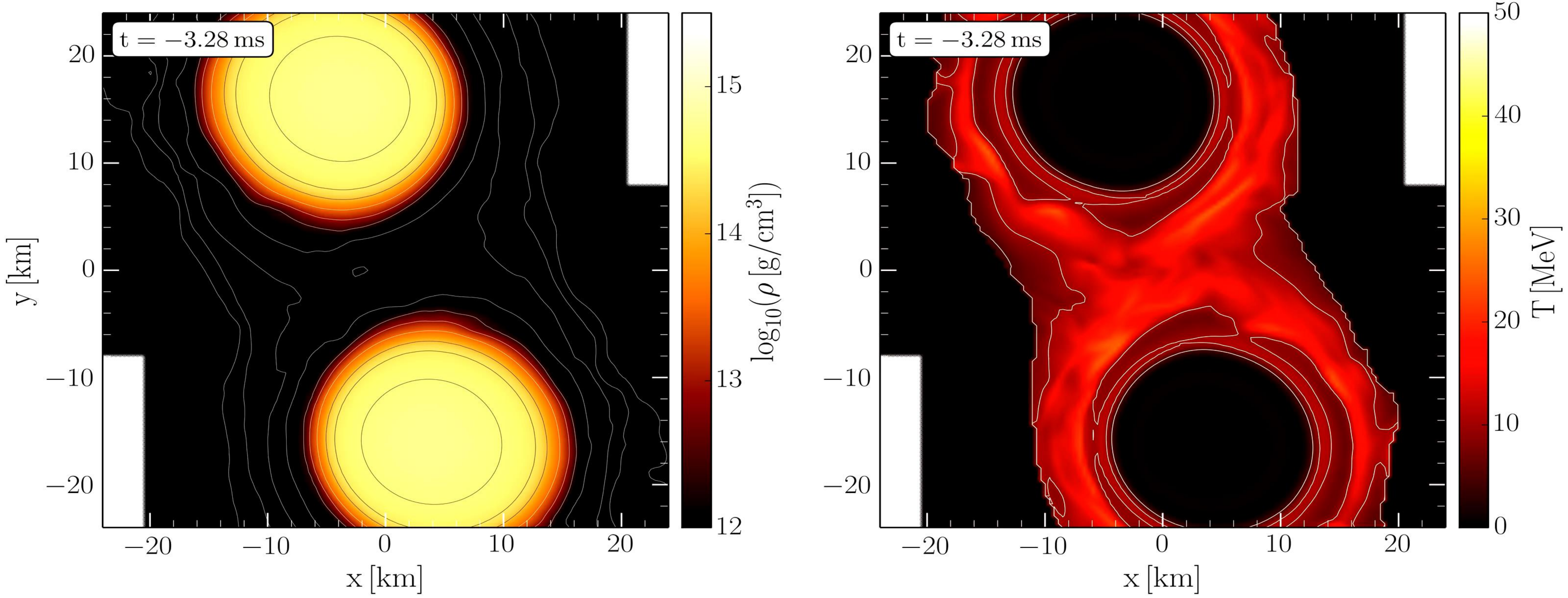

QCD Phase Diagram: The Late Inspiral Phase

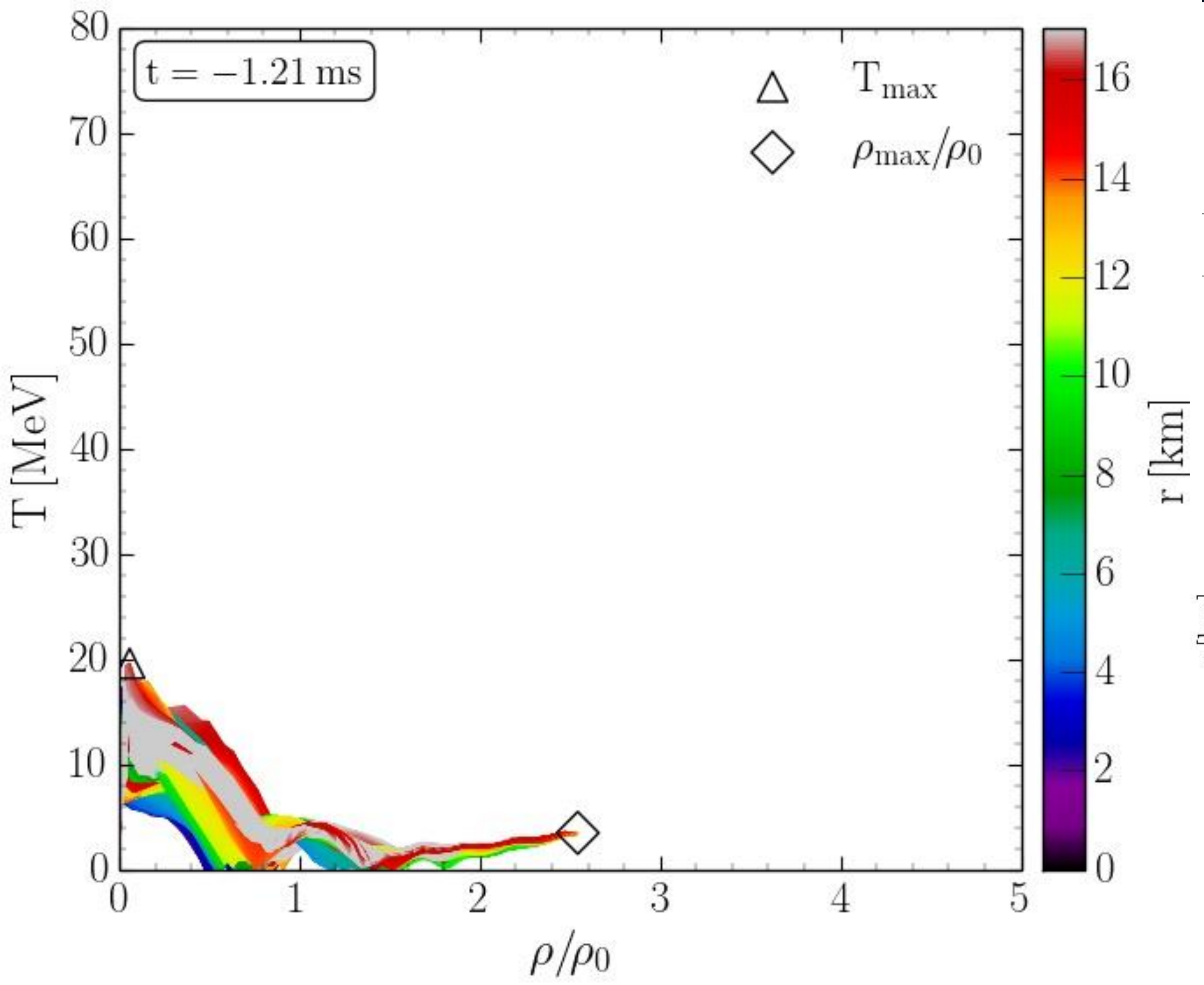

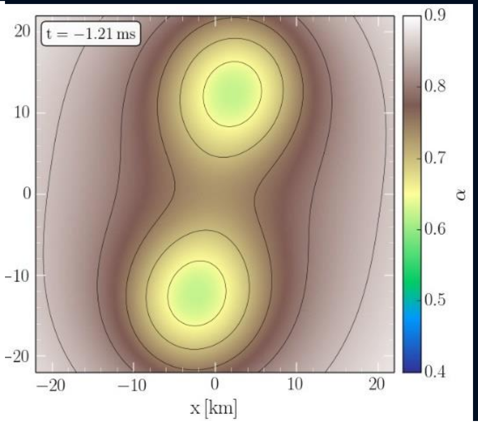

Lapse function α (left)

rest mass density ρ

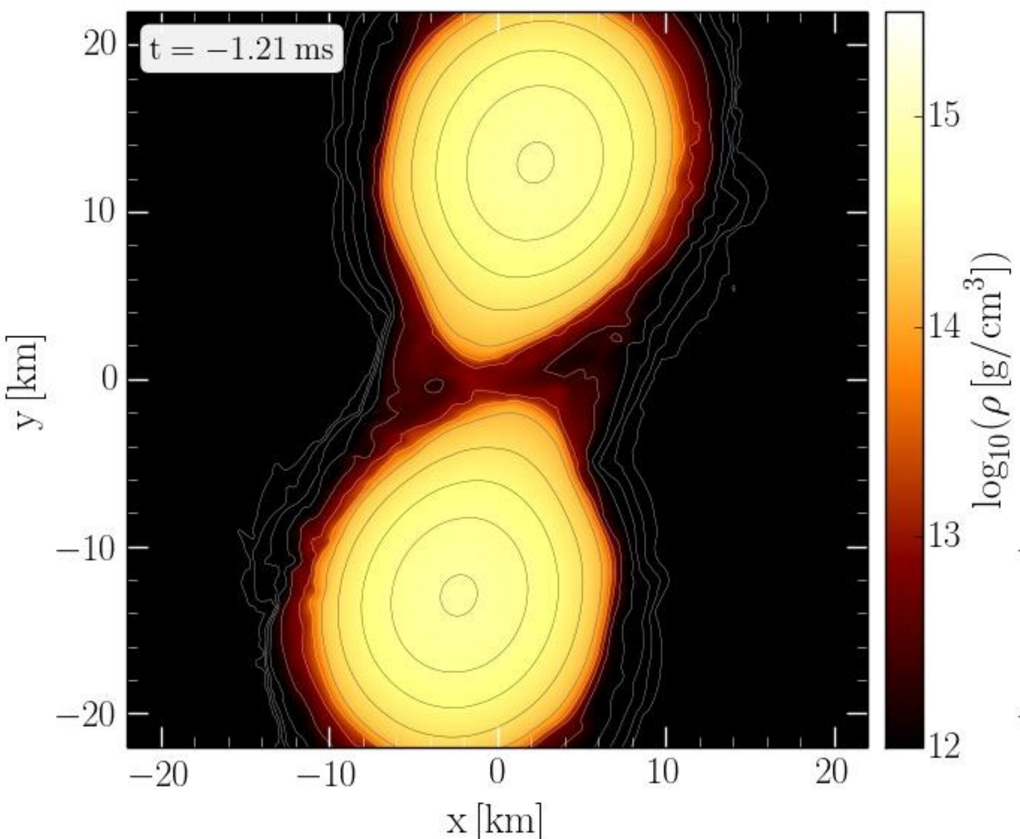

QCD Phase Diagram: The Late Inspiral Phase

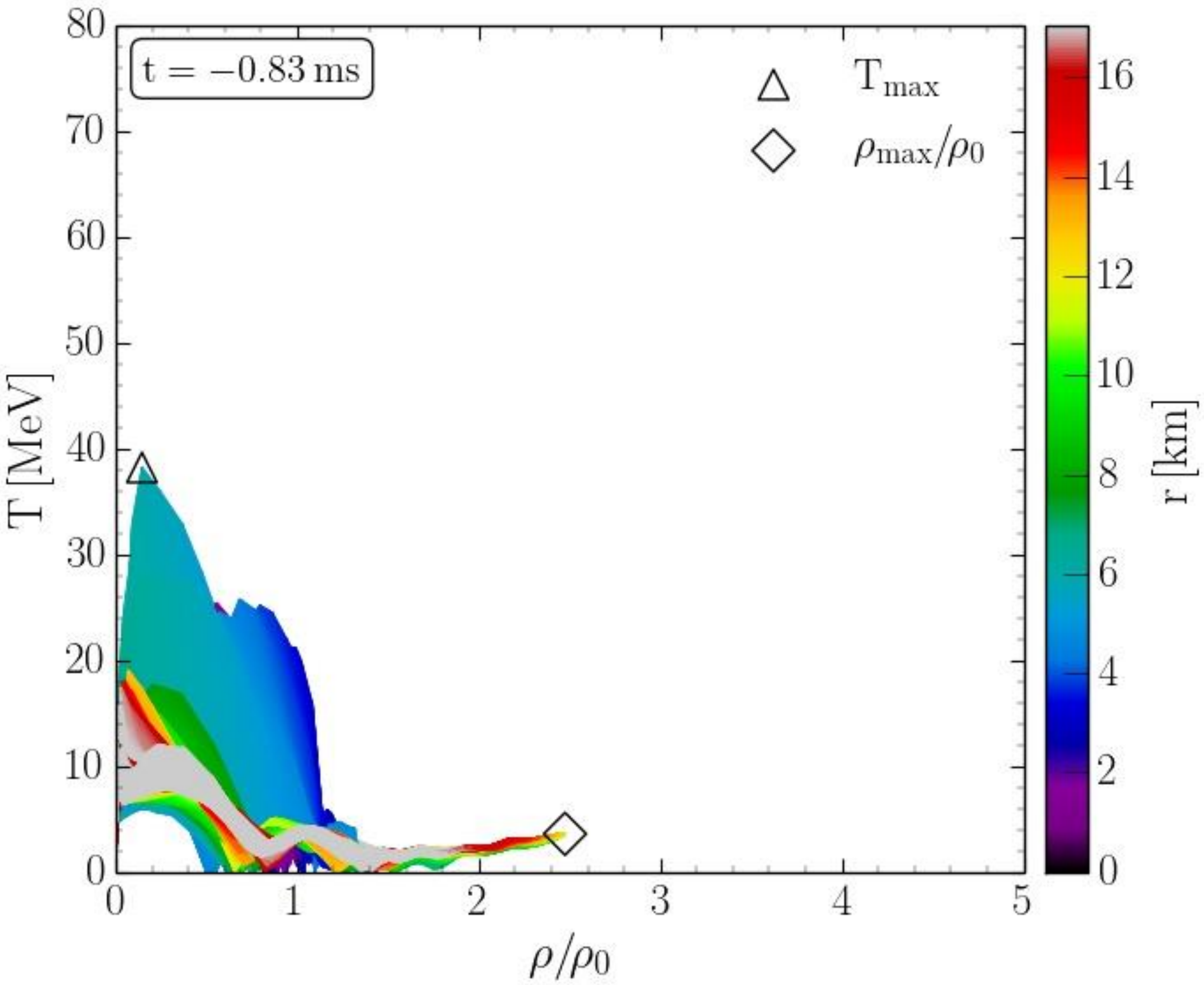

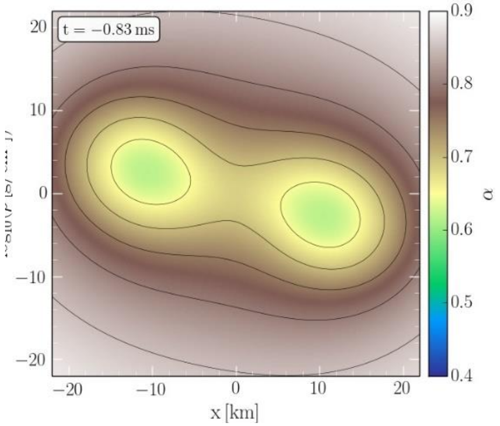

Lapse function α (left)

rest mass density ρ

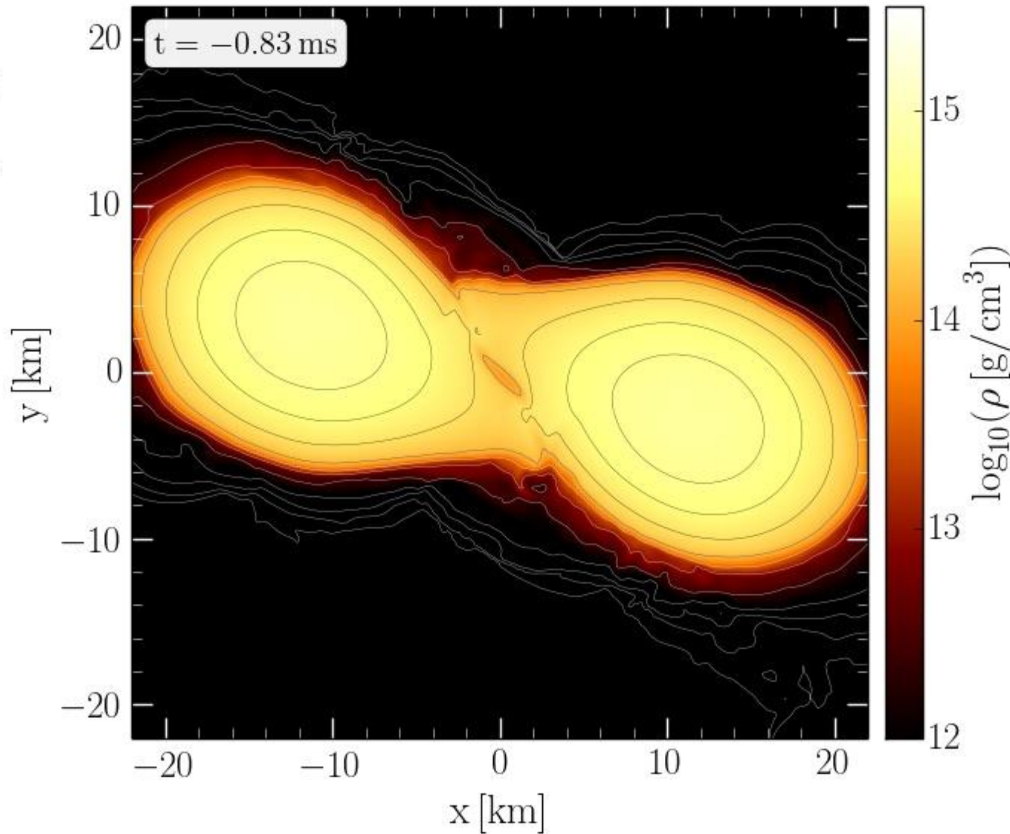

The QCD – Phase Transition and the Interior of a Hybrid Star

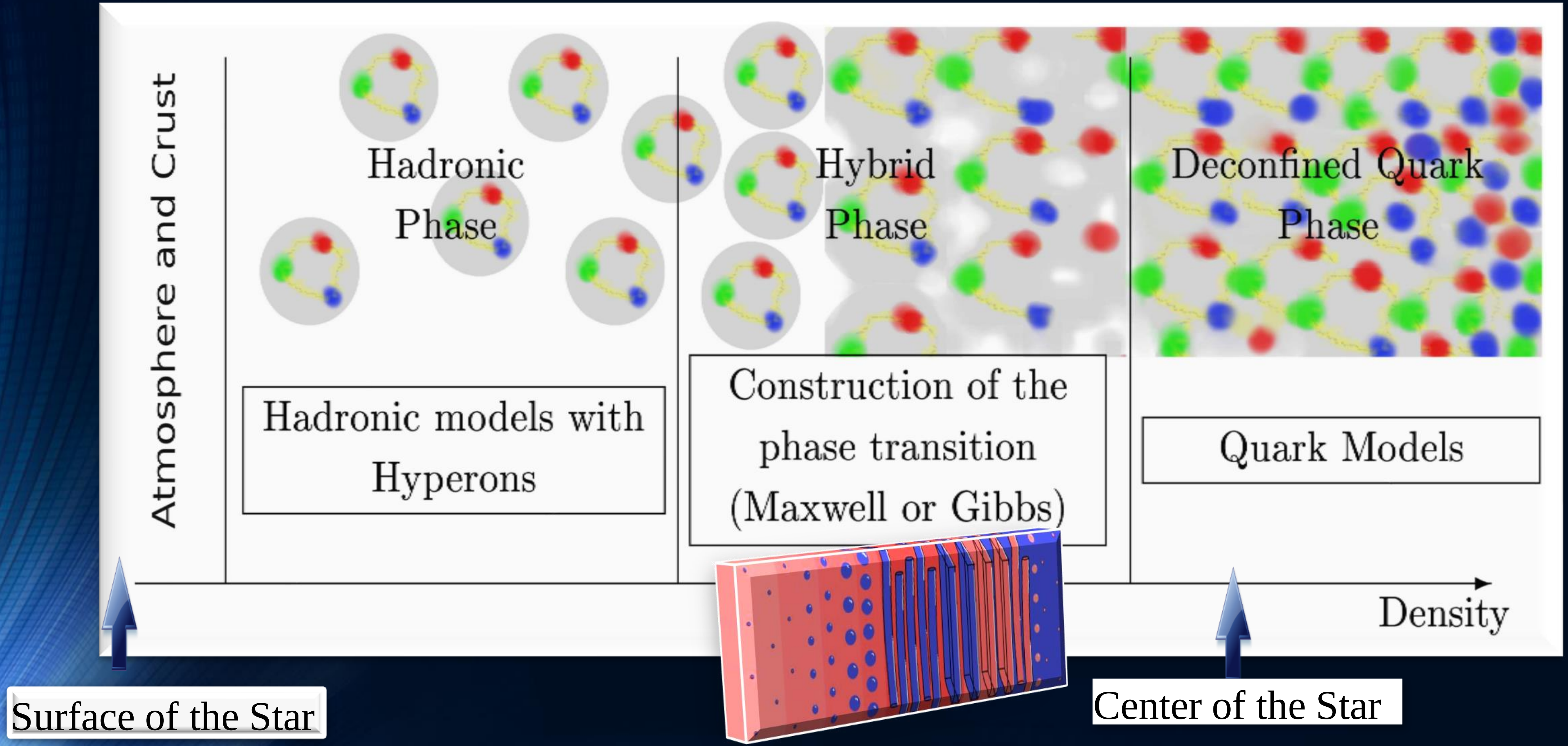

Matthias Hanauske; Doctoral Thesis:
Properties of Compact Stars within QCD-motivated Models; University Library Publication Frankfurt (2004)

The Hadron-Quark Phase Transition

The QCD Phase Diagram

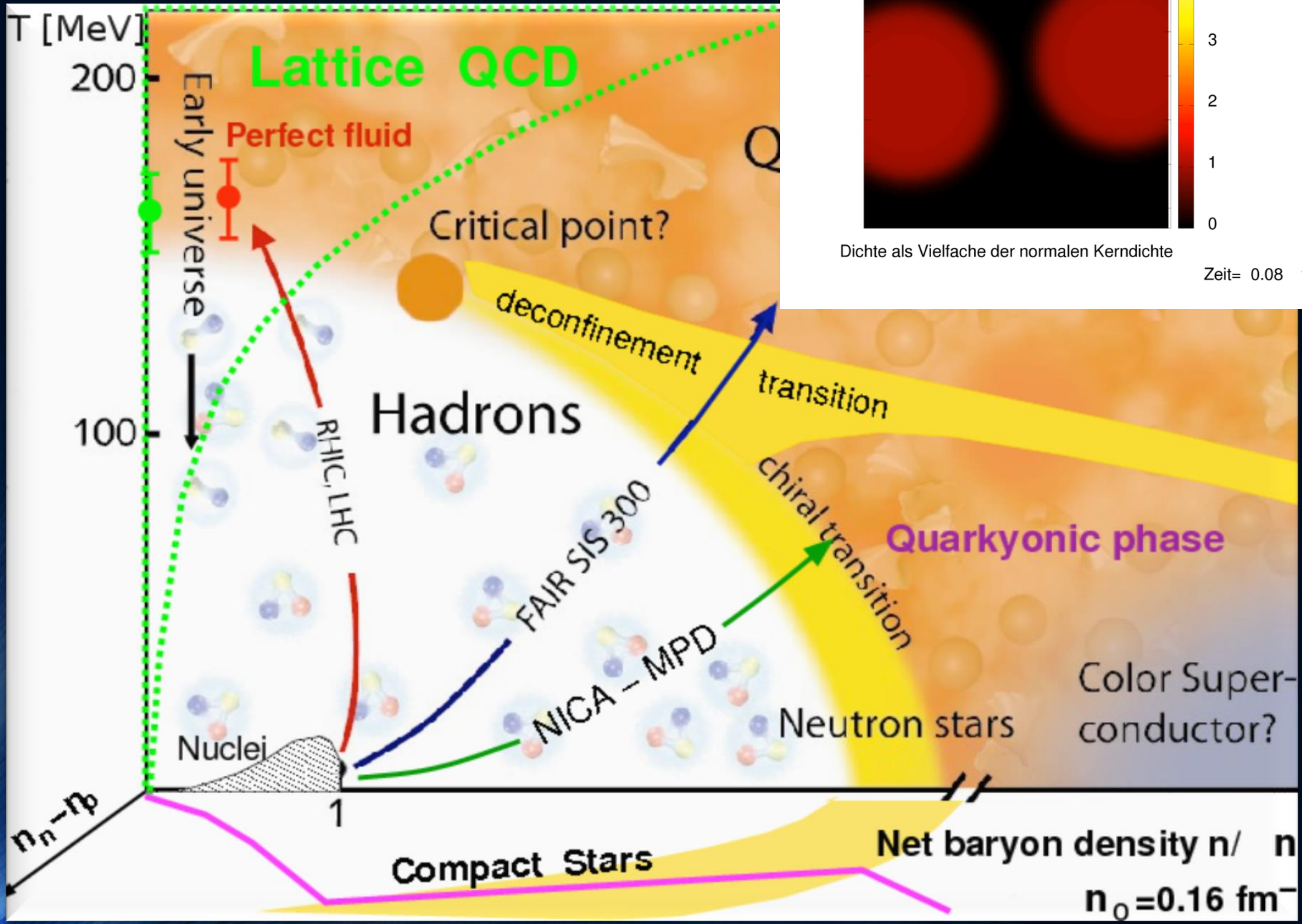

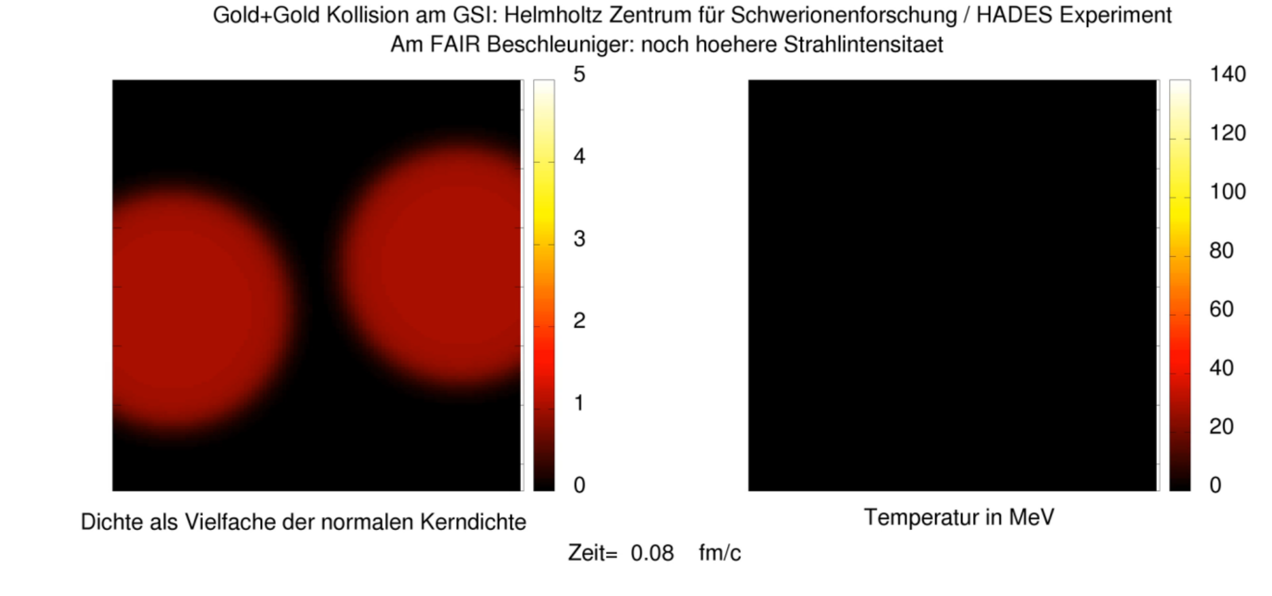

Credits:
Jan Steinheimer

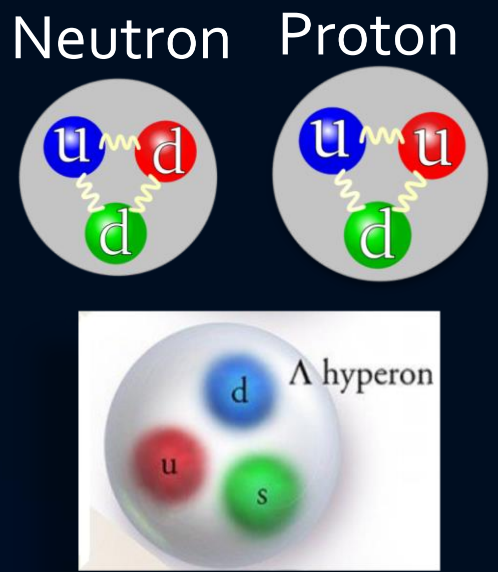

The Gibbs Construction

Hadronic and quark surface:

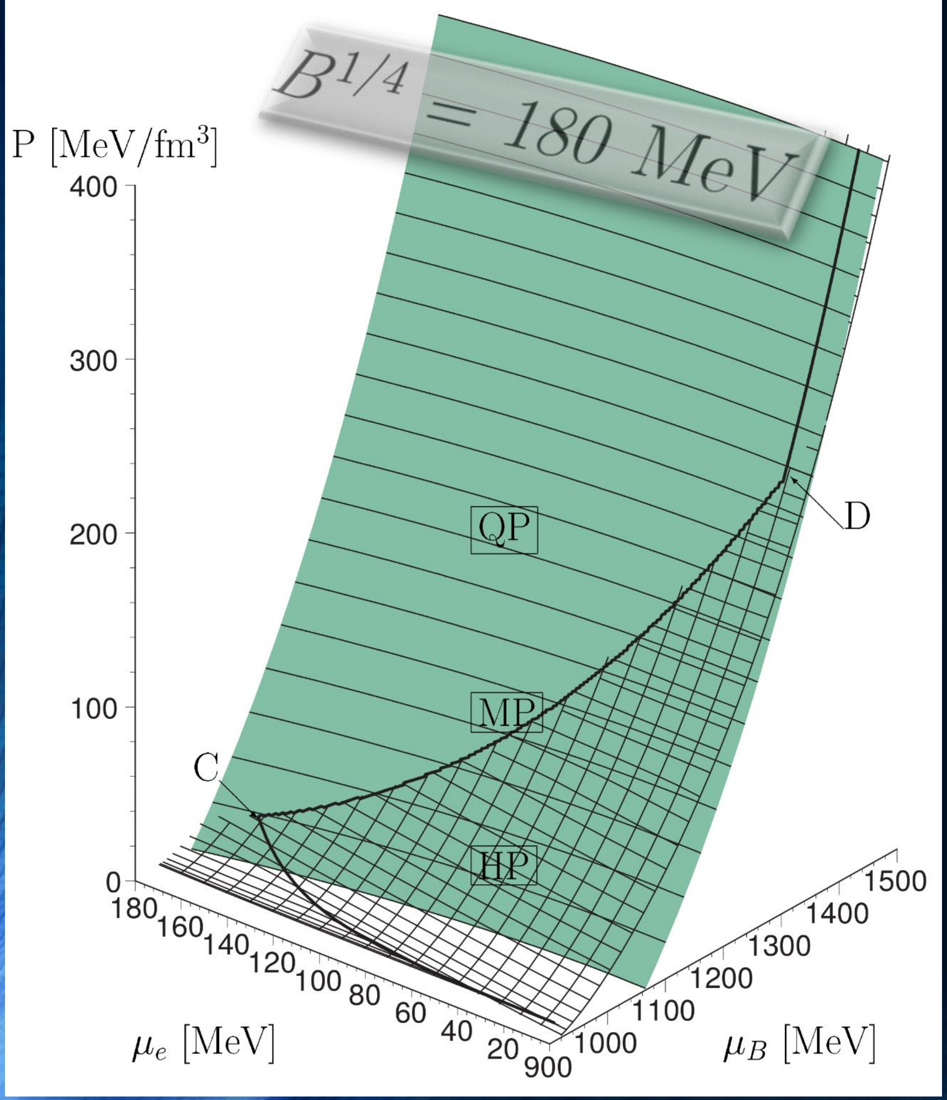

Charge neutrality condition is only globally realized

$$\rho_e := (1-\chi)\,\rho_e^H(\mu_B,\mu_e) + \chi\,\rho_e^Q(\mu_B,\mu_e) = 0\,.$$

The pressure in the mixed phase depends on two independent chemical potentials

$$\begin{aligned} P^H(\mu_B,\mu_e) &= P^Q(\mu_B,\mu_e)\,, \\ \mu_B = \mu_B^H &= \mu_B^Q\,, \\ \mu_e = \mu_e^H &= \mu_e^Q \end{aligned}$$

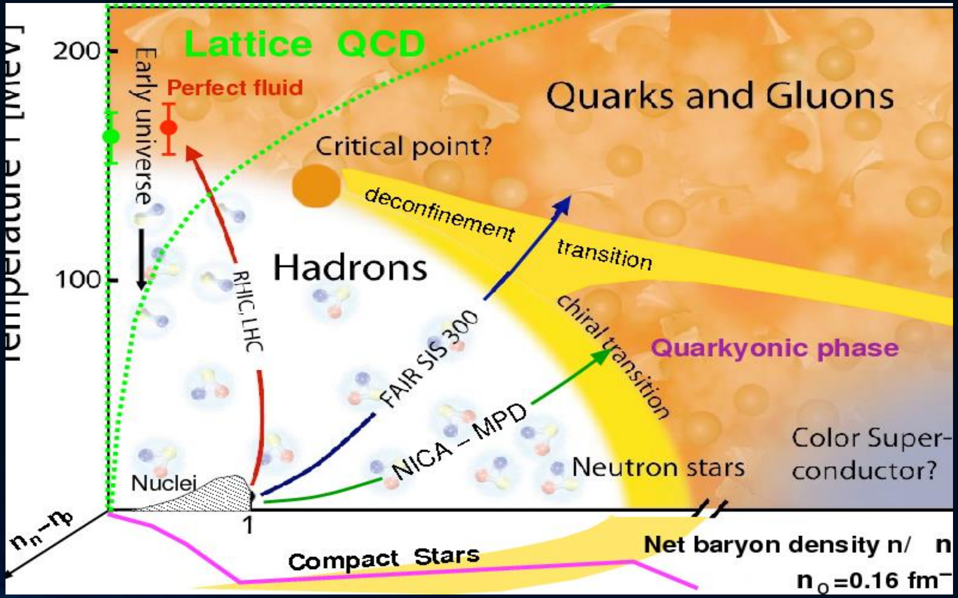

The Gibbs Construction

Hadronic and quark surface:

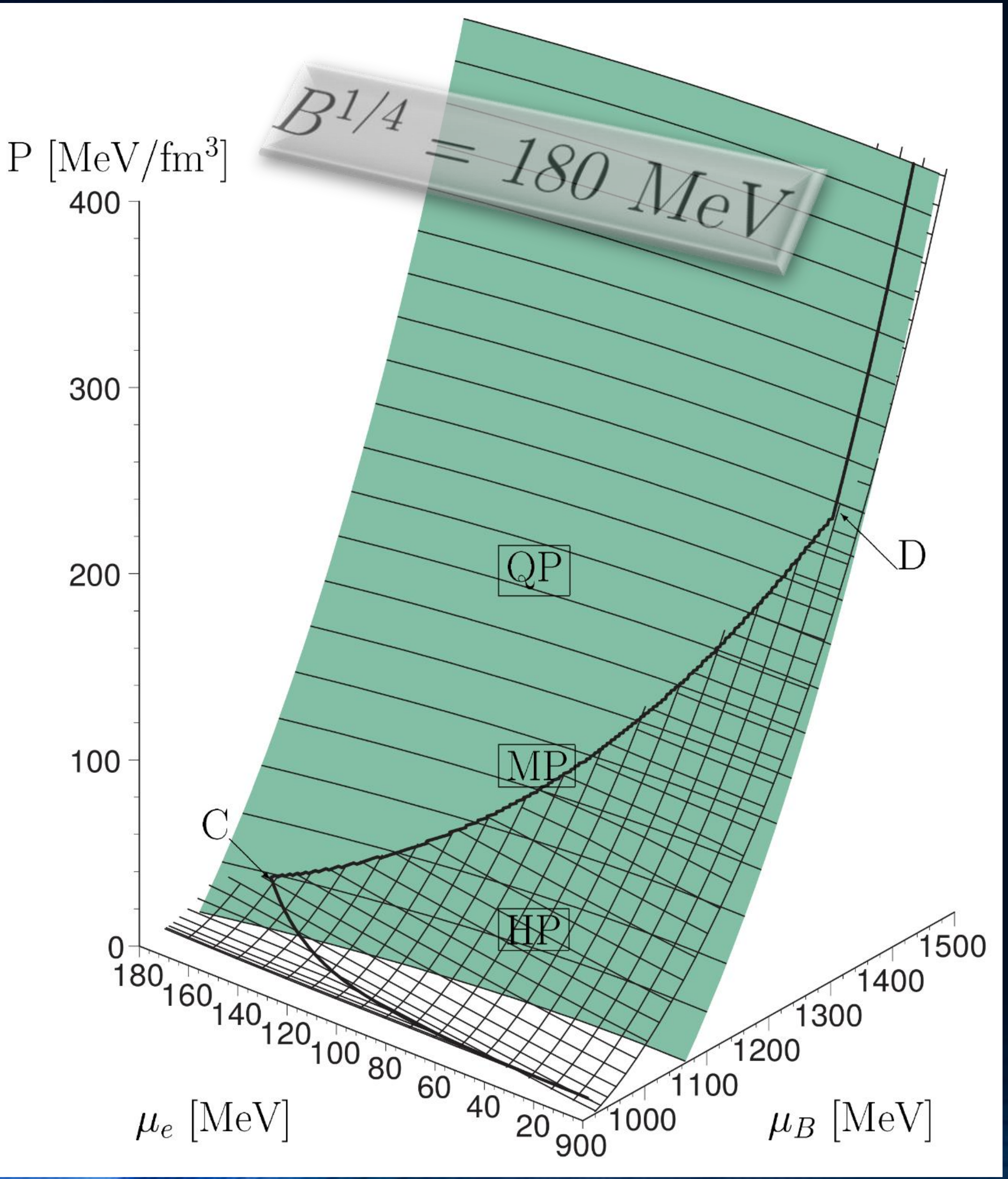

Charge neutrality condition is only globally realized

$$\rho_e := (1-\chi)\,\rho_e^H(\mu_B,\mu_e) + \chi\,\rho_e^Q(\mu_B,\mu_e) = 0\,.$$

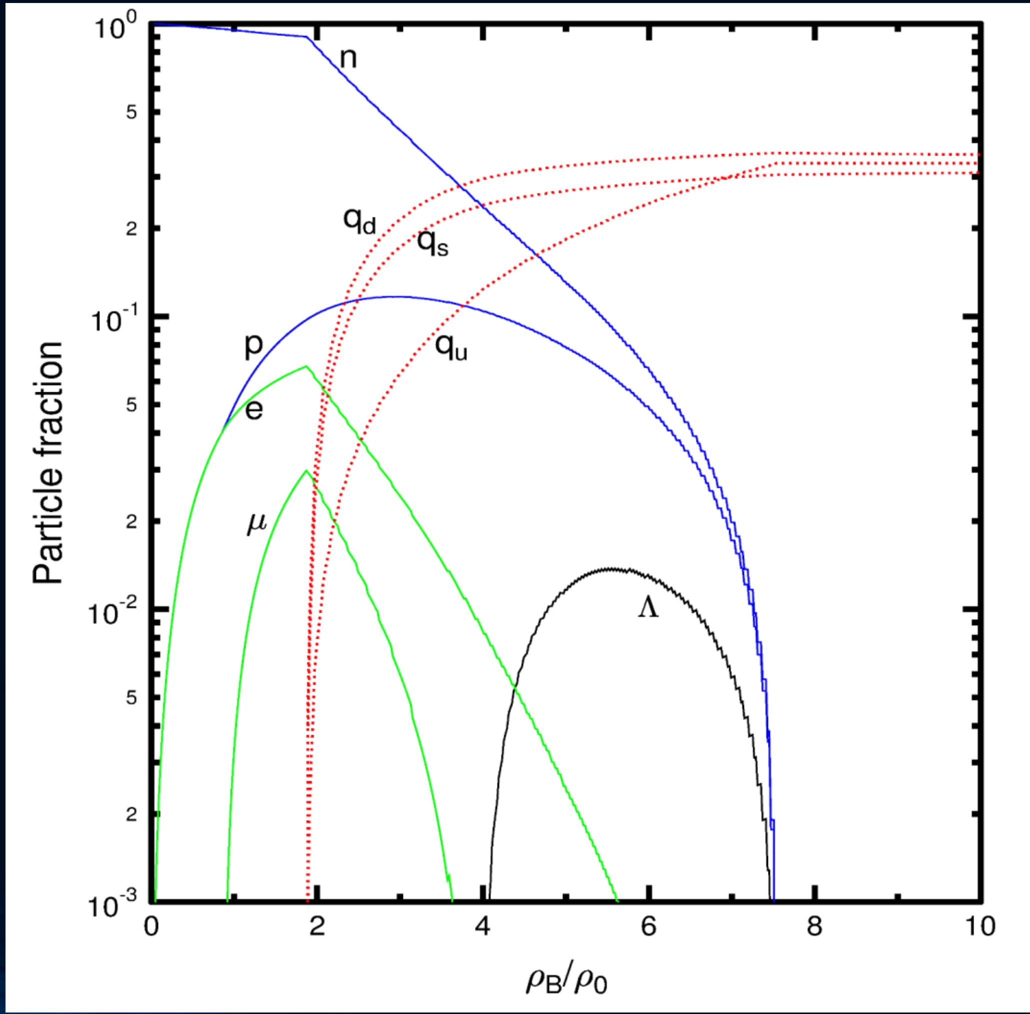

The Gibbs Construction

Hadronic and quark surface:

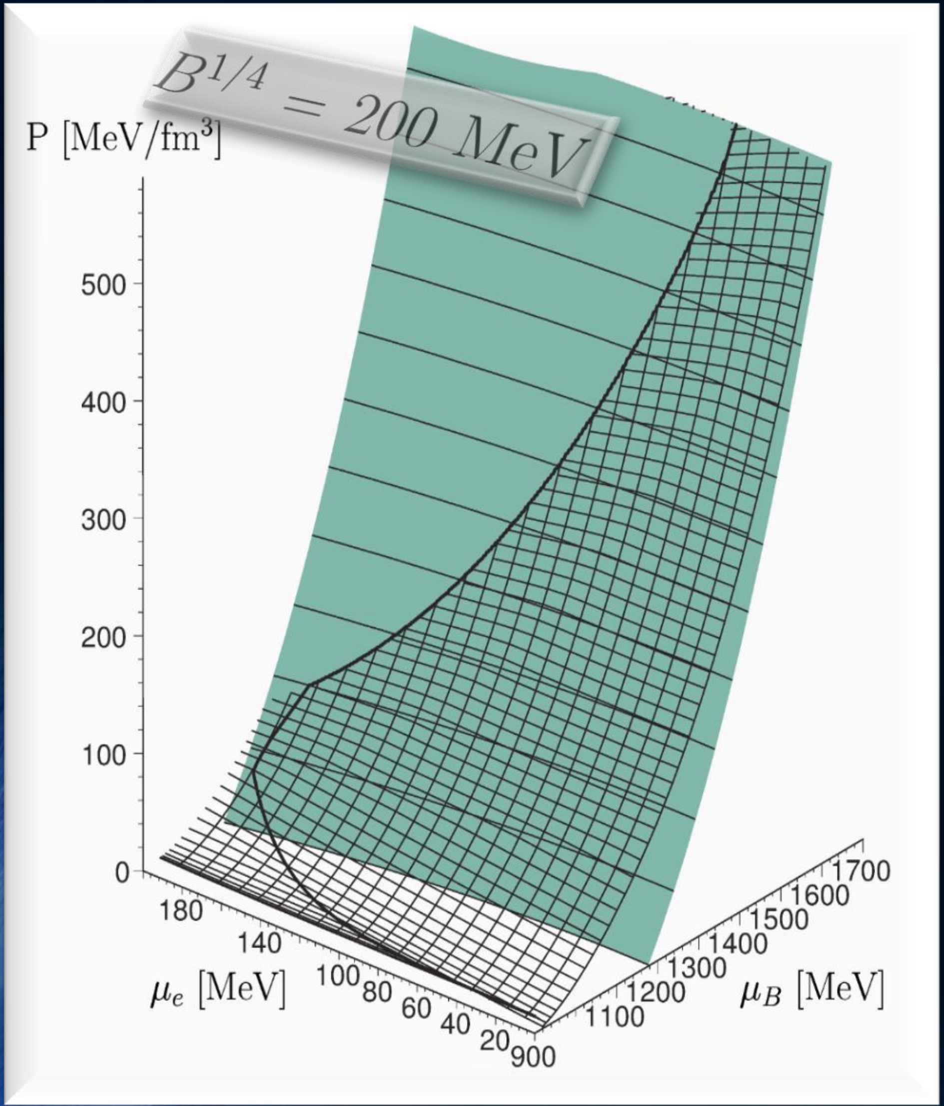

Particle composition:

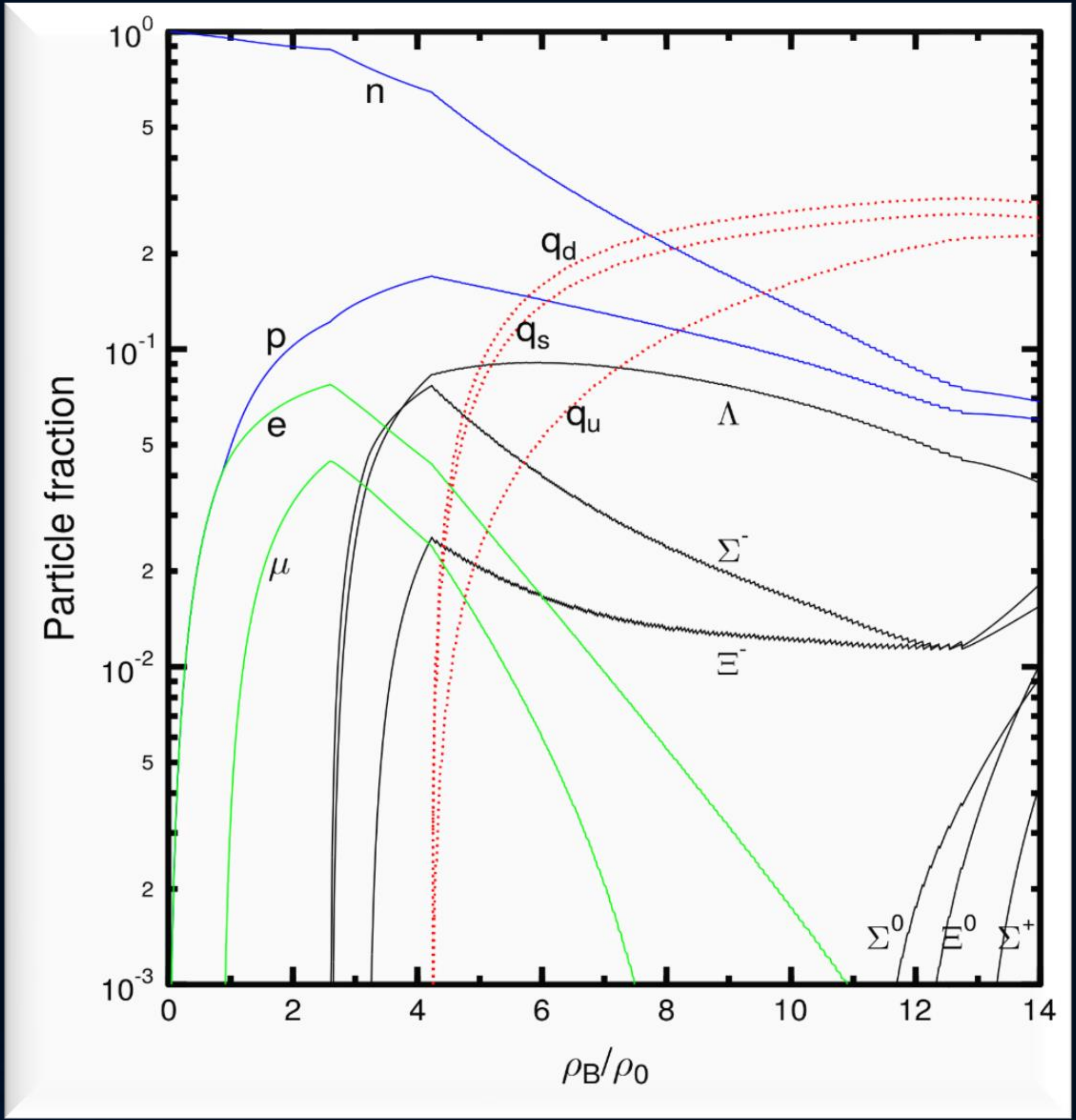

M. Hanauske, Dissertation, "Properties of Compact Stars within QCD-motivated Models"

Evolution of the density in the post merger phase

ALF2-EOS: Mixed phase region starts at $3\rho_0$ (see red curve), initial NS mass: 1.35 M_{solar}

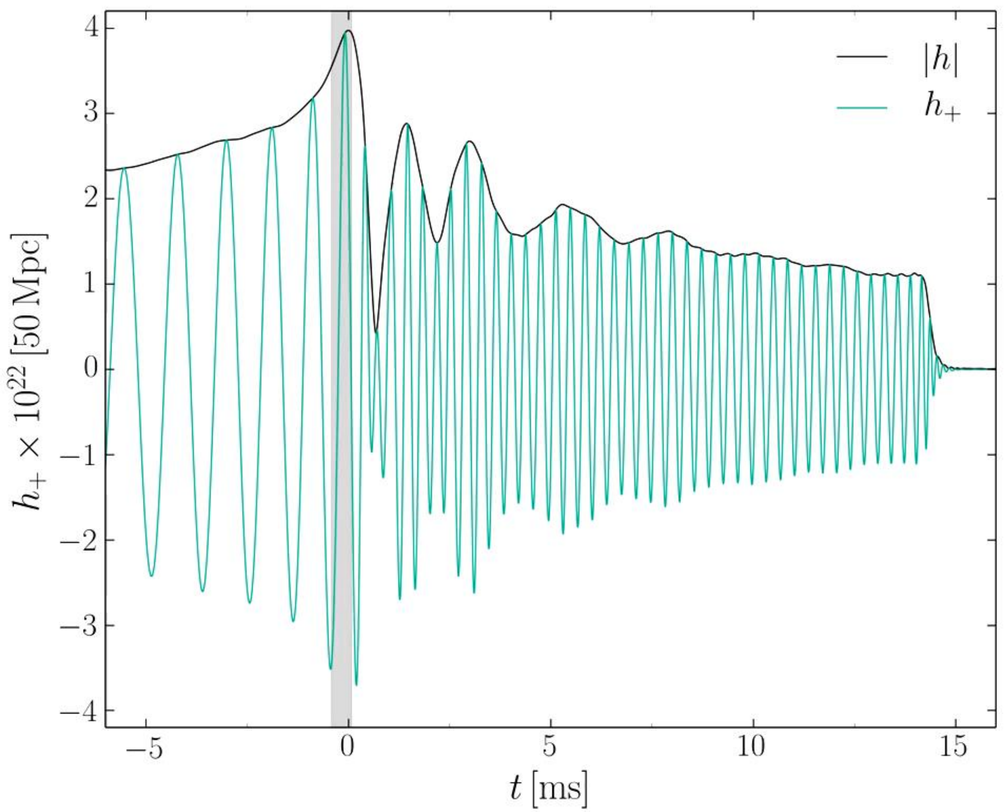

Gravitational wave amplitude
at a distance of 50 Mpc

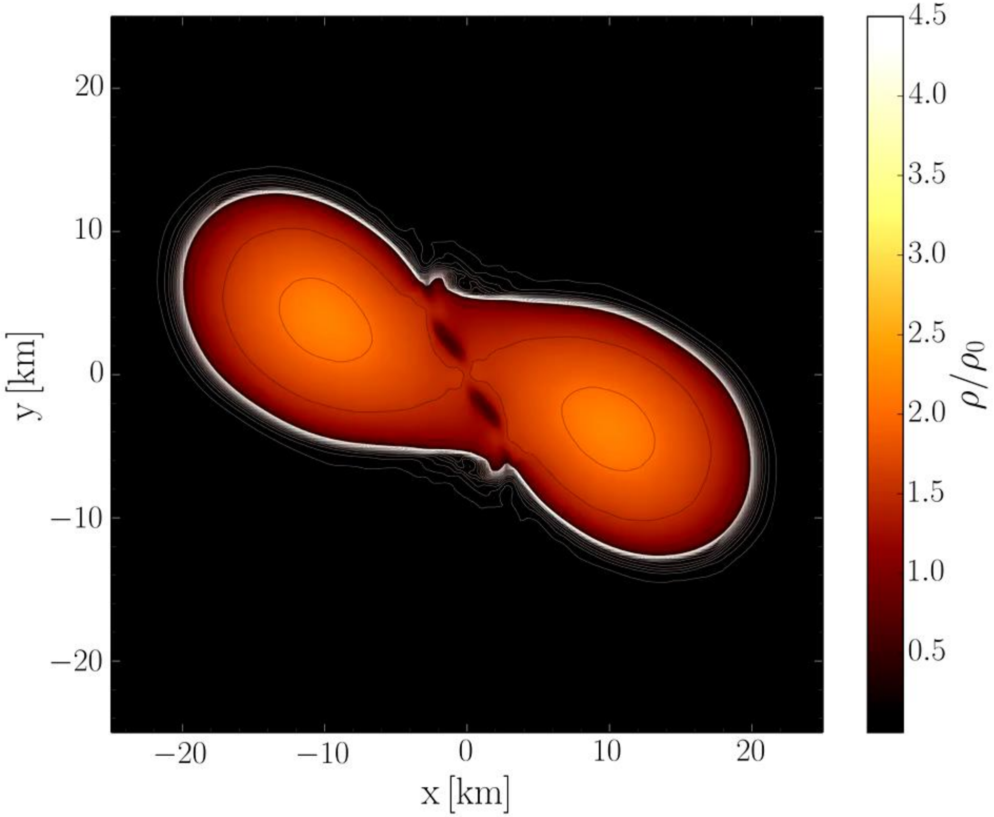

Rest mass density distribution ρ(x,y)
in the equatorial plane
in units of the nuclear matter density ρ_0

GW-Spectrum for different EOSs

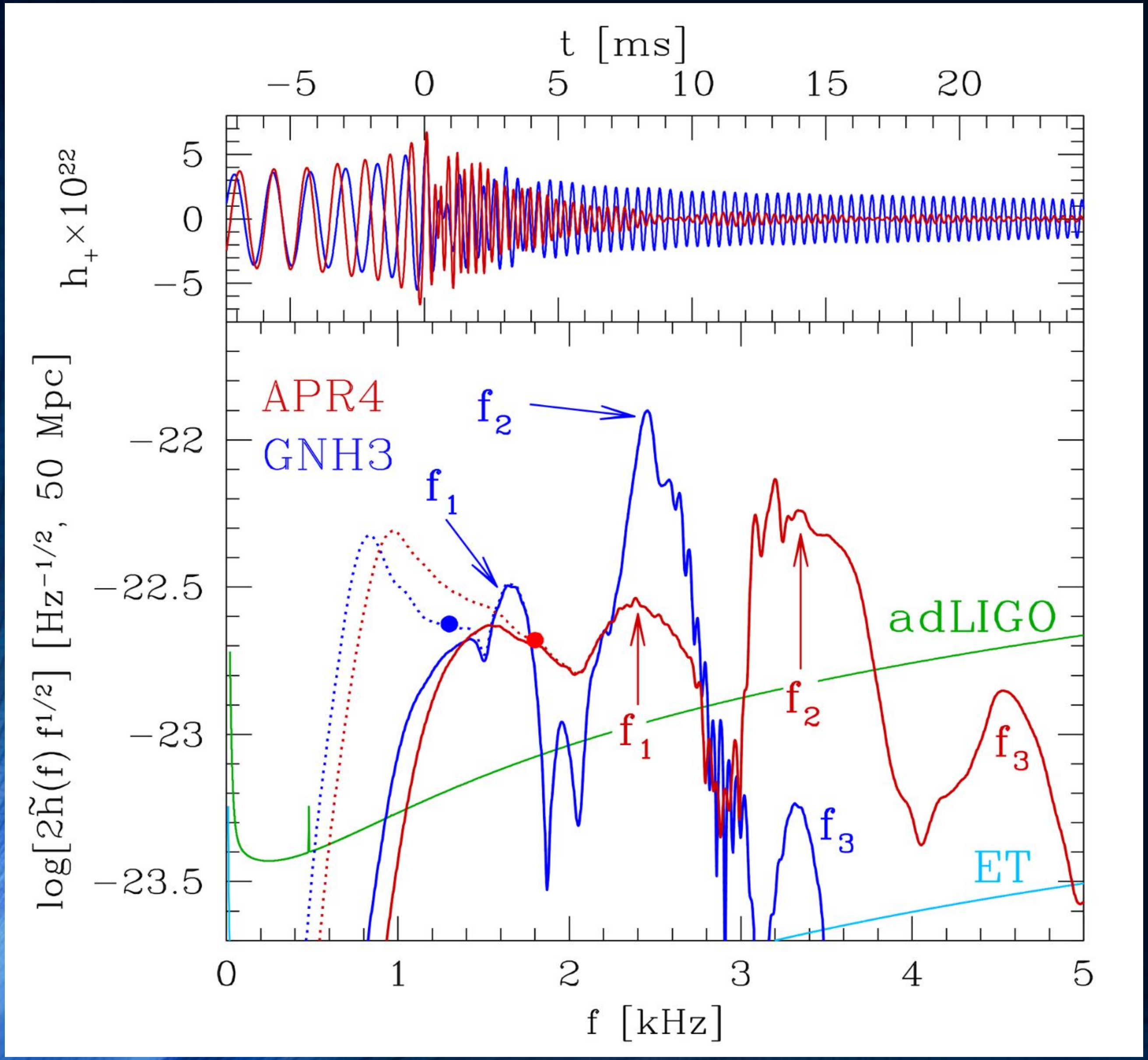

See:

Kentaro Takami, Luciano Rezzolla, and Luca Baiotti, Physical Review D 91, 064001 (2015)

Hotokezaka, K., Kiuchi, K., Kyutoku, K., Muranushi, T., Sekiguchi, Y. I., Shibata, M., & Taniguchi, K. (2013). Physical Review D, 88(4), 044026.

Bauswein, A., & Janka, H. T. (2012). Physical review letters, 108(1), 011101.

Clark, J. A., Bauswein, A., Stergioulas, N., & Shoemaker, D. (2015). arXiv:1509.08522.

Bernuzzi, S., Dietrich, T., & Nagar, A. (2015). Physical review letters, 115(9), 091101.

Time Evolution of the GW-Spectrum

The power spectral density profile of the post-merger emission is characterized by several distinct frequencies. After approximately 5 ms after merger, the only remaining dominant frequency is the f_2-frequency (See e.g. L.Rezzolla and K.Takami, PRD, 93(12), 124051 (2016))

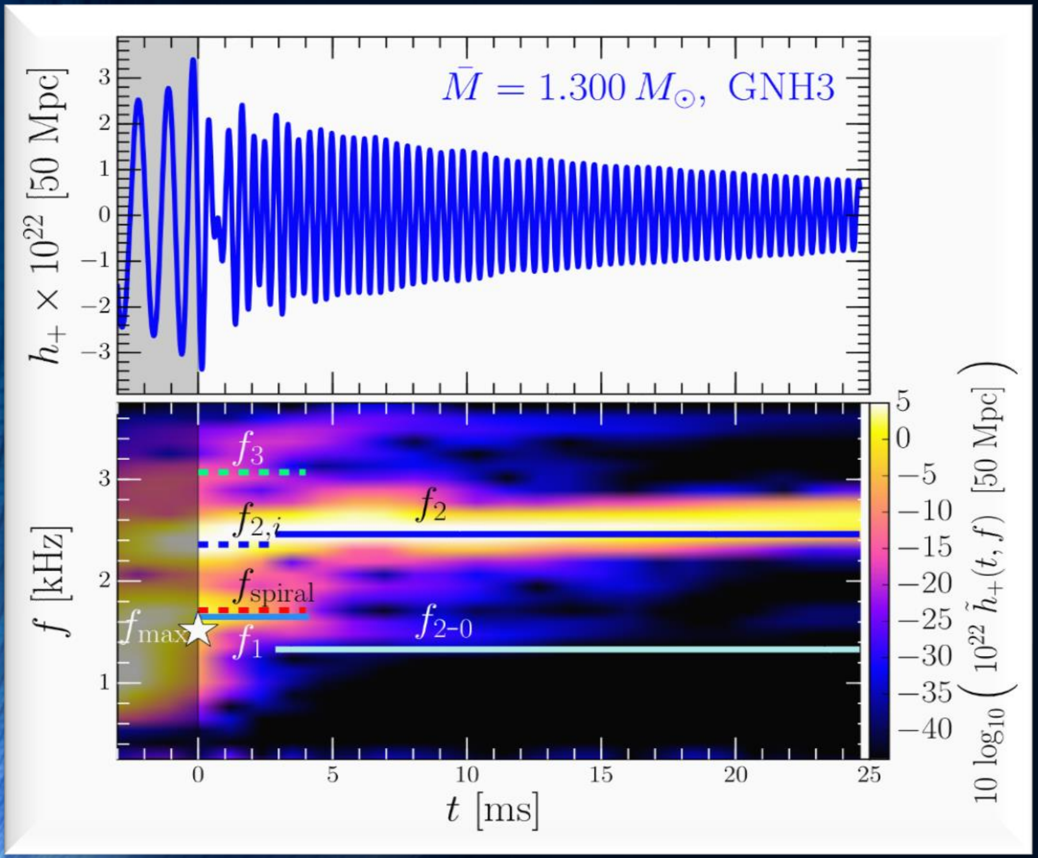

Stiff EOS

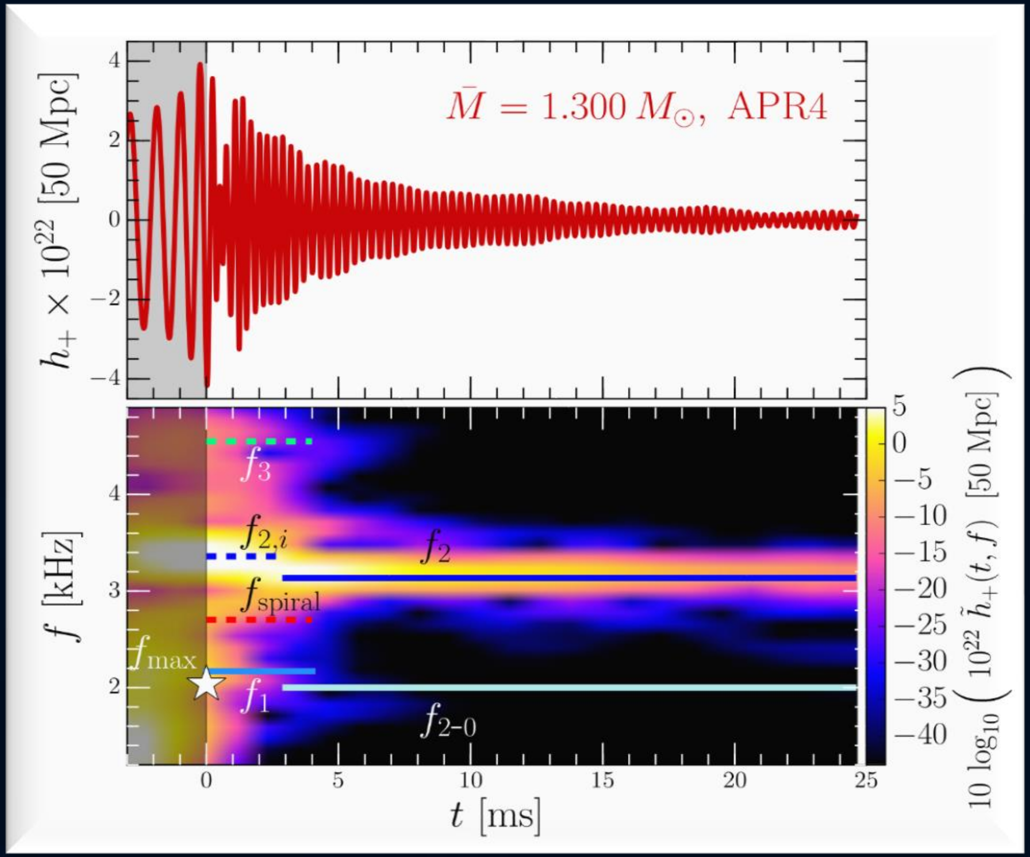

Soft EOS

Unfortunately, due to the low sensitivity at high gravitational wave frequencies, no post-merger signal has been found in GW170817.

But advanced detectors / next-generation detectors might be able to detect!!?

Evolution of the frequency spectrum of the emitted gravitational waves for the stiff GNH3 (left) and soft APR4 (right) EOS.

Density and Temperature Evolution inside the HMNS

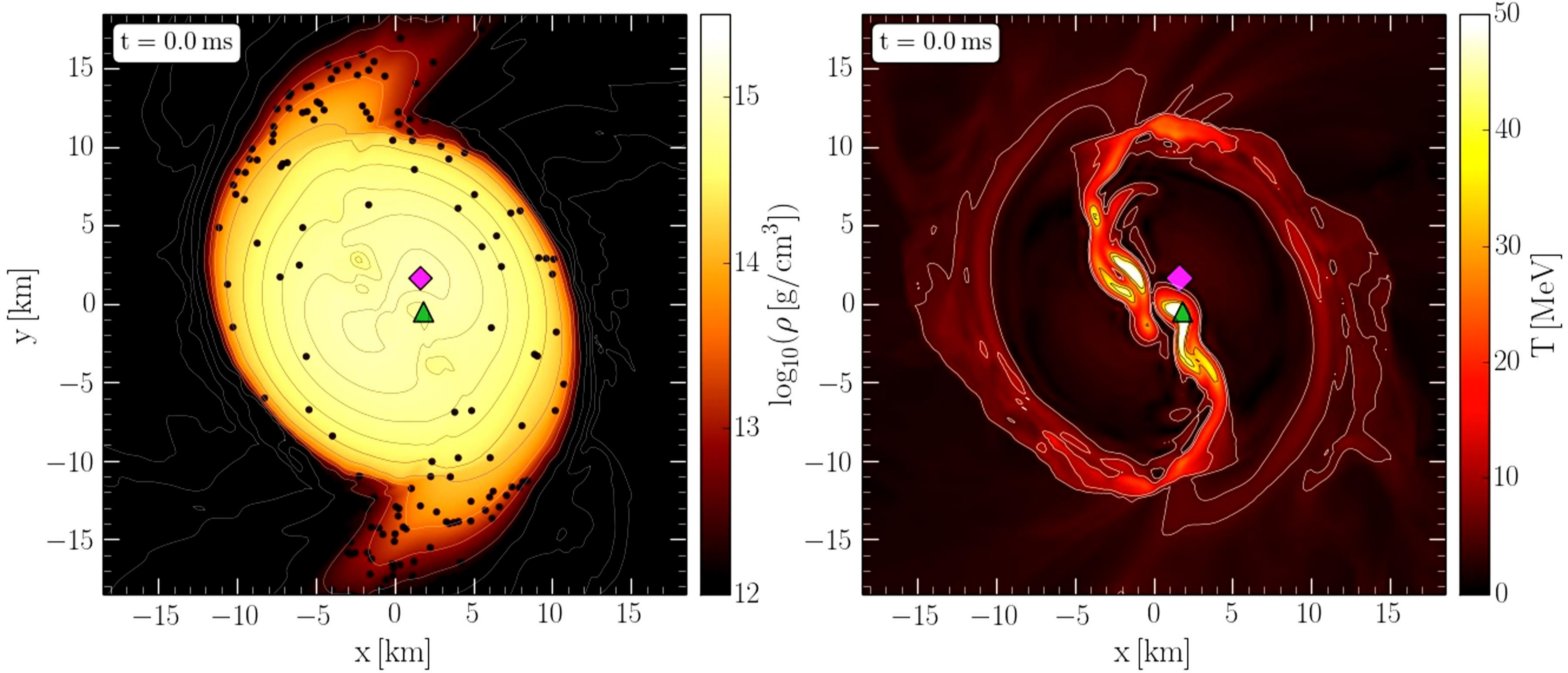

Rest mass density on the equatorial plane

Temperature on the equatorial plane

The Angular Velocity in the (3+1)-Split

The angular velocity Ω in the (3+1)-Split is a combination of the lapse function α , the ϕ-component of the shift vector β^ϕ and the 3-velocity v^ϕ of the fluid (spatial projection of the 4-velocity **u**):

(3+1)-decomposition of spacetime:

$$\Omega(x,y,z,t) = \frac{u^\phi}{u^t} = \alpha\, v^\phi \; - \; \beta^\phi$$

$$g_{\mu\nu} = \begin{pmatrix} -\alpha^2 + \beta_i \beta^i & \beta_i \\ \beta_i & \gamma_{ij} \end{pmatrix}$$

Angular velocity Ω

Lapse function α

Φ-component of 3-velocity v^φ

Frame-dragging β^φ

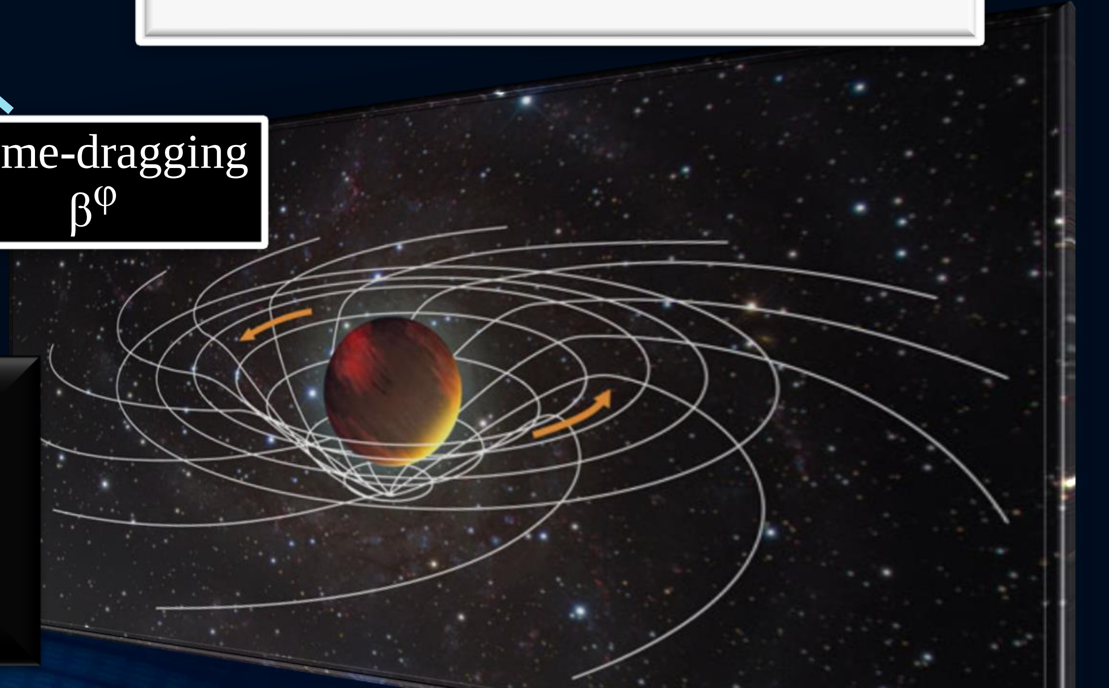

Focus: Inner core of the differentially rotating HMNS

M. Shibata, K. Taniguchi, and K. Uryu, Phys. Rev. D 71, 084021 (2005)
M. Shibata and K. Taniguchi, Phys. Rev. D 73, 064027 (2006)
F. Galeazzi, S. Yoshida and Y. Eriguchi, A&A 541, p. A156 (2012)
W. Kastaun and F. Galeazzi, Phys. Rev. D 91, p. 064027 (2015)

Temperature Angular Velocity

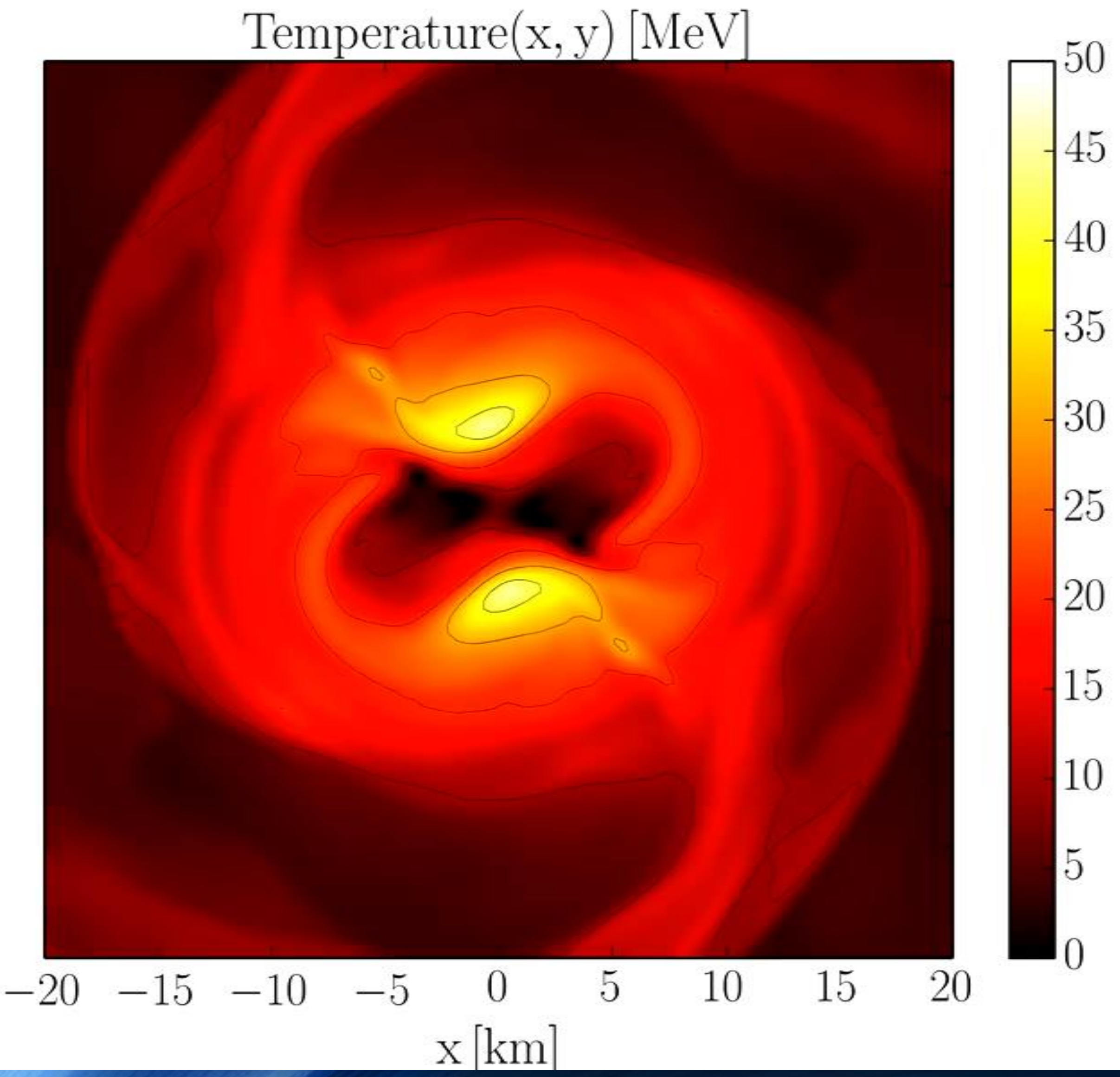

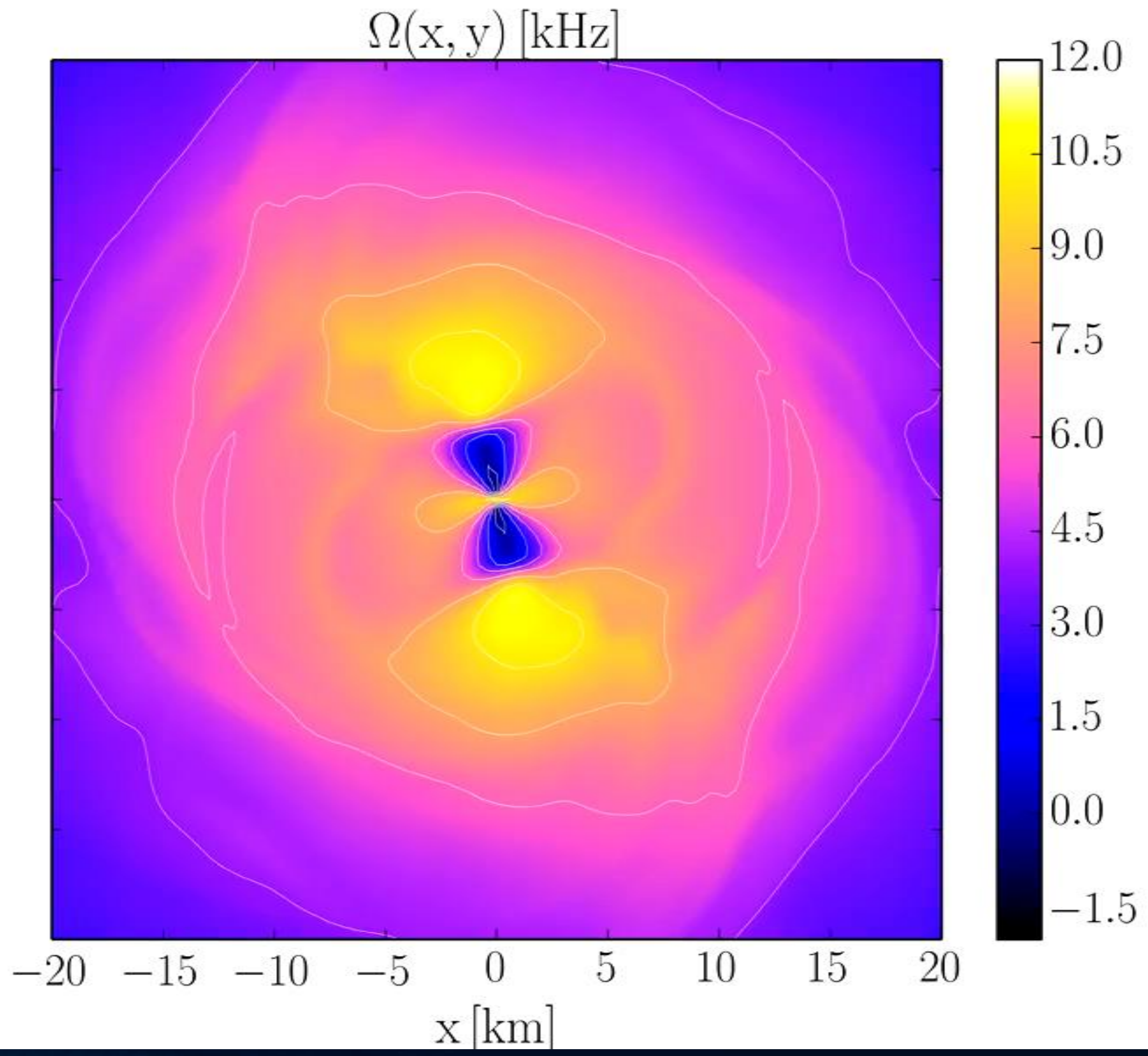

EOS: LS200 , Mass: 1.32 M_{Solar}

Binary Neutron Star Mergers in the QCD Phase Diagram

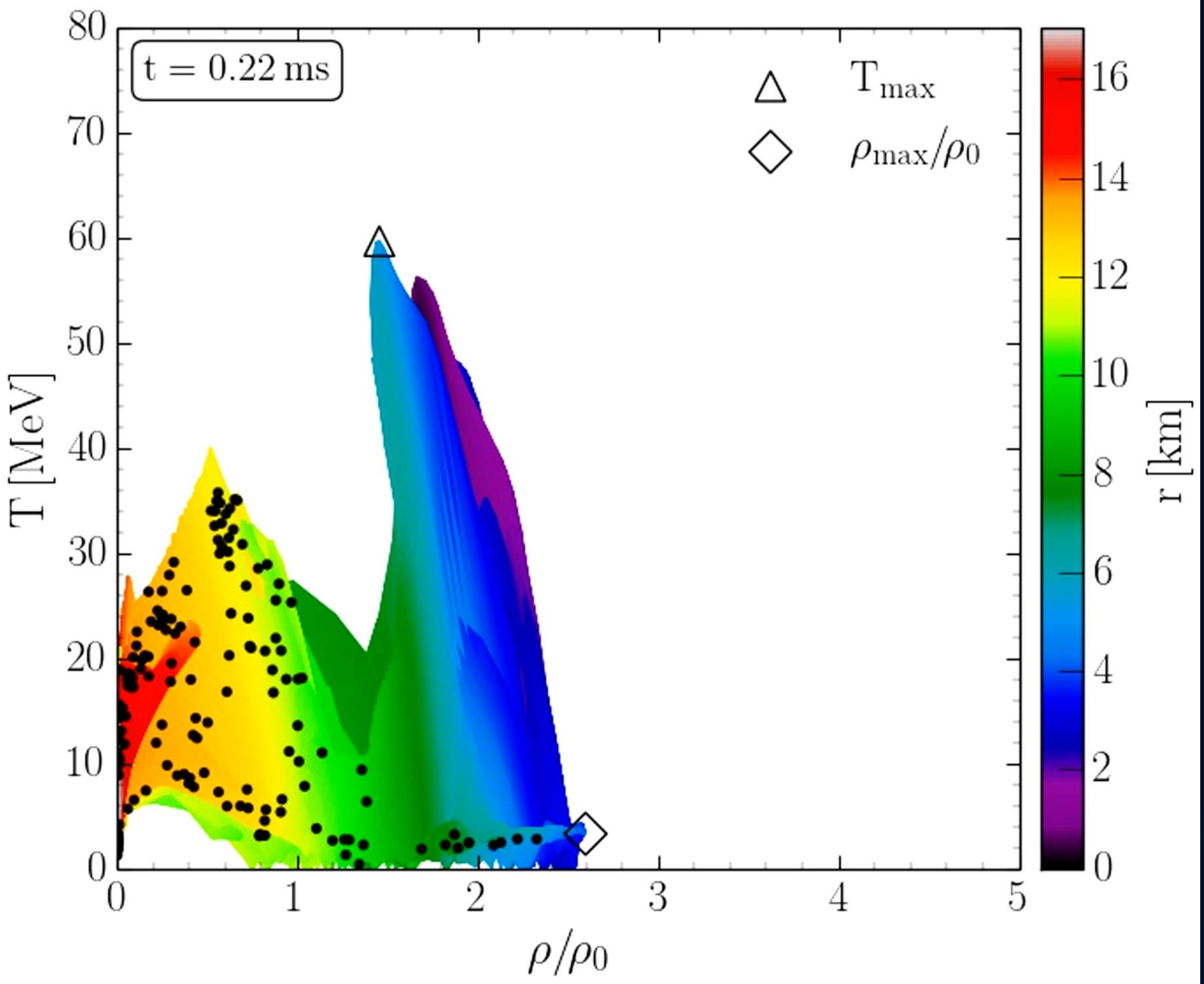

Evolution of hot and dense matter inside the inner area of a hypermassive neutron star simulated within the LS220 EOS with a total mass of M_{total}=2.7 M_{solar} in the style of a (T- ρ) QCD phase diagram plot

The color-coding indicate the radial position r of the corresponding (T- ρ) fluid element measured from the origin of the simulation (x , y) = (0 , 0) on the equatorial plane at z = 0.

The open triangle marks the maximum value of the temperature while the open diamond indicates the maximum of the density.

Hybrid Star Mergers with T-dependent EOS *(PRL paper 1)*

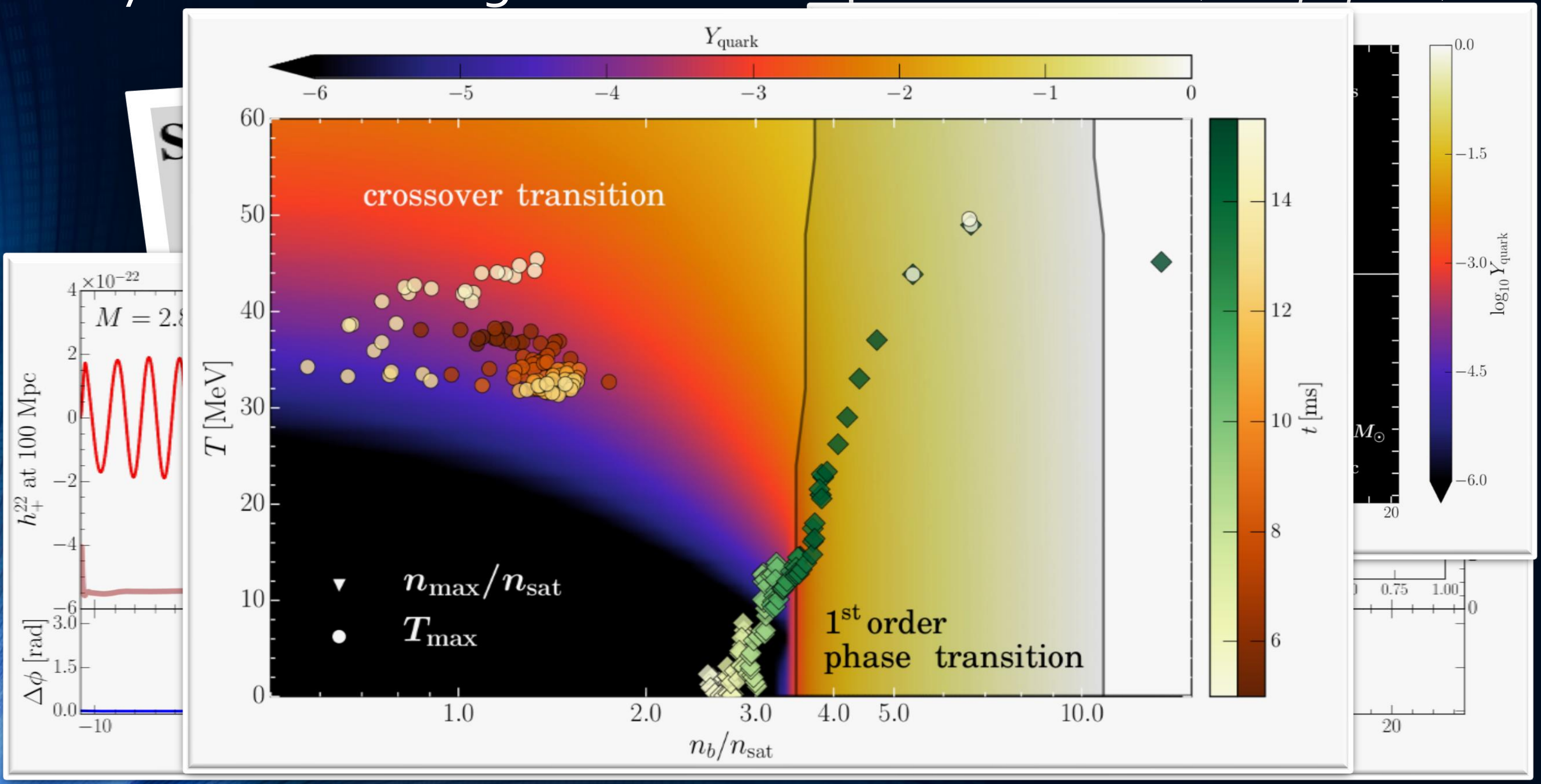

Hybrid Star Mergers with T-dependent EOS *(PRL paper 2)*

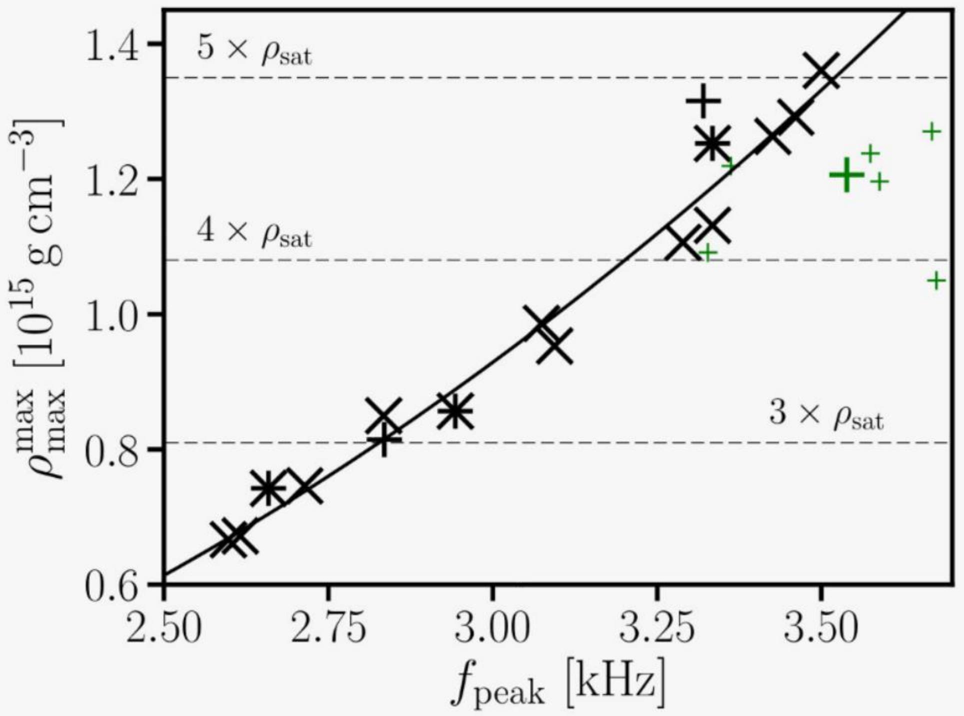

FIG. 4: Maximum rest-mass density ρ_{max}^{max} during the first milliseconds of the postmerger phase as function of the dominant postmerger GW frequency f_{peak} for 1.35-1.35 $M_\odot$ mergers. Green symbols display results for DD2F-SF (big symbol for DD2F-SF-1). Asterisks indicate models with hyperons. Black plus signs display ALF2/4. Solid curve is a second order polynomial least square fit to the data excluding hybrid EOSs.

ximum res
DD2F (b
ontal dot
hase trans

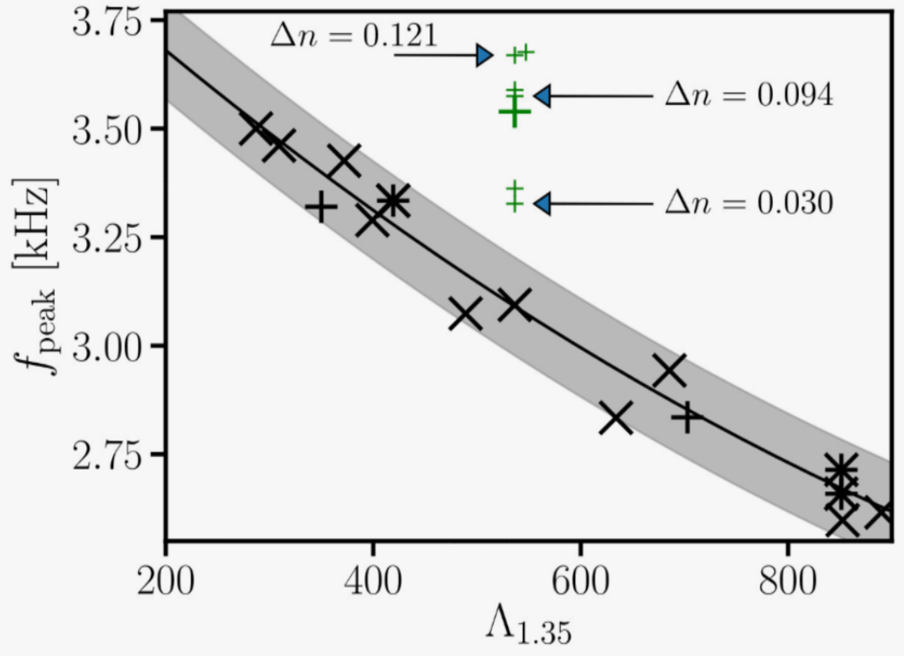

FIG. 3: Dominant postmerger GW frequency f_{peak} as function of tidal deformability Λ for 1.35-1.35 $M_\odot$ mergers. The DD2F-SF models with a phase transition to deconfined quark matter (green symbols) appear as clear outliers (big symbol for DD2F-SF-1). Solid curve displays the least square fit Eq. (1) for all purely hadronic EOSs (including three models with hyperons marked by asterisks). ALF2 and ALF4 are marked by black plus signs. EOSs incompatible with GW170817 are not shown. Arrows mark DD2F-SF models 3, 6 and 7, which feature differently strong density jumps Δn (in fm^{-3}) with roughly the same onset density and stiffness of quark matter.

GW170817: Constraining the maximum mass of Neutron Stars

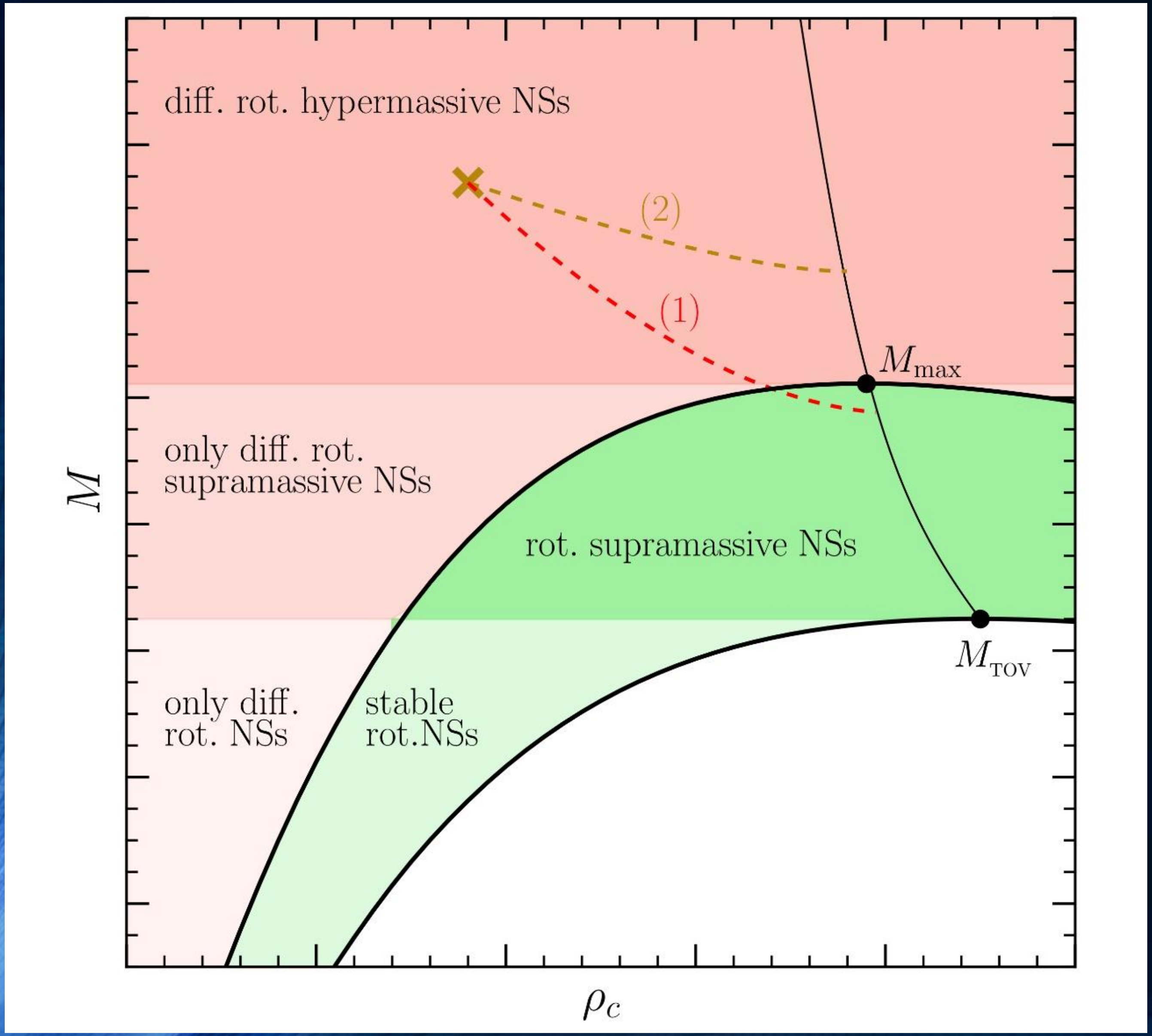

The highly differentially rotating hypermassive/supramassive neutron star will spin down and redistribute its angular momentum (e.g. due to viscosity effects, magnetic braking). After ~1 second it will cross the stability line as a uniformly rotating supramassive neutron star (close to M_{max}) and collapse to a black hole. Parts of the ejected matter will fall back into the black hole producing the gamma-ray burst.

L.Rezzolla, E.Most, L.Weih, "Using Gravitational Wave Observations and Quasi-Universal Relations to constrain the maximum Mass of Neutron Stars",The Astrophysical Journal Letters 852, L25 (2018): 2.01 +/-0.04 < M_{TOV} < 2.16 +/-0.17

See also: S.Lawrence et al. ,APJ808,186, 2015
Margalit & Metzger, The Astrophysical Journal Letters 850, L19 (2017): M_{TOV} < 2.17 (90%)
Zhou, Zhou, Li, PRD 97, 083015 (2018)
Ruiz, Shapiro, Tsokaros, PRD 97,021501 (2018)

GW170817: Constraining the Neutron Star Radius and EOS

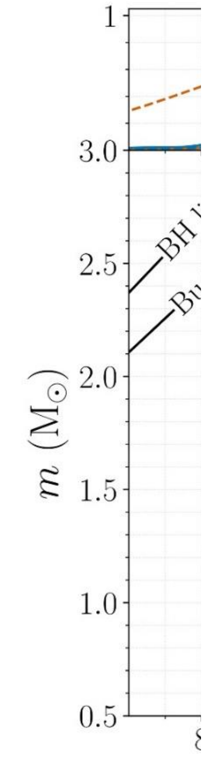

FIG. 3. Margin
and a parametr
posterior corre
the top left der
used for the po
of the 90% cre

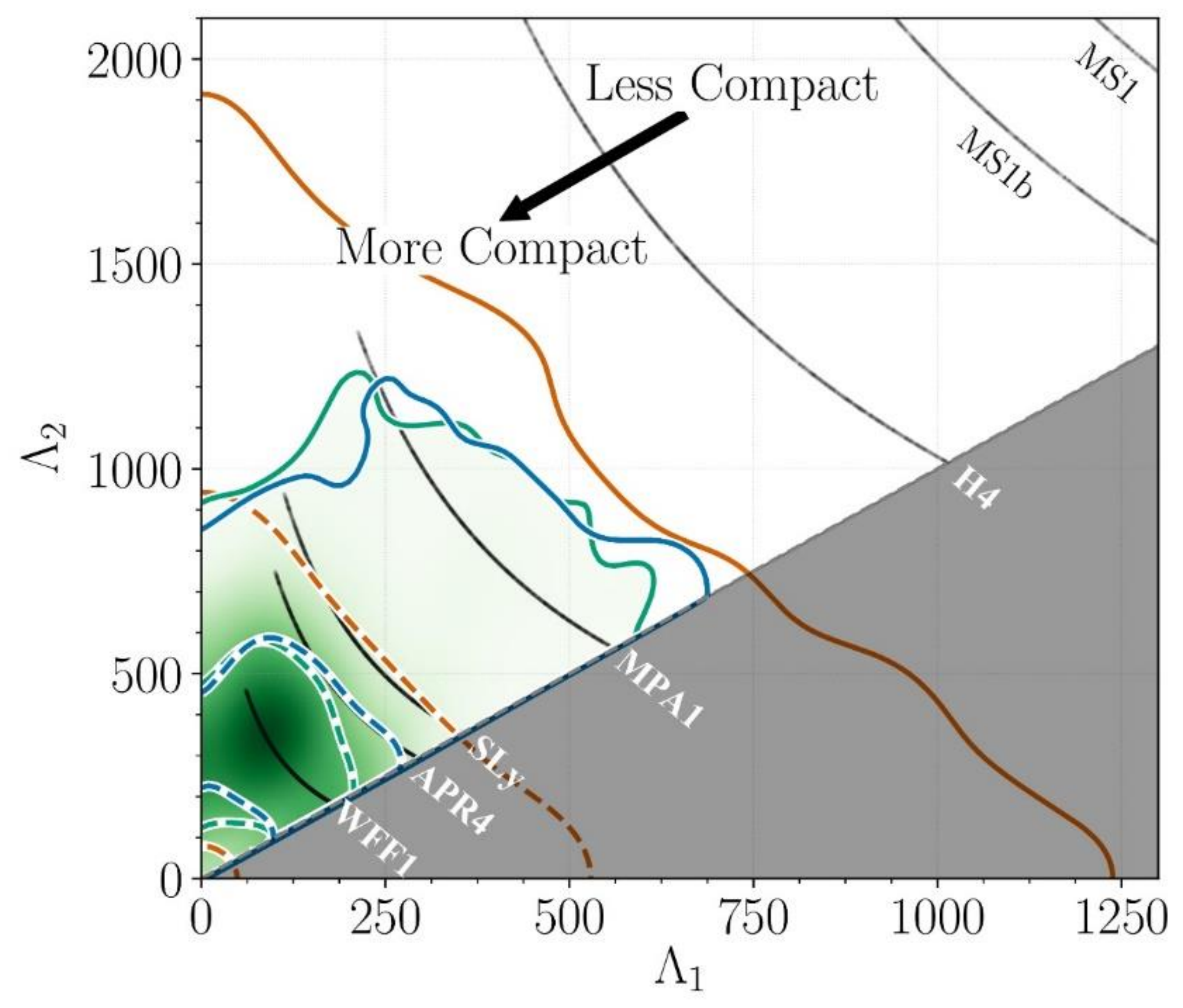

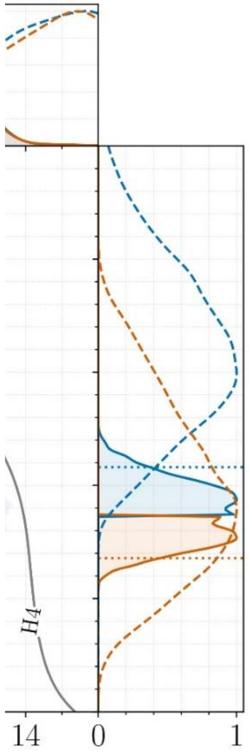

relations (left panel)
lue (bottom orange)
n grey. The lines in
plots, solid lines are
used for the bounds

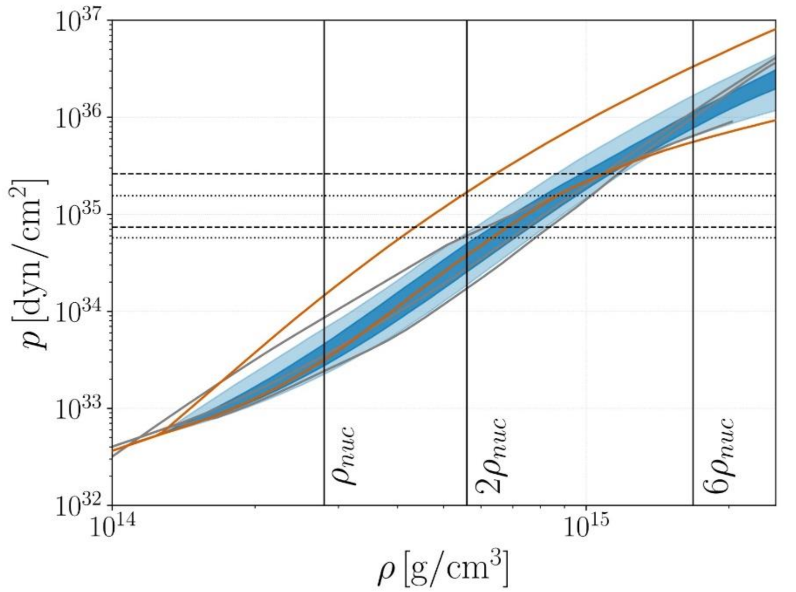

FIG. 2. Marginalized posterior (blue) and prior (orange) for the pressure p as a function of the rest-mass density ρ of the NS interior using the spectral EOS parametrization and imposing a lower limit on the maximum NS mass supported by the EOS of 1.97 $M_\odot$. The dark (light) blue shaded region corresponds to the 50% (90%) posterior credible level and the orange lines show the 90% prior credible interval. Horizontal lines denote the 90% credible interval for the central pressure of the heavier (dashed) and the lighter (dotted) binary components. Vertical lines correspond to once, twice, and six times the nuclear saturation density. Overplotted in grey are representative EOS models [121, 122, 124], using data taken from [19]; from top to bottom at $2\rho_{\rm nuc}$ we show H4, APR4, and WFF1.

GW170817: Measurements of neutron star radii and equation of state, *The LIGO /Virgo Collaboration*, arXiv:1805.11581v1

GW170817: [partially hidden] us

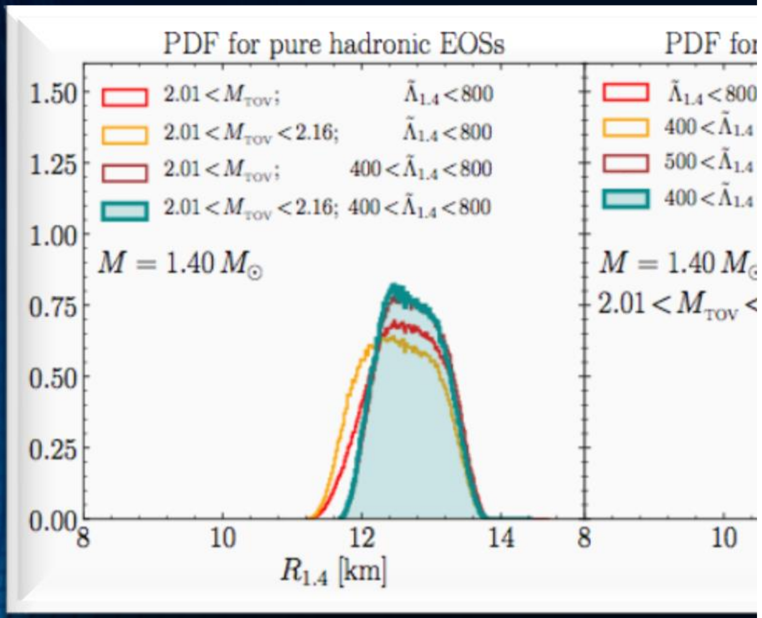

Reference	R_i [km]
Without a phase transition	
Bauswein et al. [42]	$10.68^{+0.15}_{-0.03} \leq R_{1.6}$
Most et al. [51]	$12.00 \leq R_{1.4} \leq 13.45$
Burgio et al. [54]	$11.8 \leq R_{1.5} \leq 13.1$
Tews et al. [55]	$11.3 \leq R_{1.4} \leq 13.6$
De et al. [56]	$8.9 \leq R_{1.4} \leq 13.2$
LIGO/Virgo [57]	$10.5 \leq R_{1.4} \leq 13.3$
With a phase transition	
Annala et al. [46]	$R_{1.4} \leq 13.6$
Most et al. [51]	$8.53 \leq R_{1.4} \leq 13.74$
Burgio et al. [54]	$R_{1.5} = 10.7$
Tews et al. [55]	$9.0 \leq R_{1.4} \leq 13.6$
This work	
NS	$R_{1.4} = 13.11$
HS `Model-2`	$12.9 \leq R_{1.4} \leq 13.11$
HS_T `Model-1`	$10.1 \leq R_{1.4} \leq 12.9$
HS_T `Model-2`	$10.4 \leq R_{1.4} \leq 11.9$

TABLE II. Constraints on the radius of neutron stars from GW170817 for models without a phase transition (top), works considering the possibility of a transition to quark matter (middle) and for EOSs of *Category III* in the present work (bottom).

$$12.00 < R_{1.4}/\text{km} < 13.45$$

$$8.53 < R_{1.4}/\text{km} < 13.74 \quad \bar{R}$$

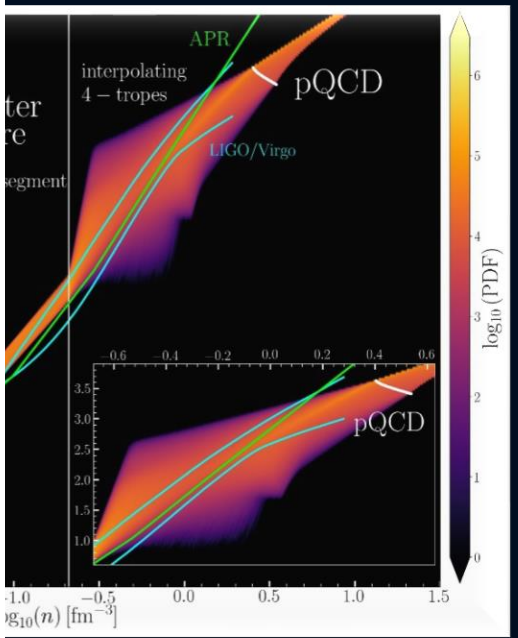

t, L.Weih, L.Rezzolla, J. fner-Bielich "New aints on radii and tidal mabilities of neutron rom GW170817", 1803.00549, pted in PRL)

See also: De, Finstad, Lattimer, Brown, Berger, Biwe… 172702 (2018) ; Nandi & Char, Astrophys. J. 857, 12 (201… Annala, Gorda, Kurkela, Vuorinen, PRL 120, 172703 (201… …v, Piekarewicz, Horowitz, PRL 120, …ros, PRD 97, 021501 (2018) ;

The Hadron-Quark Phase Transition and the Third Family of Compact Stars (Twin Stars)

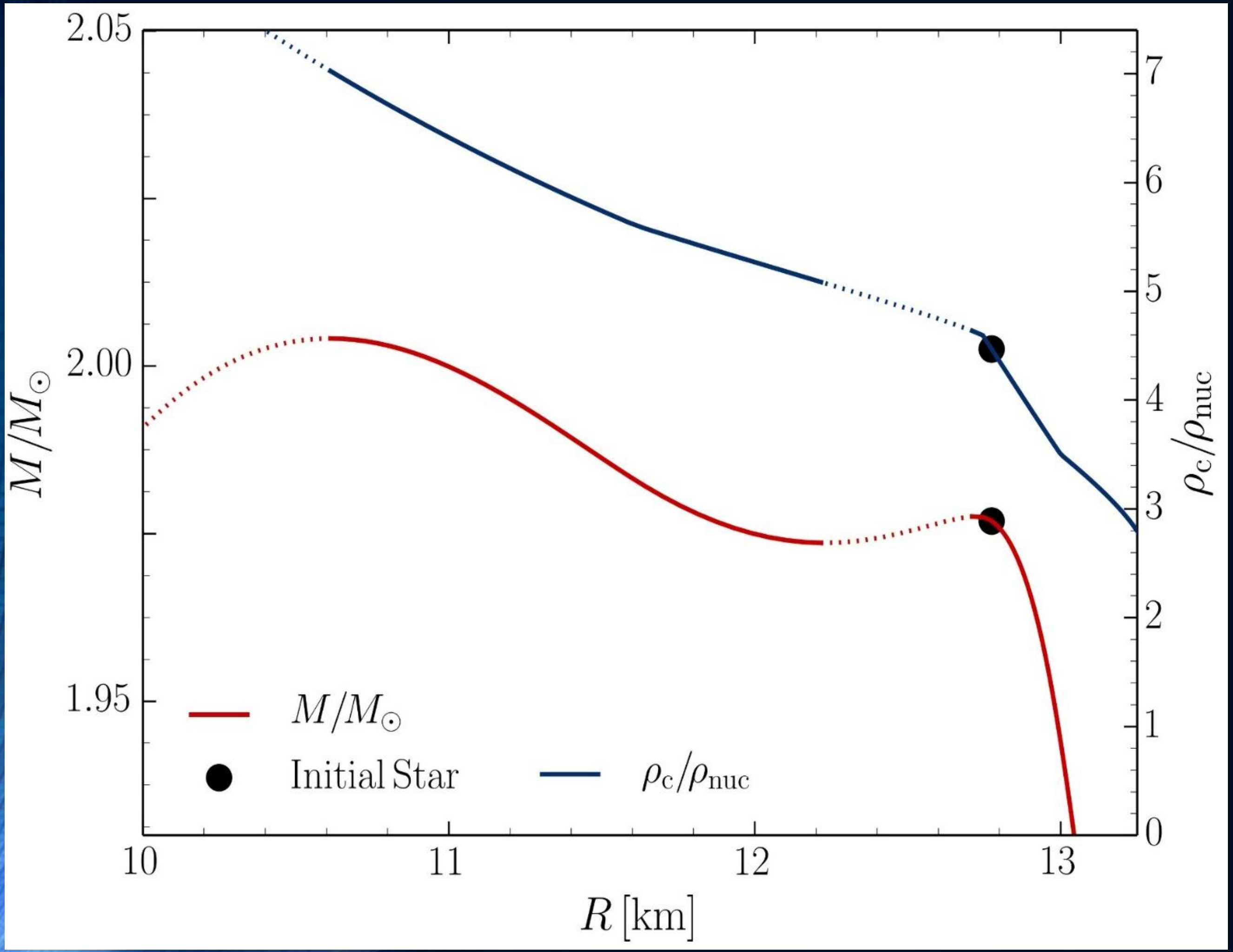

Glendenning, N. K., & Kettner, C. (1998). Nonidentical neutron star twins. Astron. Astrophys., 353(LBL-42080), L9.

Sarmistha Banik, Matthias Hanauske, Debades Bandyopadhyay and Walter Greiner, Rotating compact stars with exotic matter, Phys.Rev.D 70 (2004) p.12304

I.N. Mishustin, M. Hanauske, A. Bhattacharyya, L.M. Satarov, H. Stöcker, and W. Greiner, Catastrophic rearrangement of a compact star due to quark core formation, Physics Letters B 552 (2003) p.1-8

M.Alford and A. Sedrakian, Compact stars with sequential QCD phase transitions. Physical review letters, 119(16), 161104 (2017)..

D.Alvarez-Castillo and D.Blaschke, High-mass twin stars with a multipolytrope equation of state. Physical Review C, 96(4), 045809 (2017) .

A. Ayriyan, N.-U. Bastian, D. Blaschke, H. Grigorian, K. Maslov, D. N. Voskresensky, How robust is a third family of compact stars against pasta phase effects?, arXiv:1711.03926 [nucl-th]

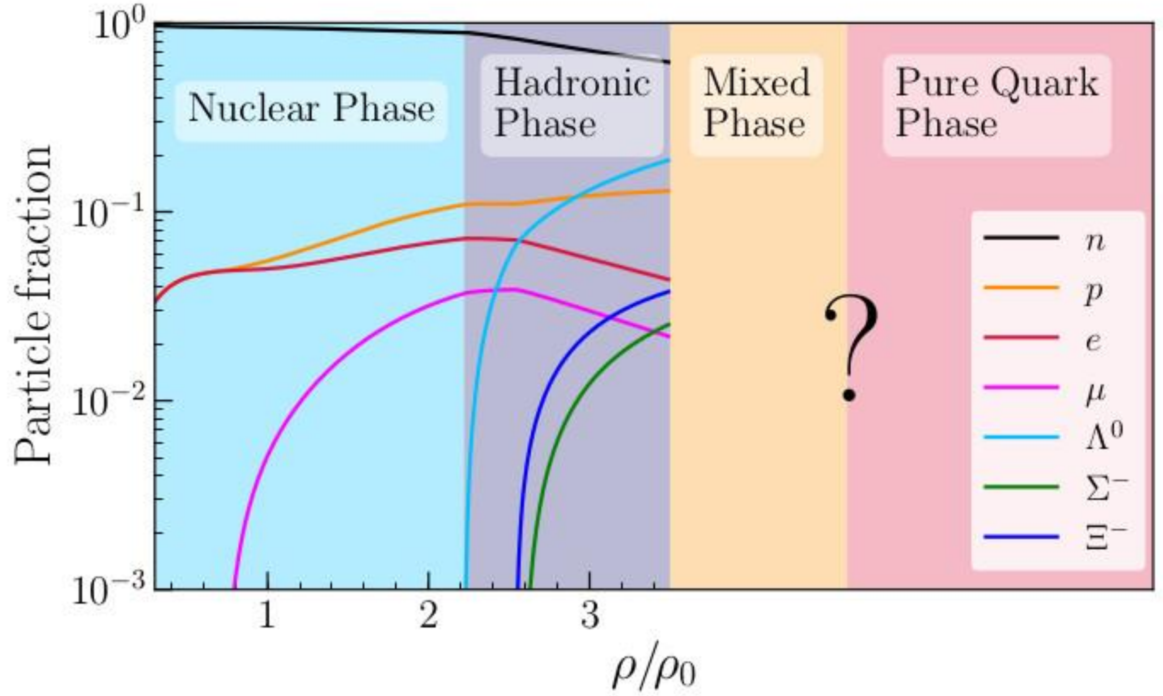

FIG. 1. Particle fractions as functions of the baryonic density for the FSU2H model [69, 70] up to the point where the HQPT is implemented, giving rise to a phase of deconfined quark matter which can be separated from the nuclear (or hadronic) phase by a mixed phase of hadrons and quarks. We note that the actual fractions of nucleons/hyperons and quarks u, d, s in the mixed and quark phases cannot be determined with the parametrizations used in this work.

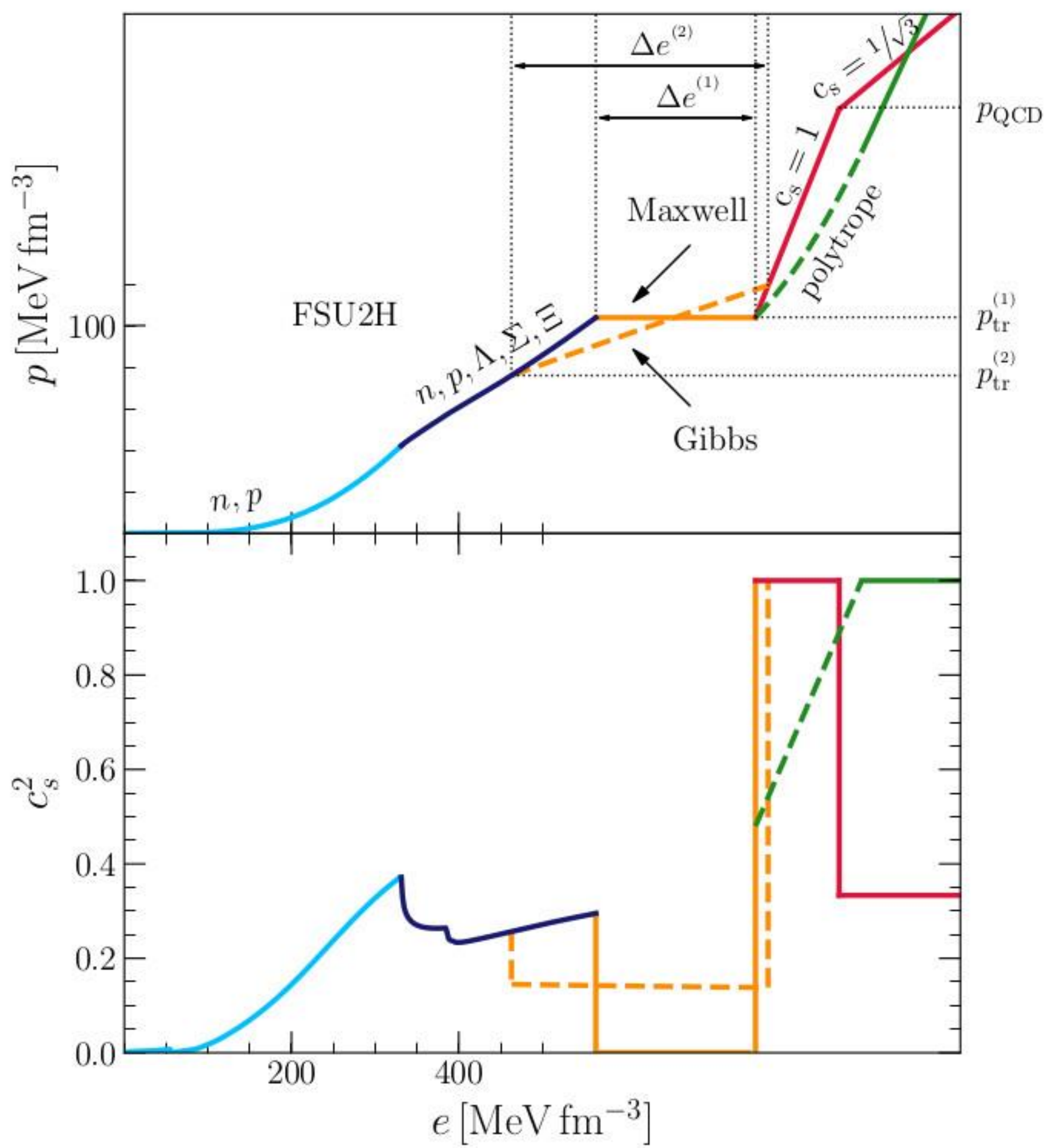

Mass-Radius Relations for Twin-Star EOSs

The mass and radius of a single, non-rotating and spherically symmetric neutron star can be easily calculated by solving the static TOV equation numerically for a given EOS.

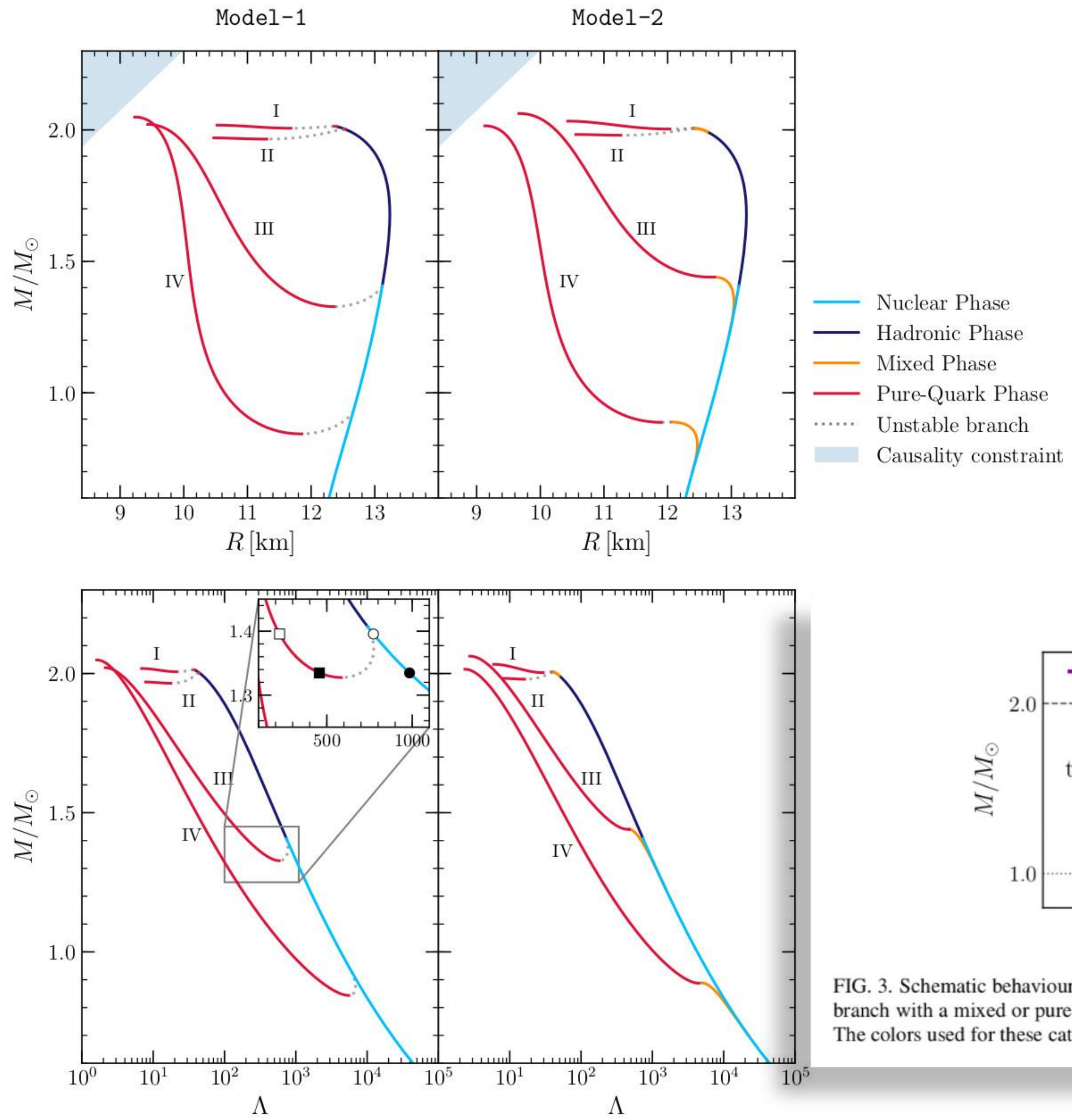

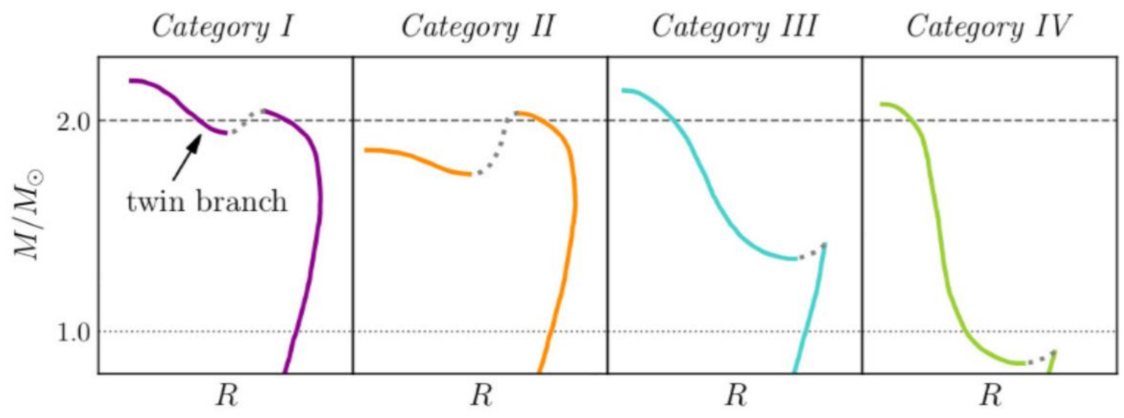

FIG. 3. Schematic behaviour of the mass–radius relation for the twin-star categories *I–IV* defined in the text. Note the appearance of a “twin” branch with a mixed or pure-quark phase; the twin branch has systematically smaller radii than the branch with a nuclear or hadronic phase. The colors used for these categories will be employed also in the subsequent figures.

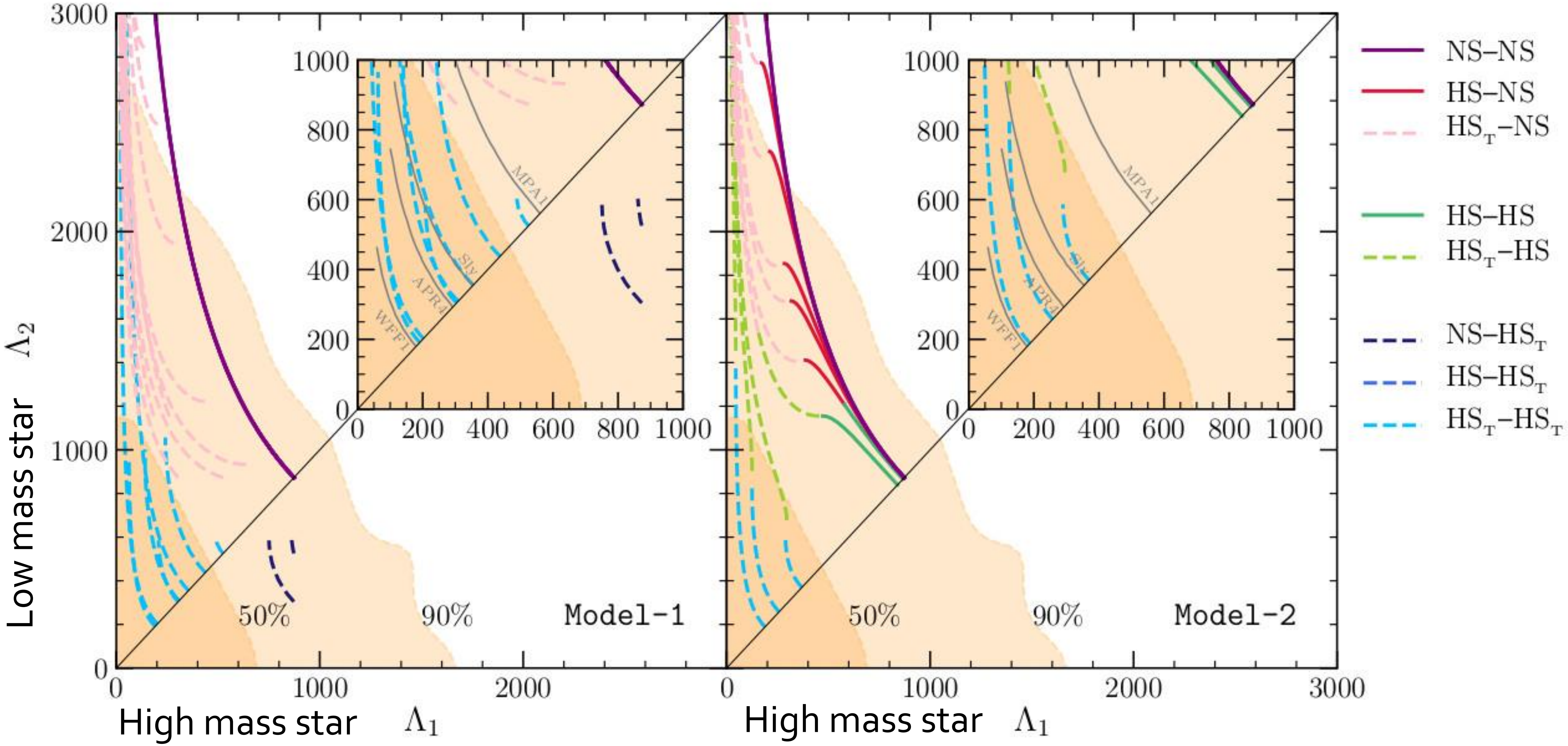

In a binary hybrid star merger the two masses of the individual stars can be different (q<1). As a result, the tidal deformability and the stars composition can be different. In this plot the total mass of the binary system has been fixed to the measured chirp mass of GW170817 (M=1.188 M_{solar}) and the different curve show results for EOSs of Category III.

Constraining the global parameters of the phase transition with GW170817

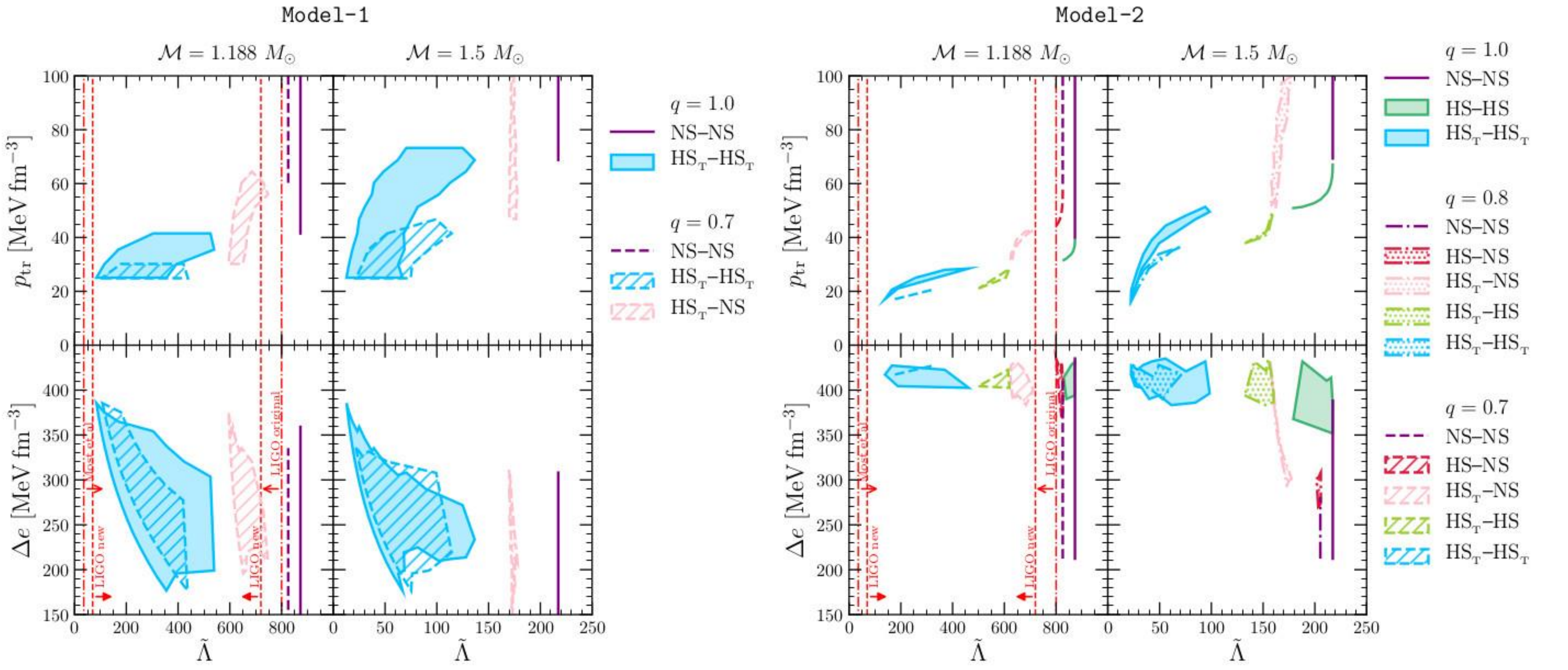

Literature

Hanauske, Matthias, and Walter Greiner. "Neutron star properties in a QCD-motivated model." *General Relativity and Gravitation* 33.5 (2001): 739-755.

Hanauske, Matthias. "How to detect the Quark-Gluon Plasma with Telescopes." *GSI Annual Report* (2003): 96.

Hanauske, M., Takami, K., Bovard, L., Rezzolla, L., Font, J. A., Galeazzi, F., & Stöcker, H. (2017). Rotational properties of hypermassive neutron stars from binary mergers. Physical Review D, 96(4), 043004

M. Hanauske, et.al., Connecting Relativistic Heavy Ion Collisions and Neutron Star Mergers by the Equation of State of Dense Hadron-and Quark Matter as signalled by Gravitational Waves, Journal of Physics: Conference Series, 878(1), p.012031 (2017)

Hanauske, Matthias, et al. "Gravitational waves from binary compact star mergers in the context of strange matter." *EPJ Web of Conferences*. Vol. 171. EDP Sciences, 2018.

Mark G. Alford, Luke Bovard, Matthias Hanauske, Luciano Rezzolla, and Kai Schwenzer (2018), Viscous Dissipation and Heat Conduction in Binary Neutron-Star Mergers. Phys. Rev. Lett. 120, 041101

Hanauske, Matthias, and Luke Bovard. "Neutron star mergers in the context of the hadron–quark phase transition." *Journal of Astrophysics and Astronomy* 39.4 (2018): 45.

Hanauske, Matthias, et al. "Neutron Star Mergers: Probing the EoS of Hot, Dense Matter by Gravitational Waves." *Particles* 2.1 (2019): 44-56.

Credits to ...

Kentaro Takami, Luke Bovard, Jose Font, Filippo Galeazzi, Jens Papenfort, Lukas Weih, Elias Most, Cosima Breu, Federico Guercilena, Natascha Wechselberger, Zekiye Simay Yilmaz, Christina Mitropoulos, Jan Steinheimer, Stefan Schramm, David Blaschke, Mark Alford, Kai Schwenzer, Antonios Nathanail, Roman Gold, Alejandro Cruz Osorio, Andreas Zacchi, Jürgen Schaffner-Bielich, Laura Tolos, Sven Köppel, Gloria Montaña, Michael Rattay, Debades Bandopadhyay,

Walter Greiner *Horst Stöcker* *Luciano Rezzolla*

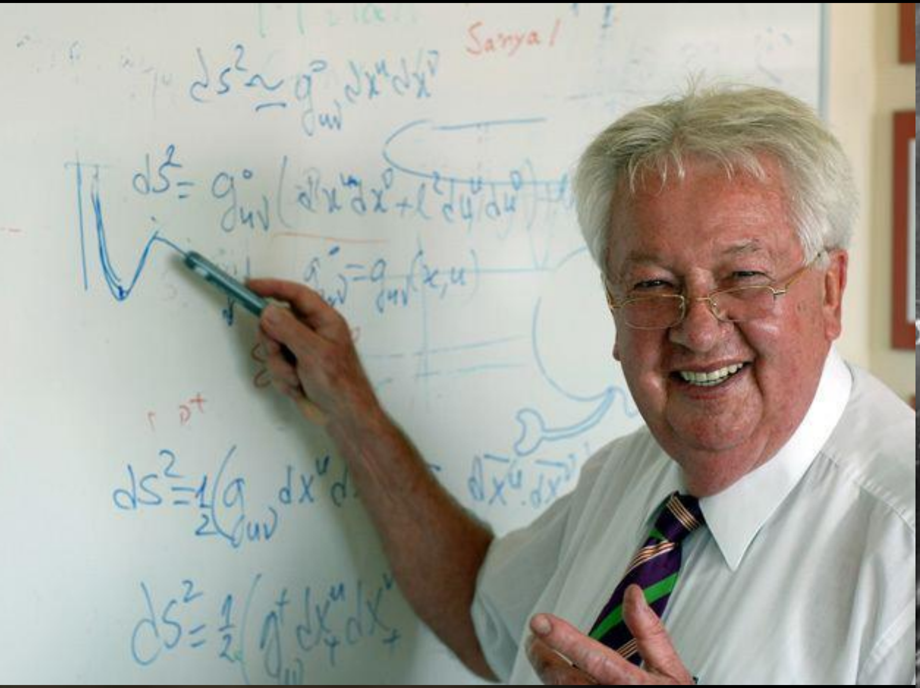
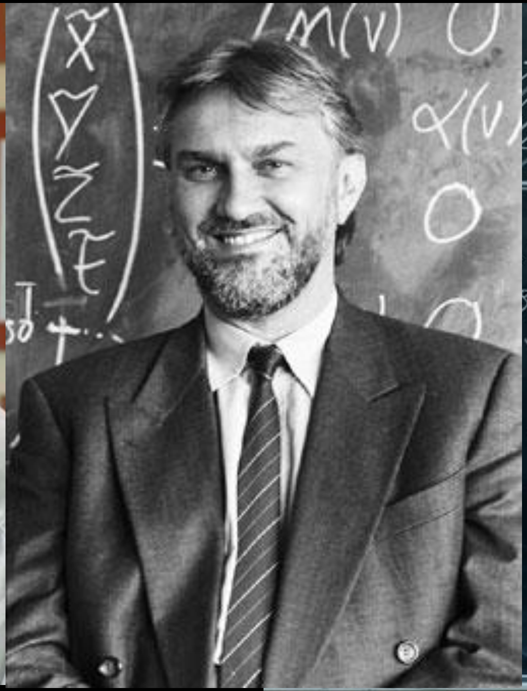
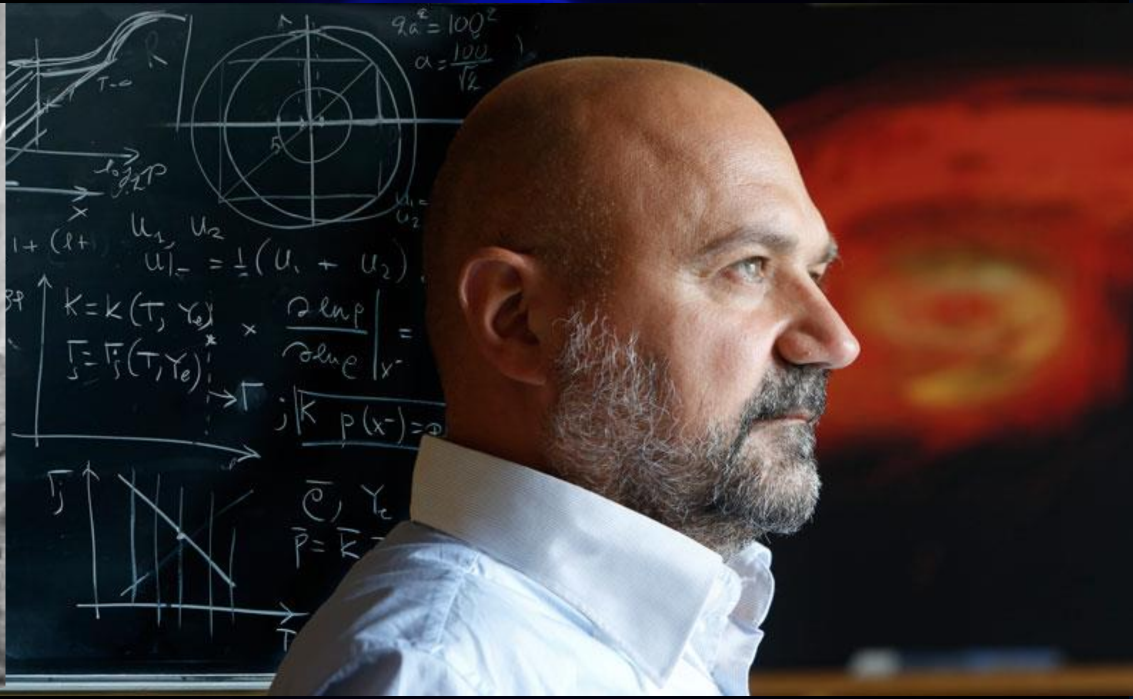

Riedberg TV, Hessisches Kompetenzzentrum für Hochleistungsrechnen und Tanzschule Wernecke

Kamera: *Pablo Rengel Lorena* Schnitt: *Luise Schulte*

Der Tanz der Neutronensterne: Vortrag an der Sternwarte Darmstadt am Sa. 16.02., 20.00 Uhr

Tanz der Neutronensterne

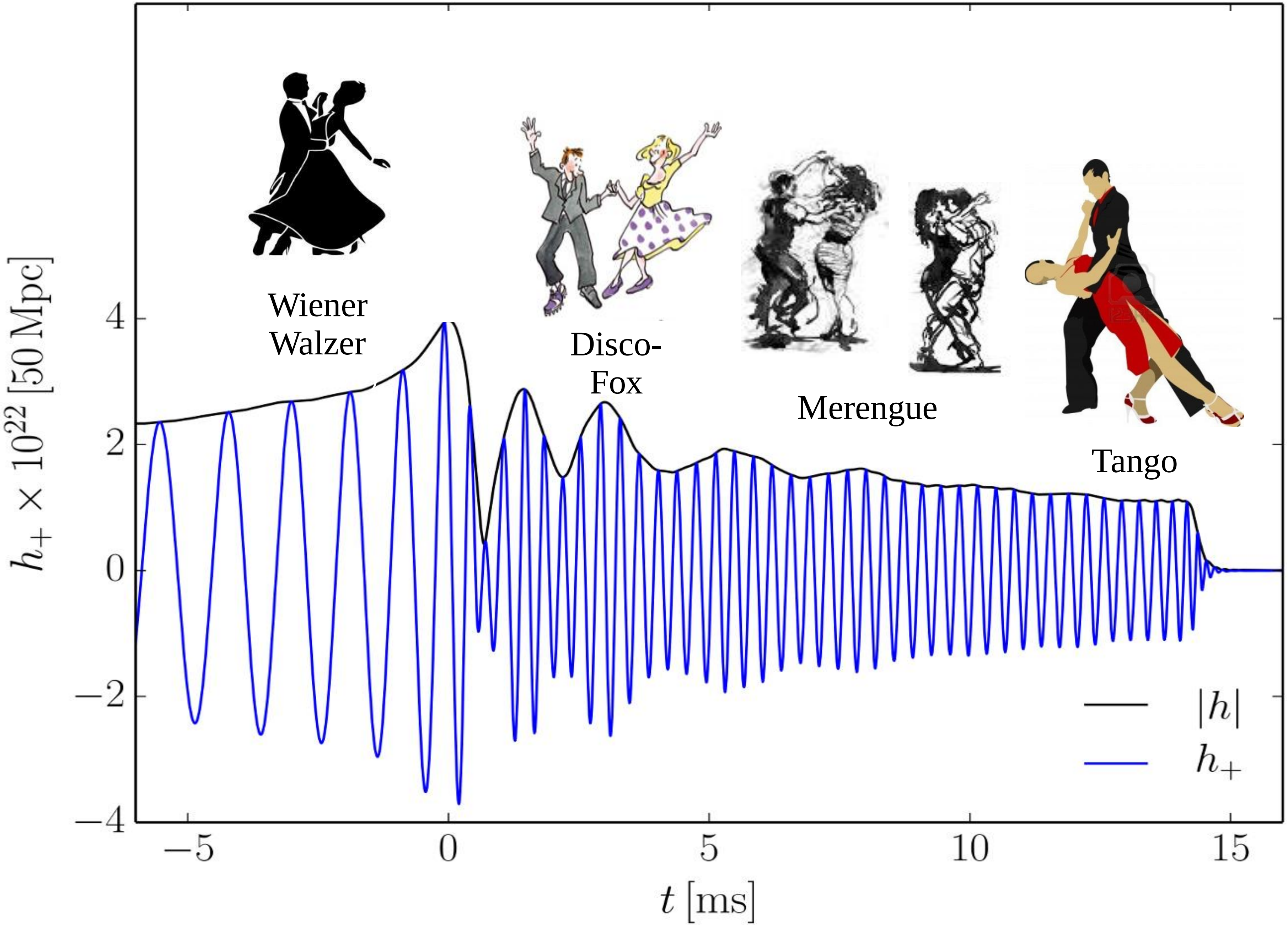

Constraining the mass and radius with GW170817

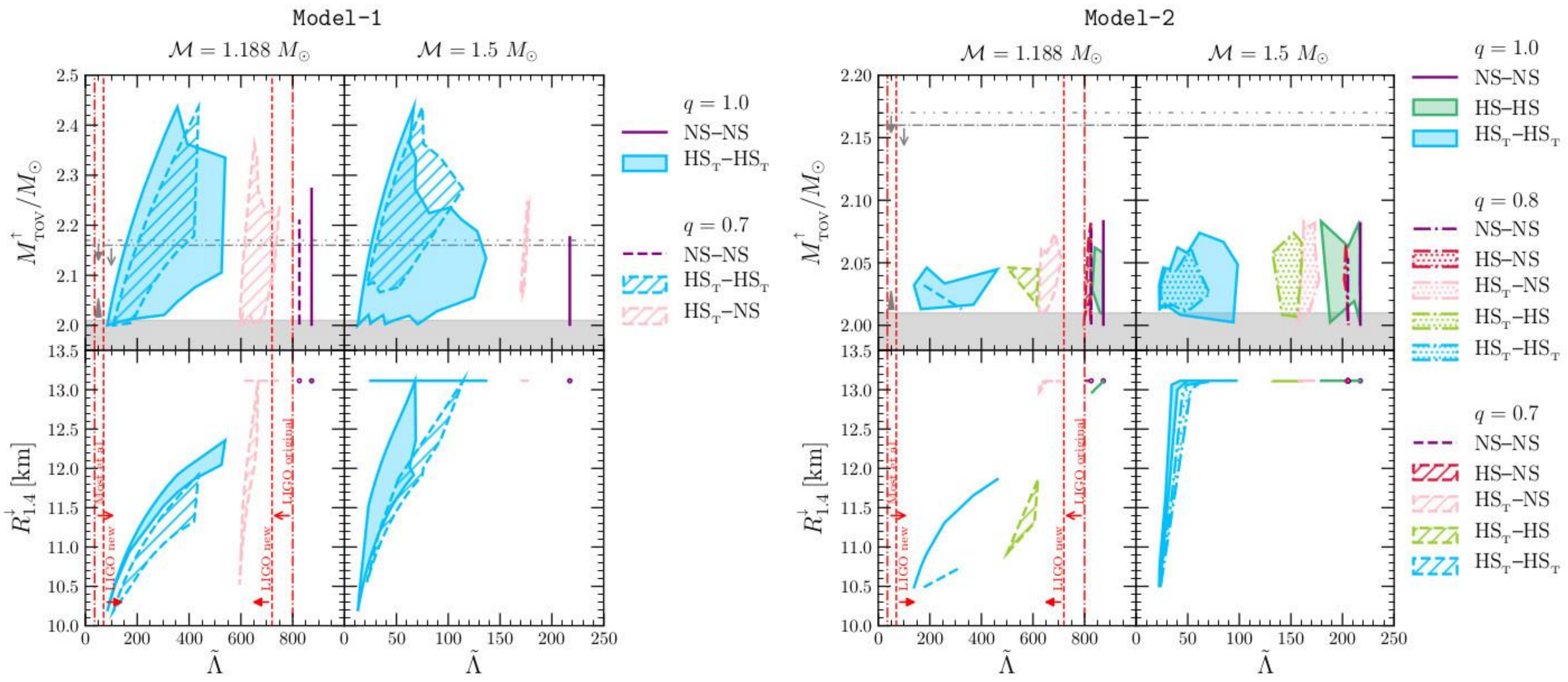

FIG. 10. Left plot: Maximum mass (upper panels) and radius of a $1.4\ M_\odot$ star (lower panels) as a function of the weighted $\tilde{\Lambda}$ for the same cases as in the left plot of Fig. 9. Right plot: Maximum mass (upper panels) and radius of a $1.4\ M_\odot$ star (lower panels) as a function of the weighted $\tilde{\Lambda}$ for the same cases as in the right plot of Fig. 9. In these plots, together with the constraints on tidal deformability, we display a lower horizontal band coming from the lower limit of $2\ M_\odot$ observations [19, 20] as well as recent constraints on the maximum mass of ~ 2.16–$2.17\ M_\odot$ from multi-messenger observations of GW170817 [41, 44].

Density

Temperature

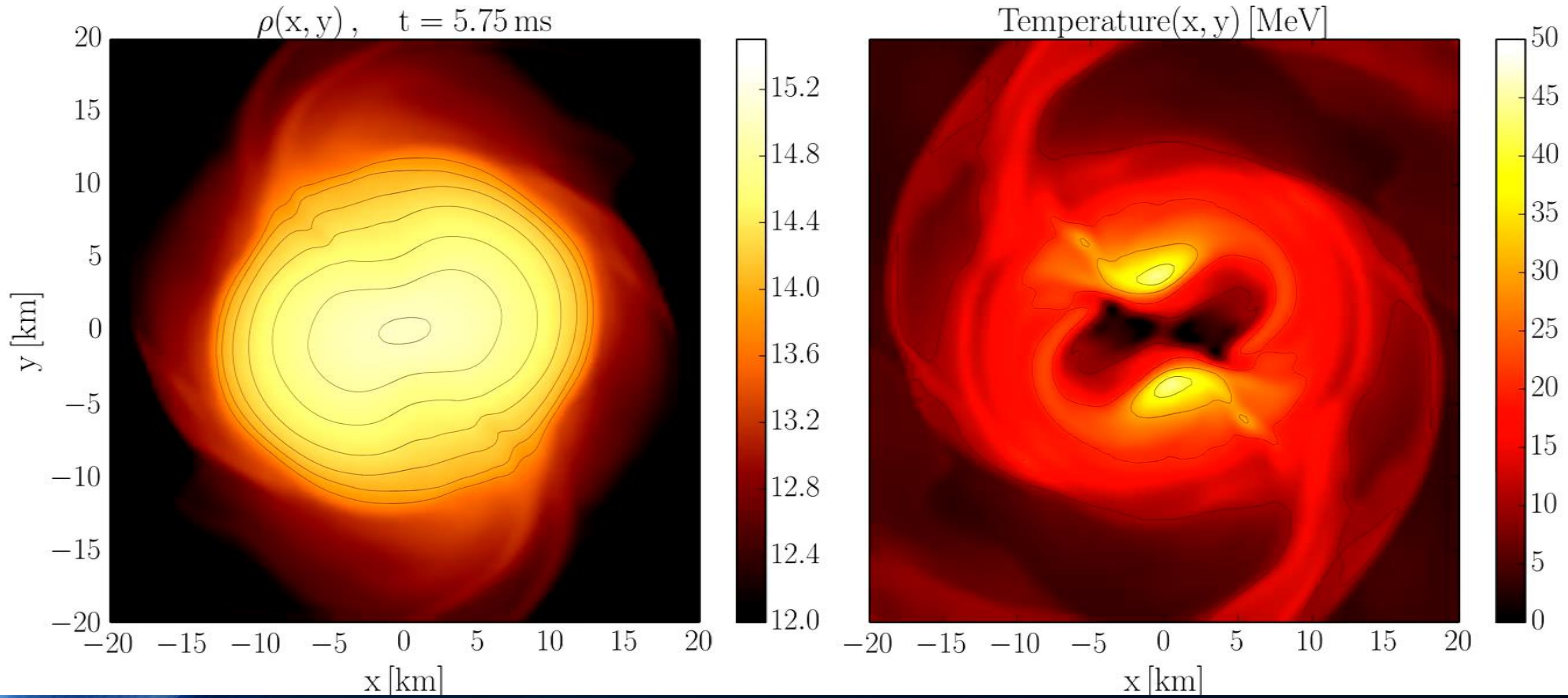

EOS: LS200 , Mass: 1.32 MSolar

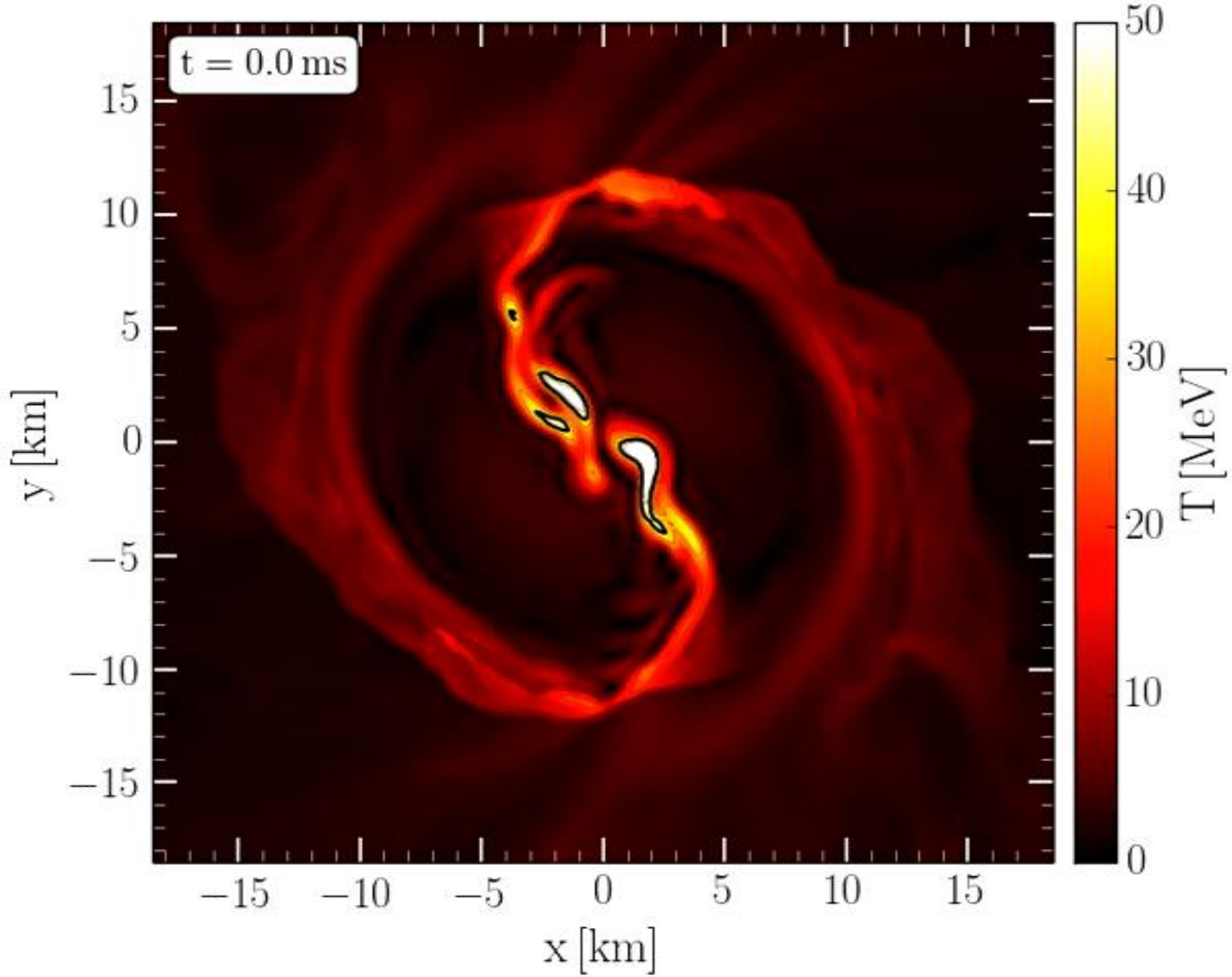

Evolution of the Temperature in the post merger phase

Hanauske, M., Takami, K., Bovard, L., Rezzolla, L., Font, J. A., Galeazzi, F., & Stöcker, H. (2017). Rotational properties of hypermassive neutron stars from binary mergers. Physical Review D, 96(4), 043004

Kastaun, W., Ciolfi, R., Endrizzi, A., & Giacomazzo, B. (2017). Structure of stable binary neutron star merger remnants: Role of initial spin. Physical Review D, 96(4), 043019

M. Hanauske, et.al., Connecting Relativistic Heavy Ion Collisions and Neutron Star Mergers by the Equation of State of Dense Hadron-and Quark Matter as signalled by Gravitational Waves, Journal of Physics: Conference Series, 878(1), p.012031 (2017)

Evolution of Tracer-particles tracking individual fluid elements in the equatorial plane of the HMNS at post-merger times

Mark G. Alford, Luke Bovard, Matthias Hanauske, Luciano Rezzolla, and Kai Schwenzer (2018) Viscous Dissipation and Heat Conduction in Binary Neutron-Star Mergers. Phys. Rev. Lett. 120, 041101

Different rotational behaviour of the quark-gluon-plasma produced in non-central ultra-relativistic heavy ion collisions
L. Adamczyk et.al., "Global Lambda-hyperon polarization in nuclear collisions: evidence for the most vortical fluid", Nature 548, 2017

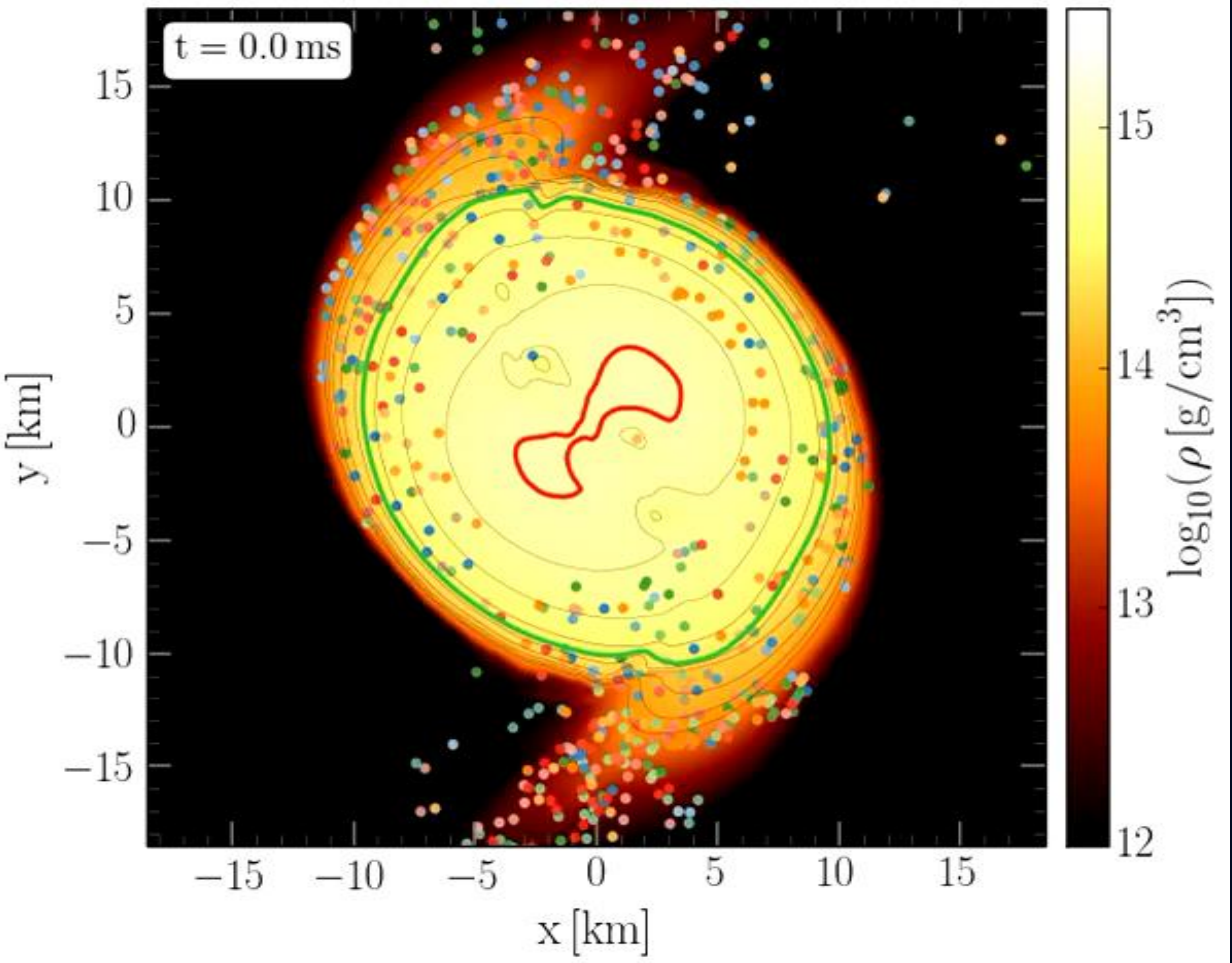

The different Phases during the Postmergerphase of the HMNS

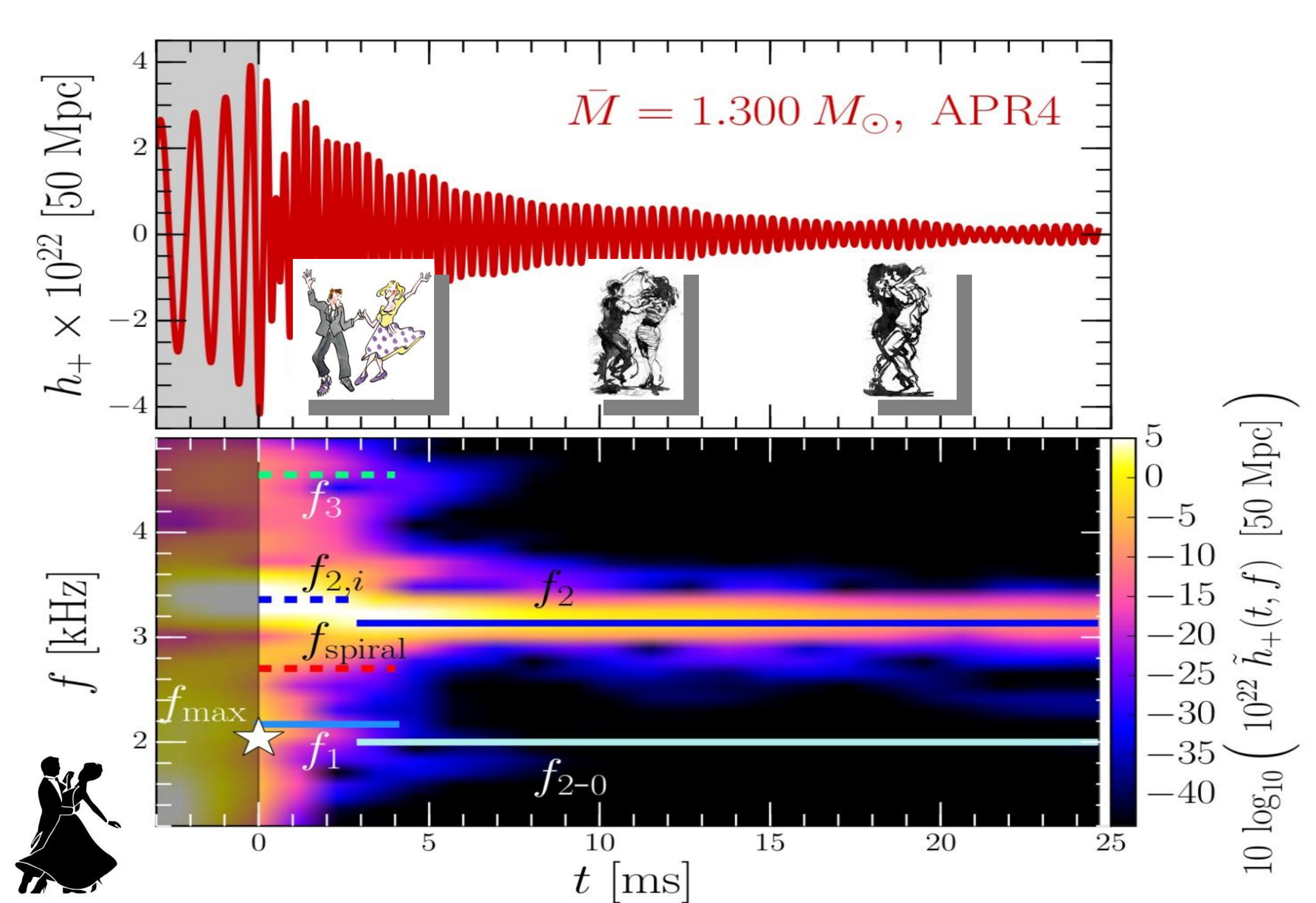

Disco-Fox, Merengue und Tango Phase

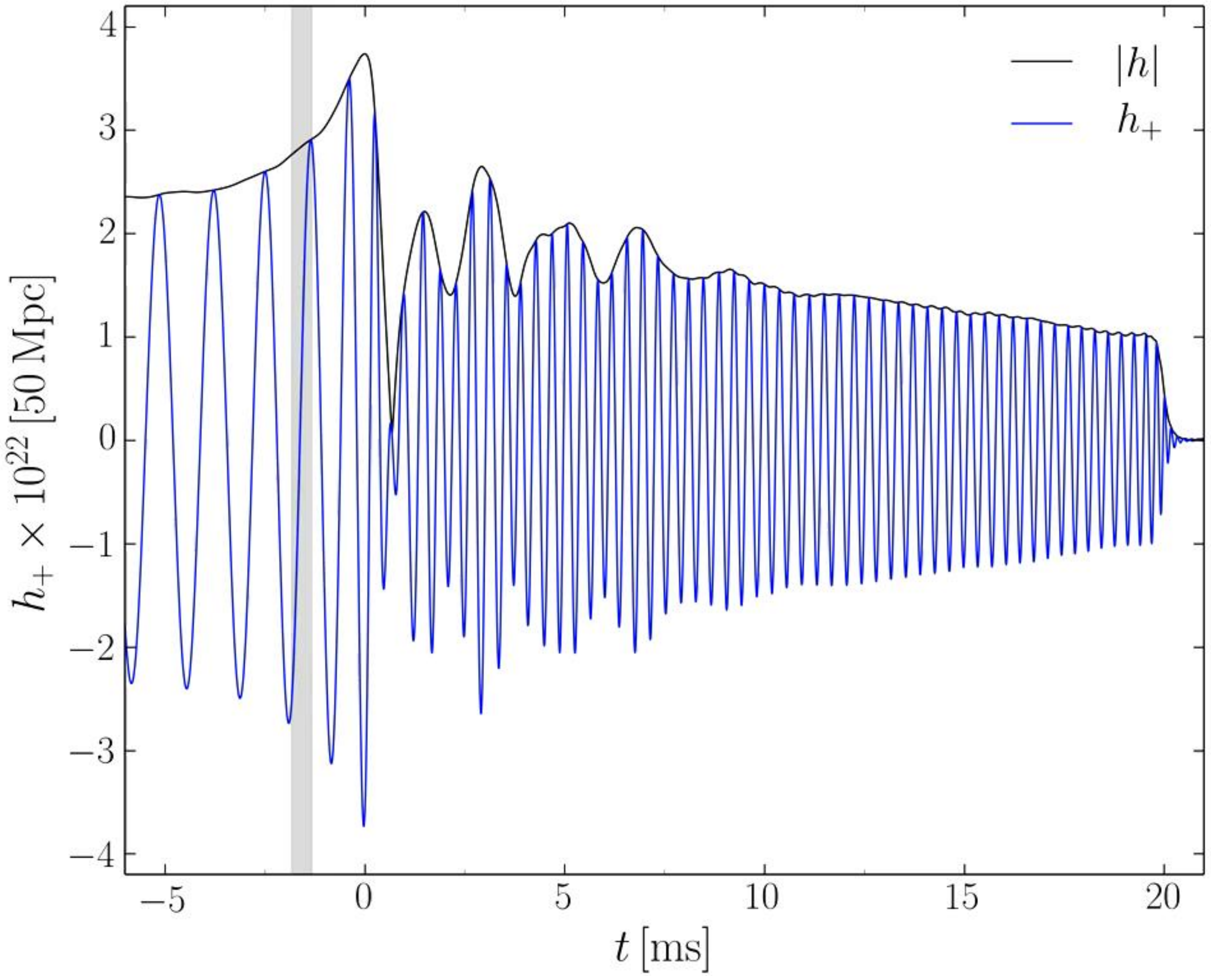

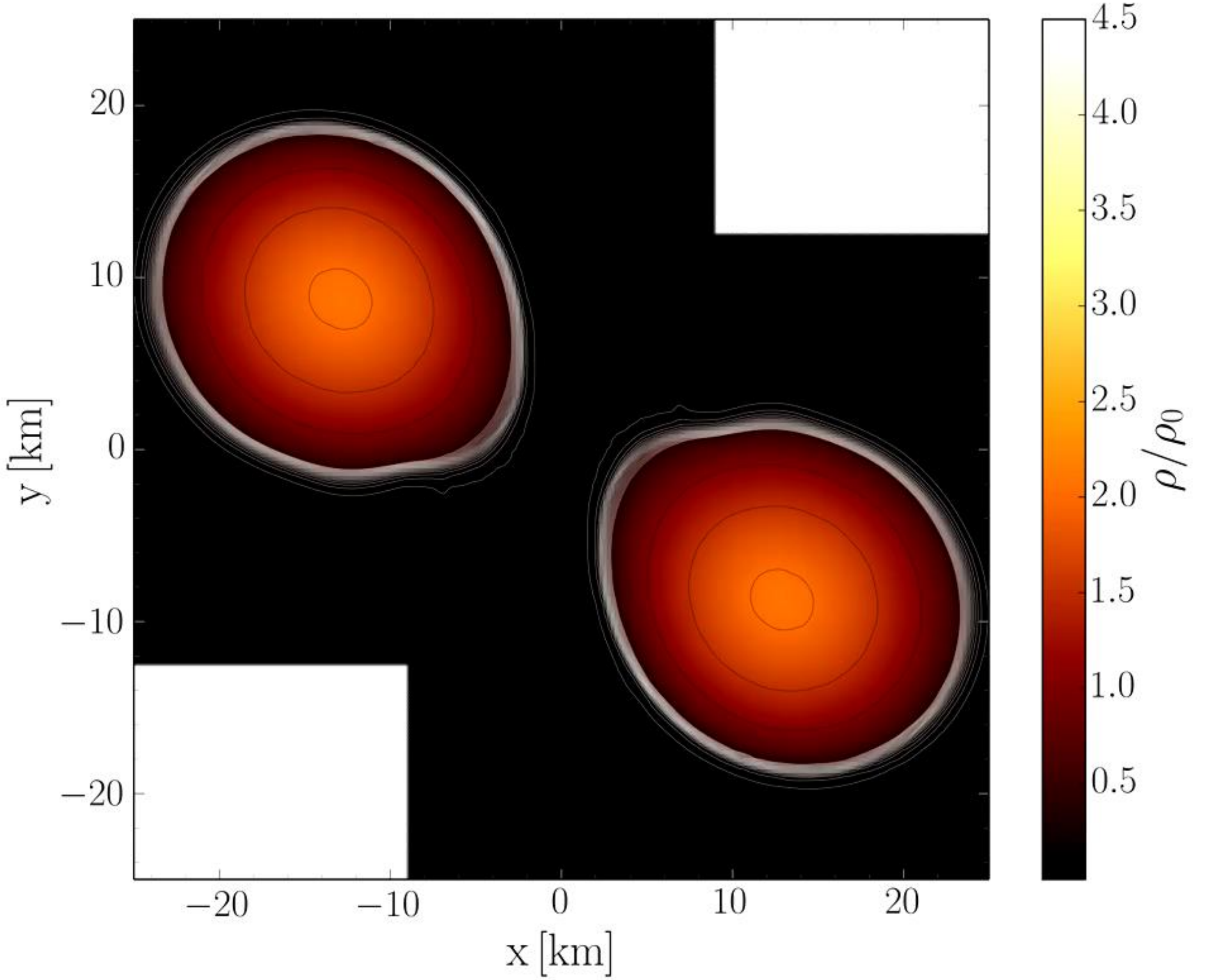

Der Ereignishorizont eines Schwarzen Loches

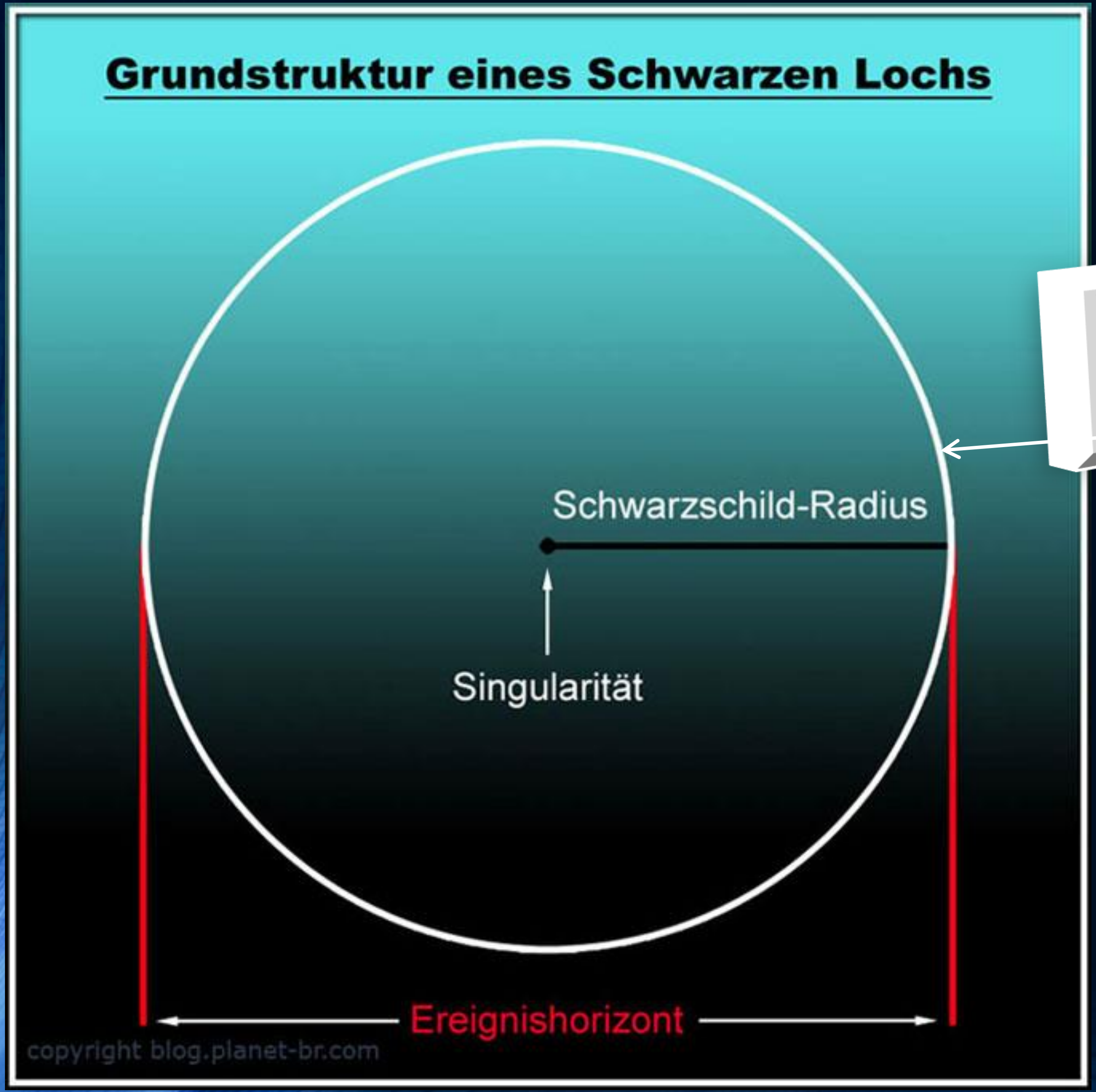

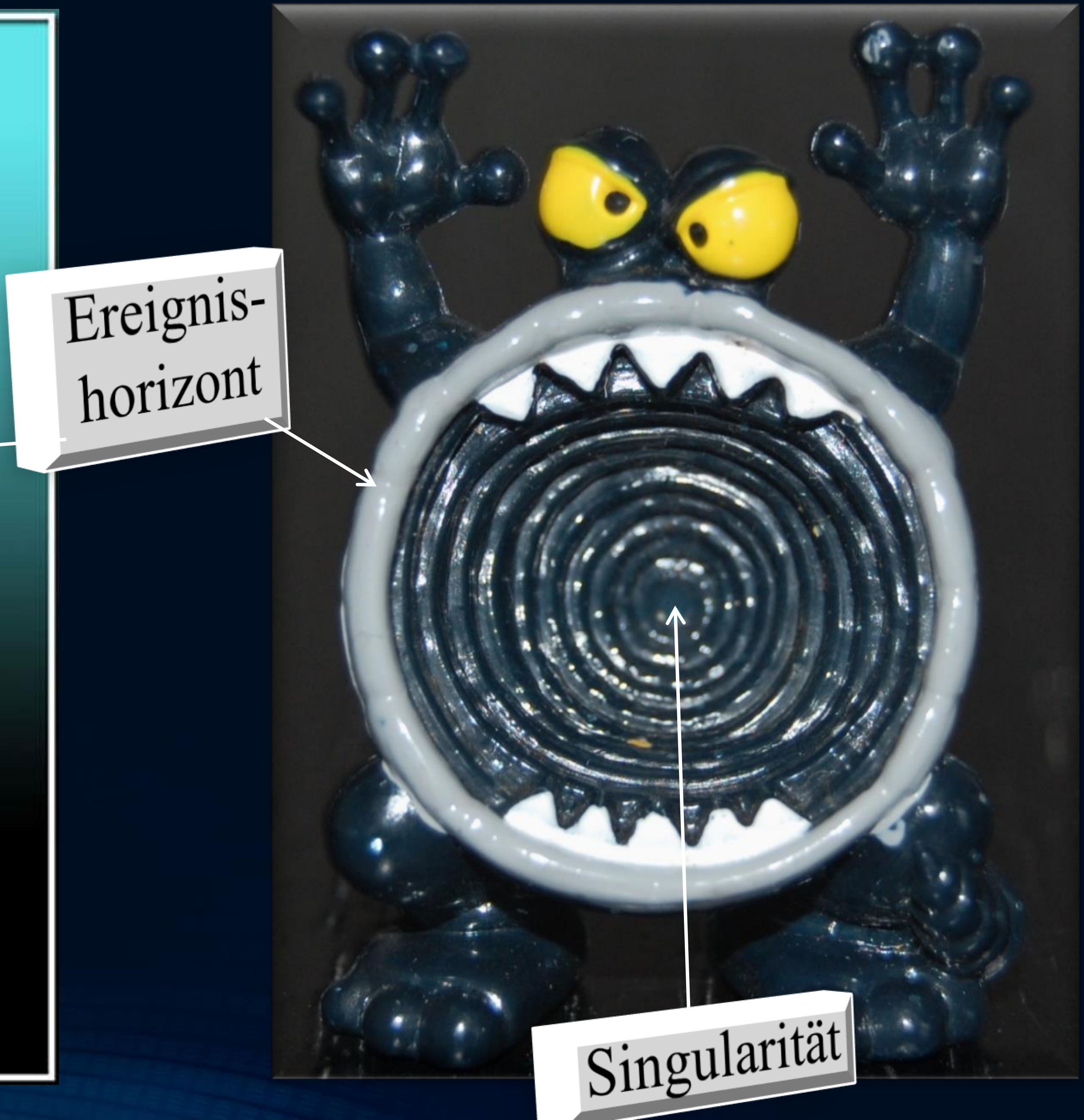

Der deutsche Bundestag in Berlin

Die wohl beste Veranschaulichung eines schwarzen Loches

Der Raumzeit-Tricher
im Reichstagsgebäude

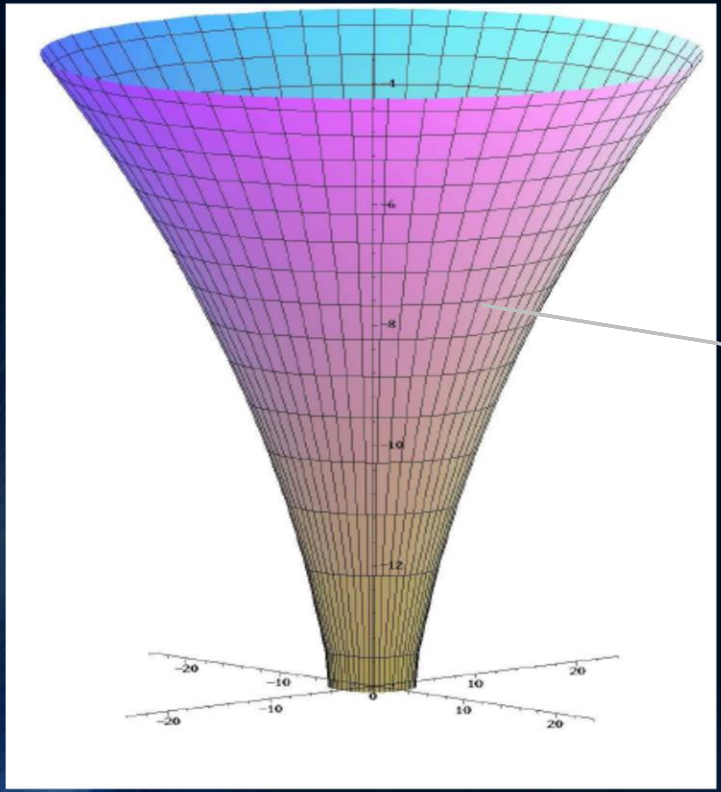

Schwarze Löcher und der deutsche Reichstag

Der deutsche Bundestag in Berlin

Die wohl beste Veranschaulichung eines schwarzen Loches

Computer Simulation einer Kollision zweier Neutronensterne

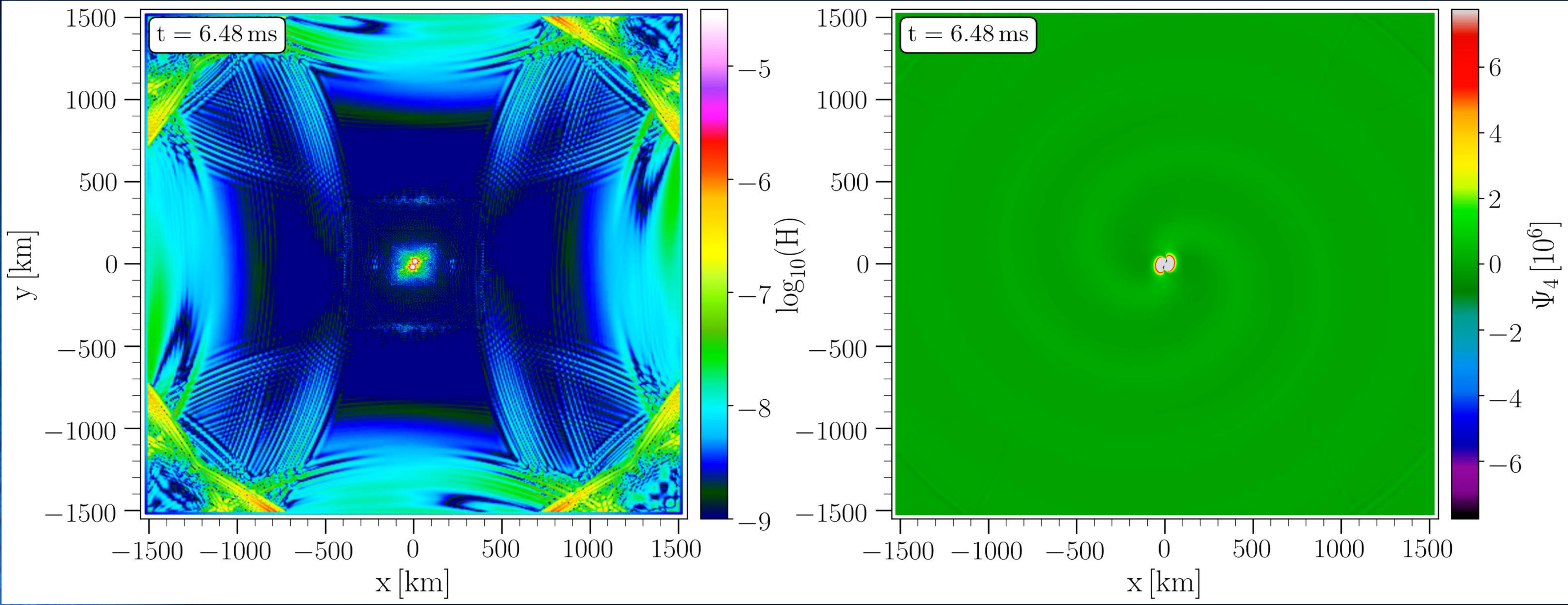

Die Gleichungen der ART werden numerisch auf einem Gitter mittels Hochleistungscomputern simuliert. Durch den Diskretisierungsprozess im Computerprogramms, sind die Nebenbedingungen (Hamilton Constraints) nicht mehr exakt erhalten. Die linke Abbildung zeigt diese Unsicherheiten des Programms. Die rechte Seite zeigt die Simulationsergebnisse der vom binären Neutronenstern System emittierten Gravitationswellen.

Computer Simulation einer Kollision zweier Neutronensterne

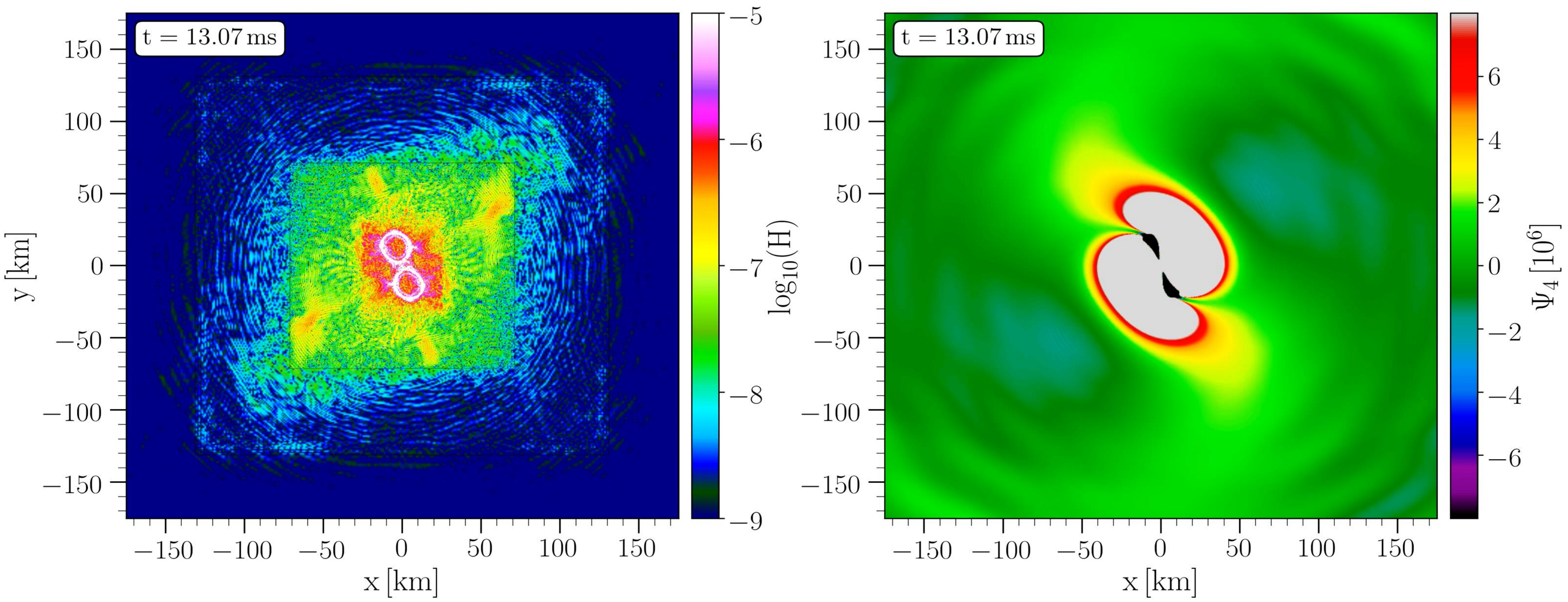

Die Gleichungen der ART werden numerisch auf einem Gitter mittels Hochleistungscomputern simuliert. Durch den Diskretisierungsprozess im Computerprogramms, sind die Nebenbedingungen (Hamilton Constraints) nicht mehr exakt erhalten. Die linke Abbildung zeigt diese Unsicherheiten des Programms. Die rechte Seite zeigt die Simulationsergebnisse der vom binären Neutronenstern System emittierten Gravitationswellen.

Computer Simulation einer Kollision zweier Neutronensterne

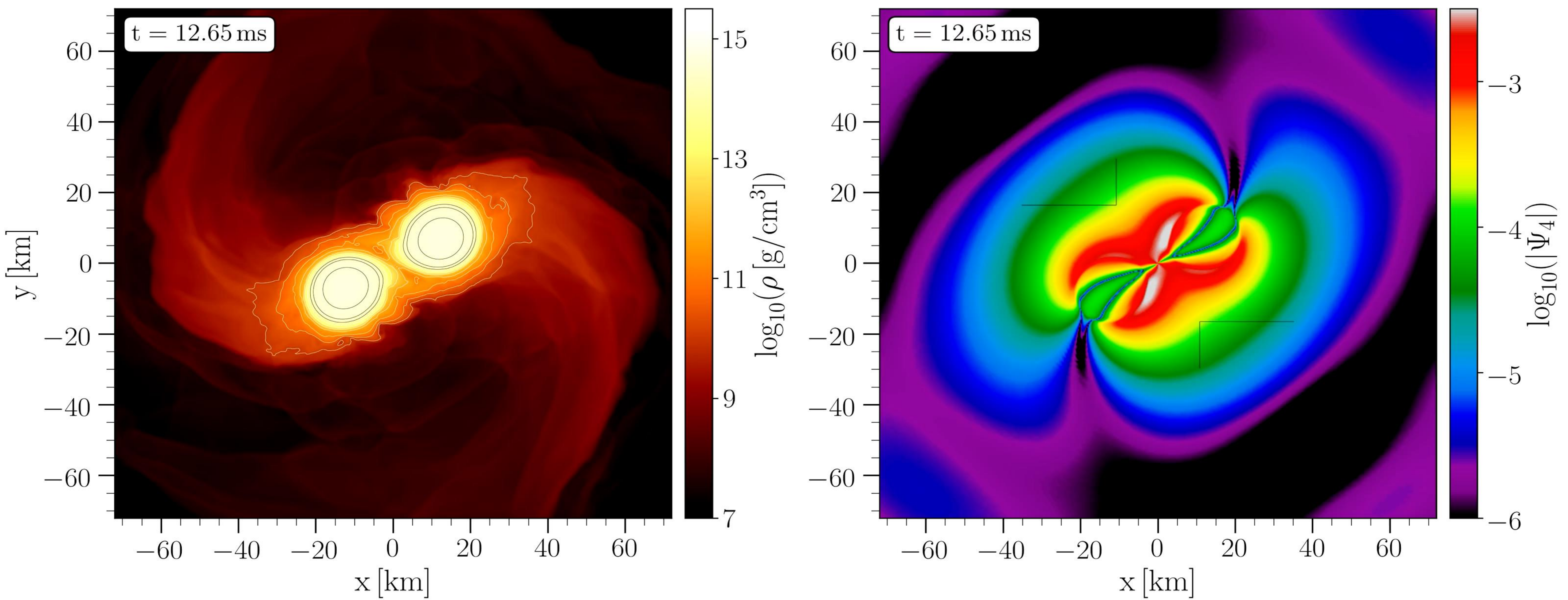

Die Gleichungen der ART werden numerisch auf einem Gitter mittels Hochleistungscomputern simuliert. Durch den Diskretisierungsprozess im Computerprogramms, sind die Nebenbedingungen (Hamilton Constraints) nicht mehr exakt erhalten. Die linke Abbildung zeigt die Dichte der Neutronensternmaterie. Die rechte Seite zeigt die Simulationsergebnisse der vom binären Neutronenstern System emittierten Gravitationswellen.

Erste Gravitationswelle im Jahr 2015 gefunden!!

Kollision zweier Schwarzer Löcher GW150914

Massen: 36 & 29 Sonnenmassen

Abstand zur Erde 410 Mpc (1.34 Milliarden Lichtjahre)

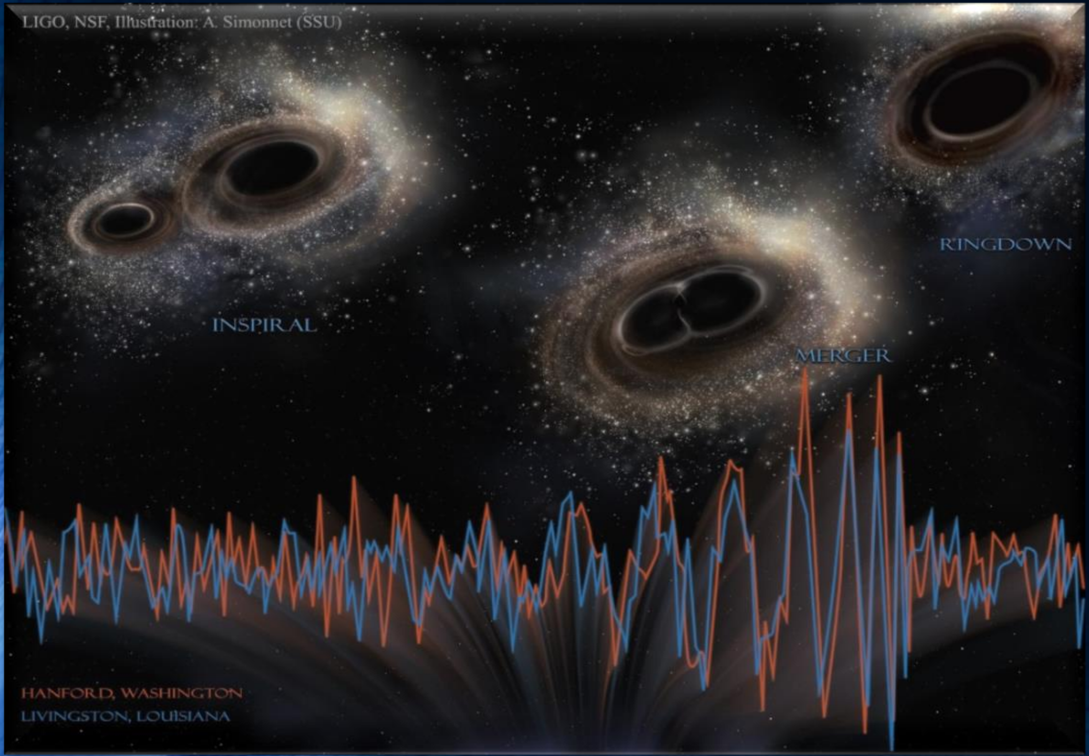

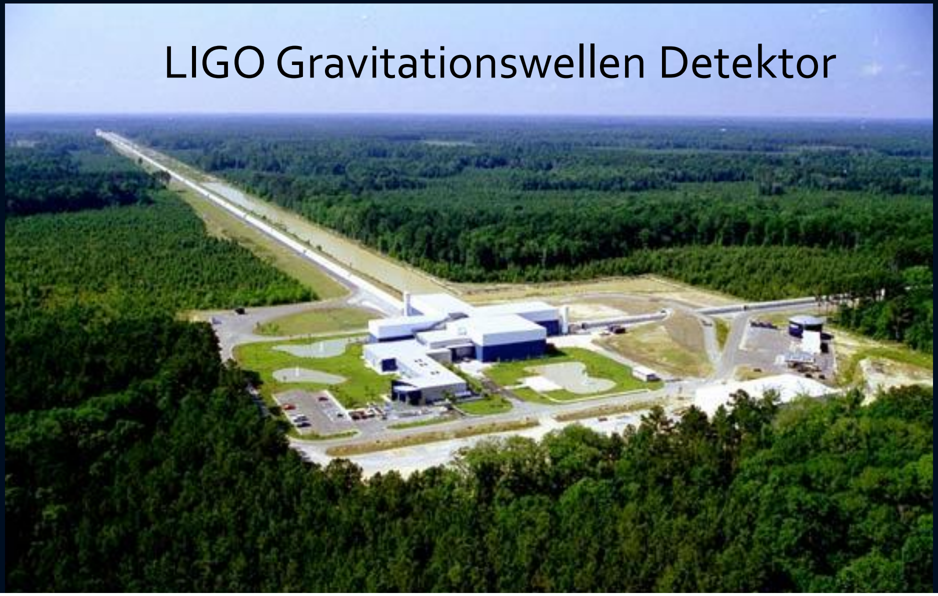

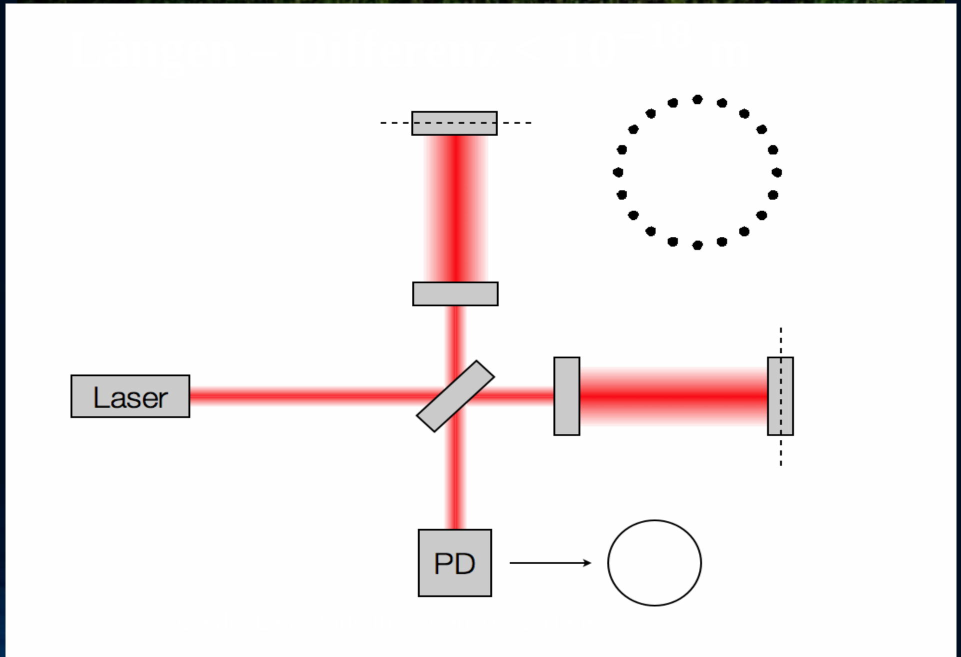

Physik Nobel Preis 2017

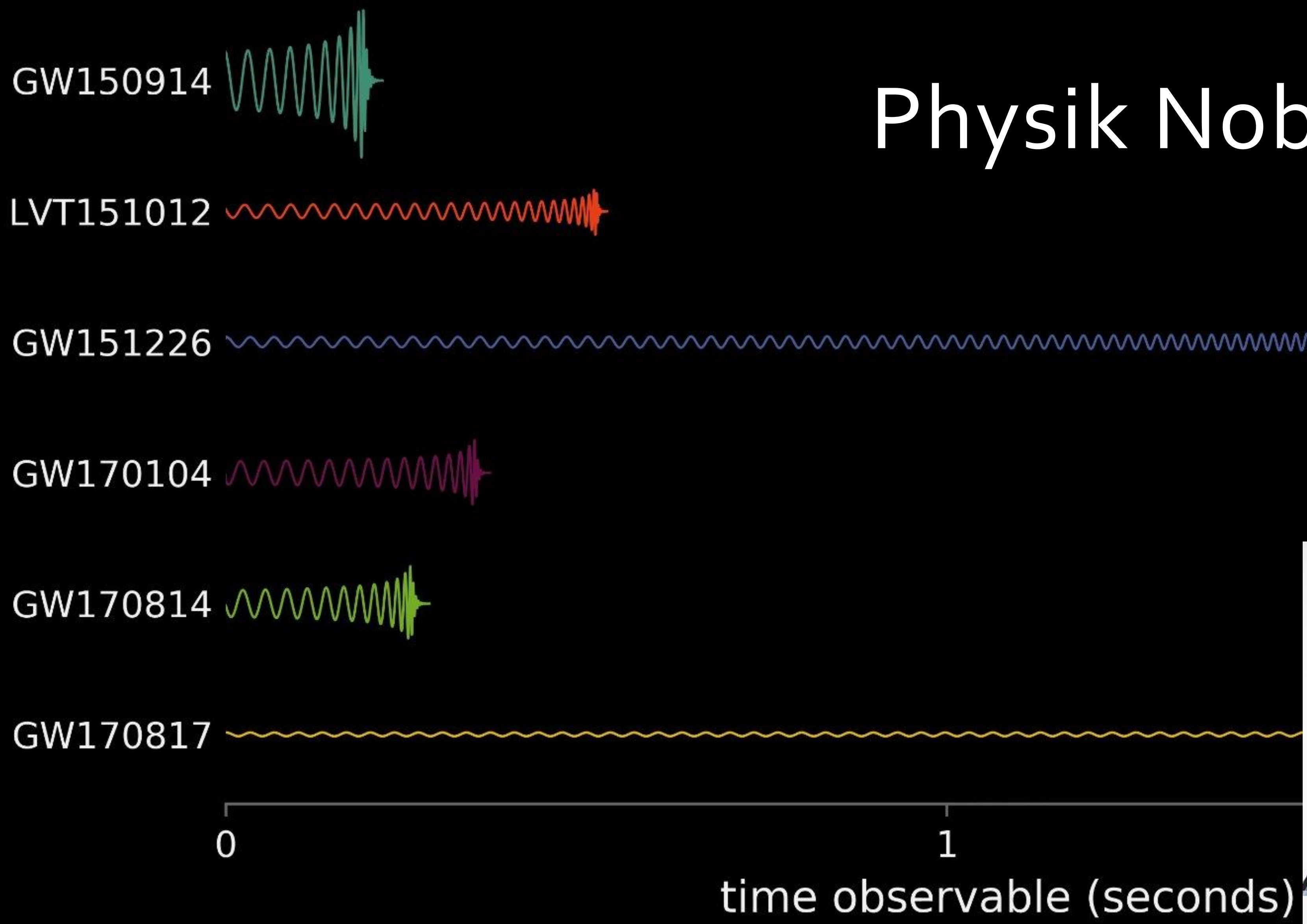

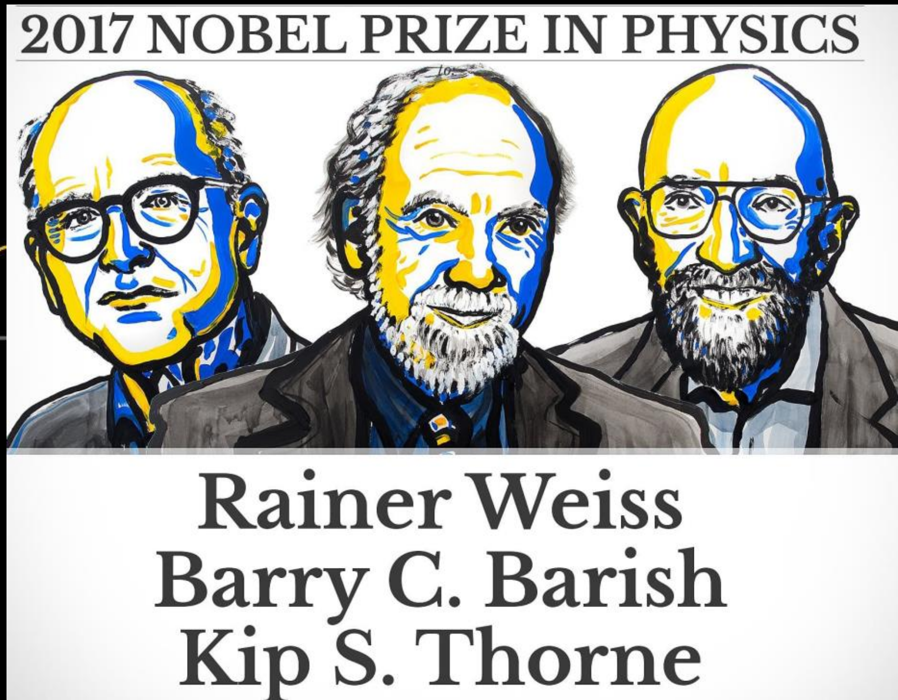

Binäre Neutronenstern Systeme

Zurzeit kennt man ca. 25 binäre Neutronenstern Systeme

Beispiel:
Der **Double Pulsar**
(PSR J0737-3039A/B):
Entdeckt im Jahre 2003
Eccentricity: 0.088
Pulsar A: P=23 ms, M=1.3381(7)
Pulsar B: P=2.7 s, M=1.2489(7)

Abstand zwischen den Sternen nur 800,000 km
Orbitale Periode: 147 Minuten

Abstand verkleinert sich langsam aufgrund der Abstrahlung von Gravitationswellen

Die beiden Neutronensterne werden erst in 85 Millionen Jahren kollidieren

Kramer, Wex, Class. Quantum Grav. 2009

McGill NCS Multimedia Services Animation by Daniel Cantin, DarwinDimensions)

Was geschieht wenn zwei Neutronensterne miteinander kollidieren?

Zwei sehr massive Neutronensterne

Zwei mittelschwere Neutronensterne

Zwei leichte Neutronensterne

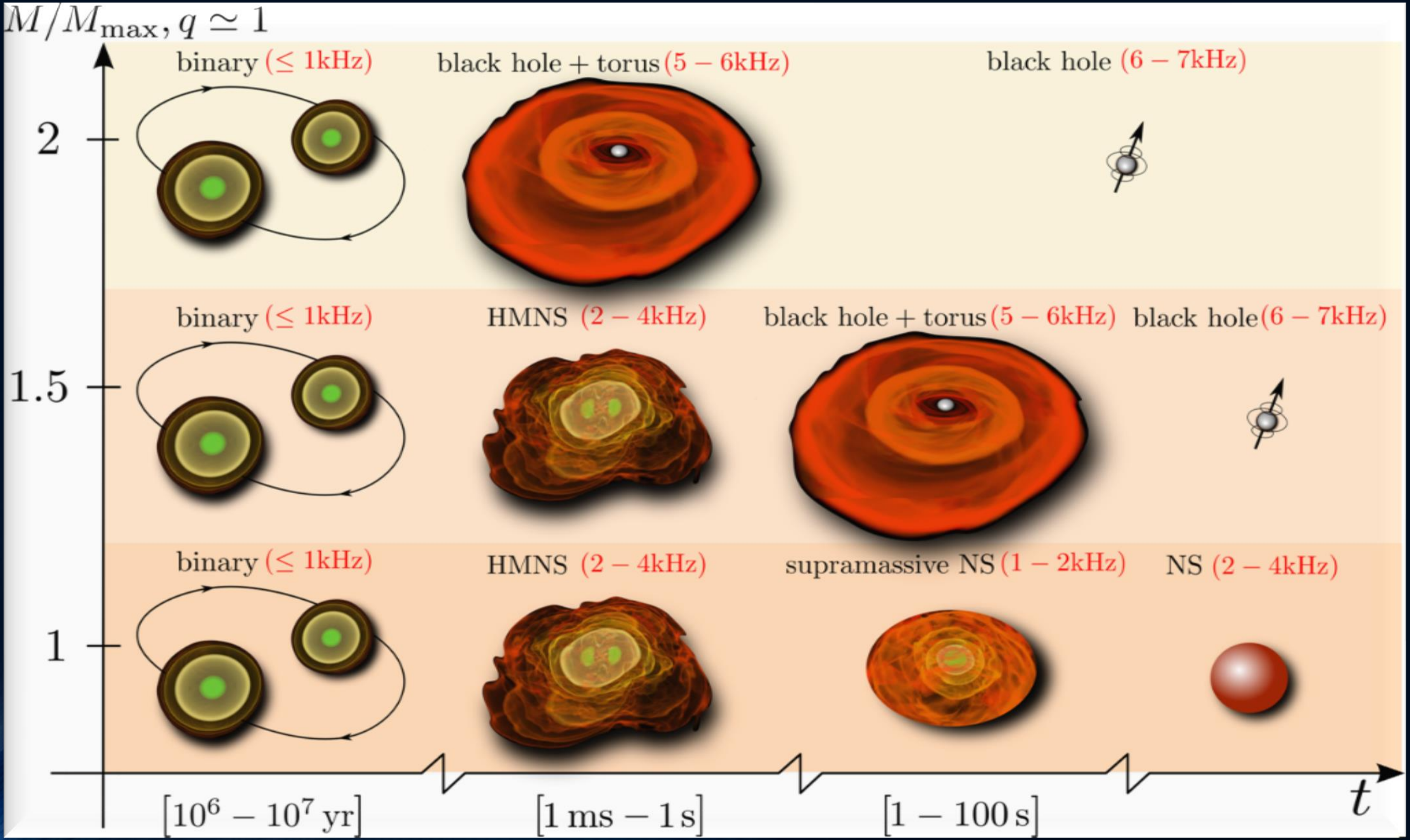

Computer Simulation einer Neutronenstern Kollision

Credits: Cosima Breu, David Radice und Luciano Rezzolla

Dichte der Neutronenstern Materie

8.5 — 14

lg(rho) [g/cm^3]

Temperatur der Neutronenstern Materie

0 — 50

T [MeV]

Binary Merger of two Neutron Stars for different EoSs

M=1.35 Msolar
for details see Hanauske, et.al. PRD, 96(4), 043004 (2017)

Central value of the lapse function α_c (upper panel) and maximum of the rest mass density ρ_{max} in units of ρ_0 (lower panel) versus time for the high mass simulations.

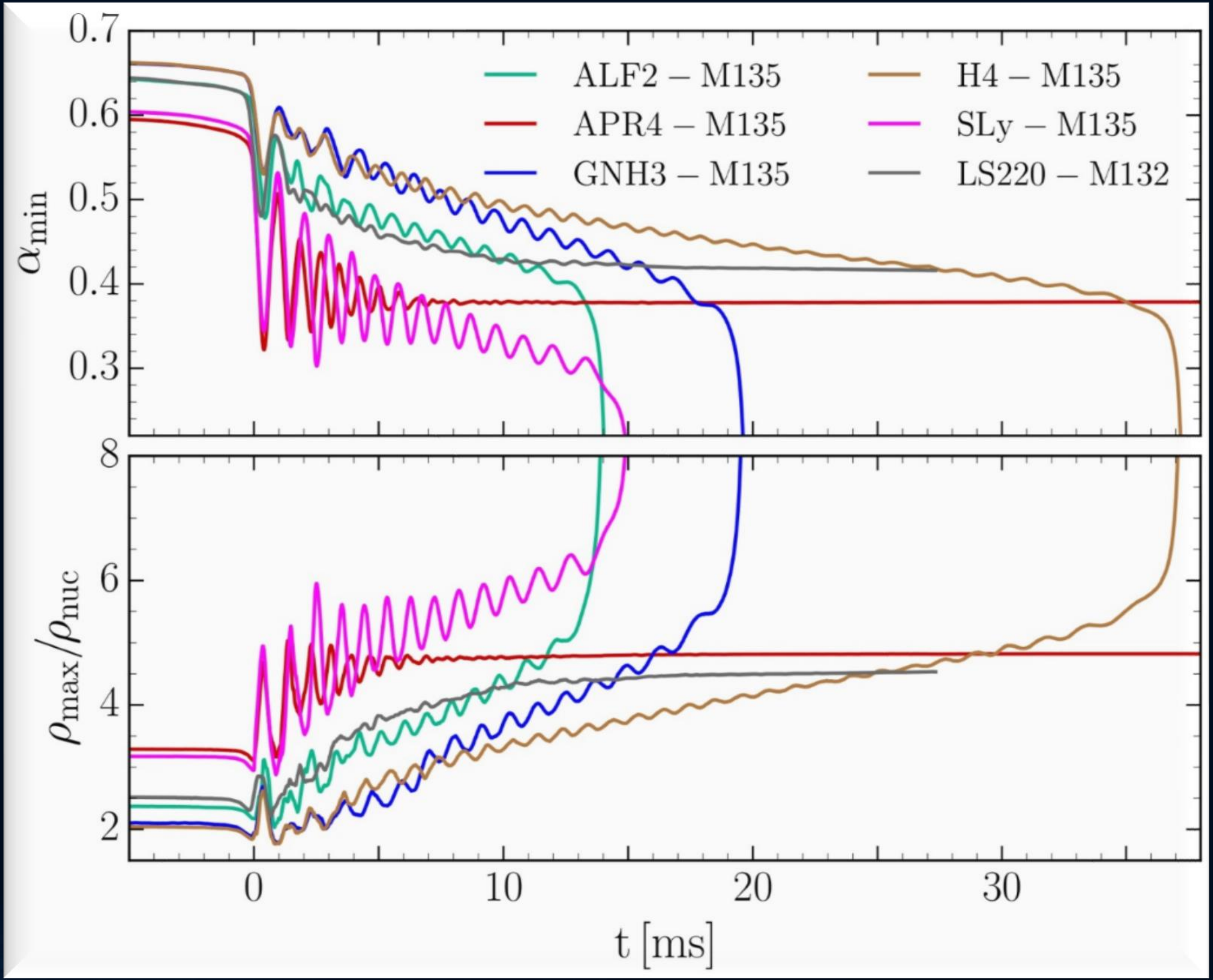

SEARCH FOR POST-MERGER GRAVITATIONAL WAVES FROM THE REMNANT OF THE BINARYNEUTRON STAR MERGER GW170817 (see arXiv:1710.09320v1)

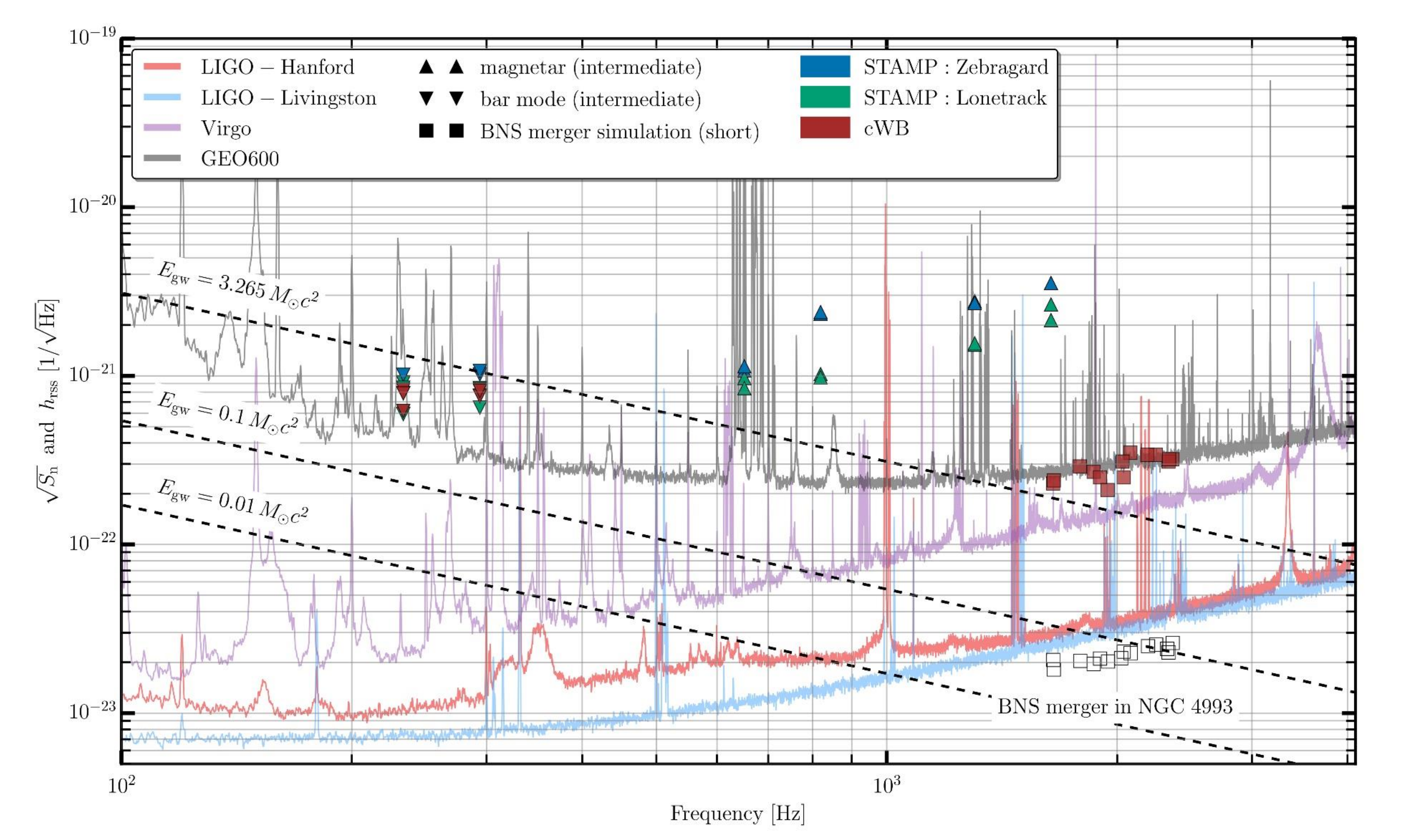

Unfortunately, due to the low sensitivity at high gravitational wave frequencies, no post-merger signal has been found in GW170817.

But, the results indicate that post-merger emission from a similar event may be detectable when advanced detectors reach design sensitivity or with next-generation detectors.

Was geschieht zwischen der Kollision und dem Kollaps zum schwarzen Loch?

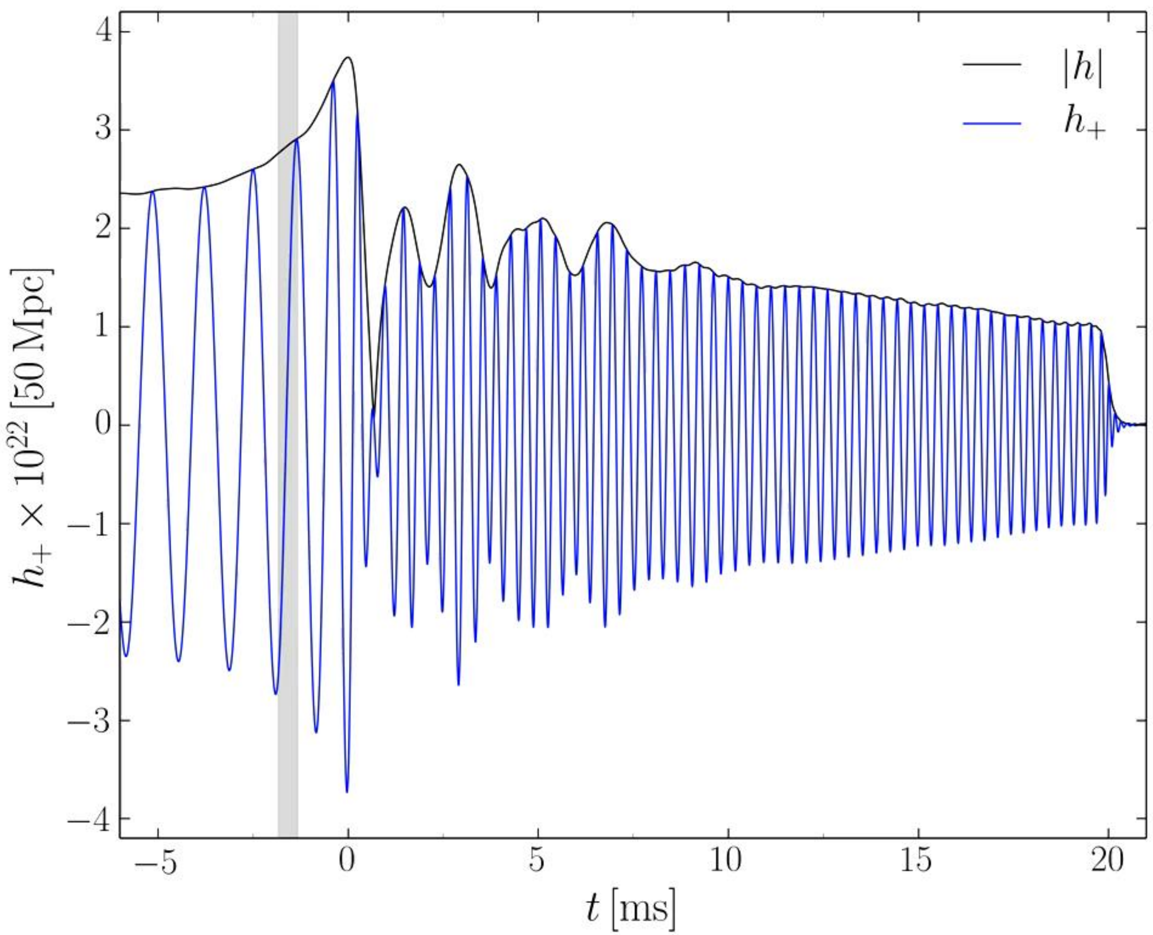

Amplitude der emittierten Gravitationswelle

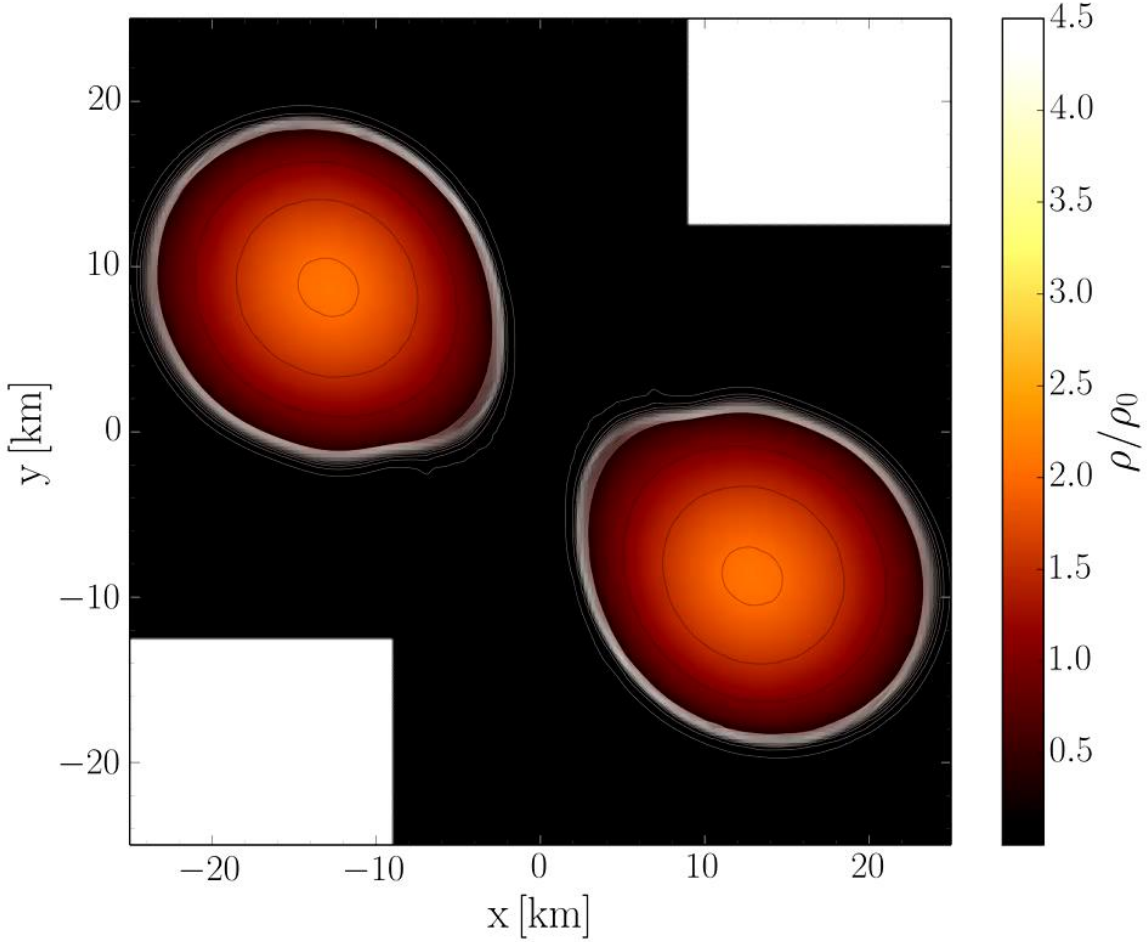

Dichteprofil in der äquatorialen Ebene

Gravitationswelle einer Neutronenstern Kollision

Neutronenstern Kollision (Simulation)

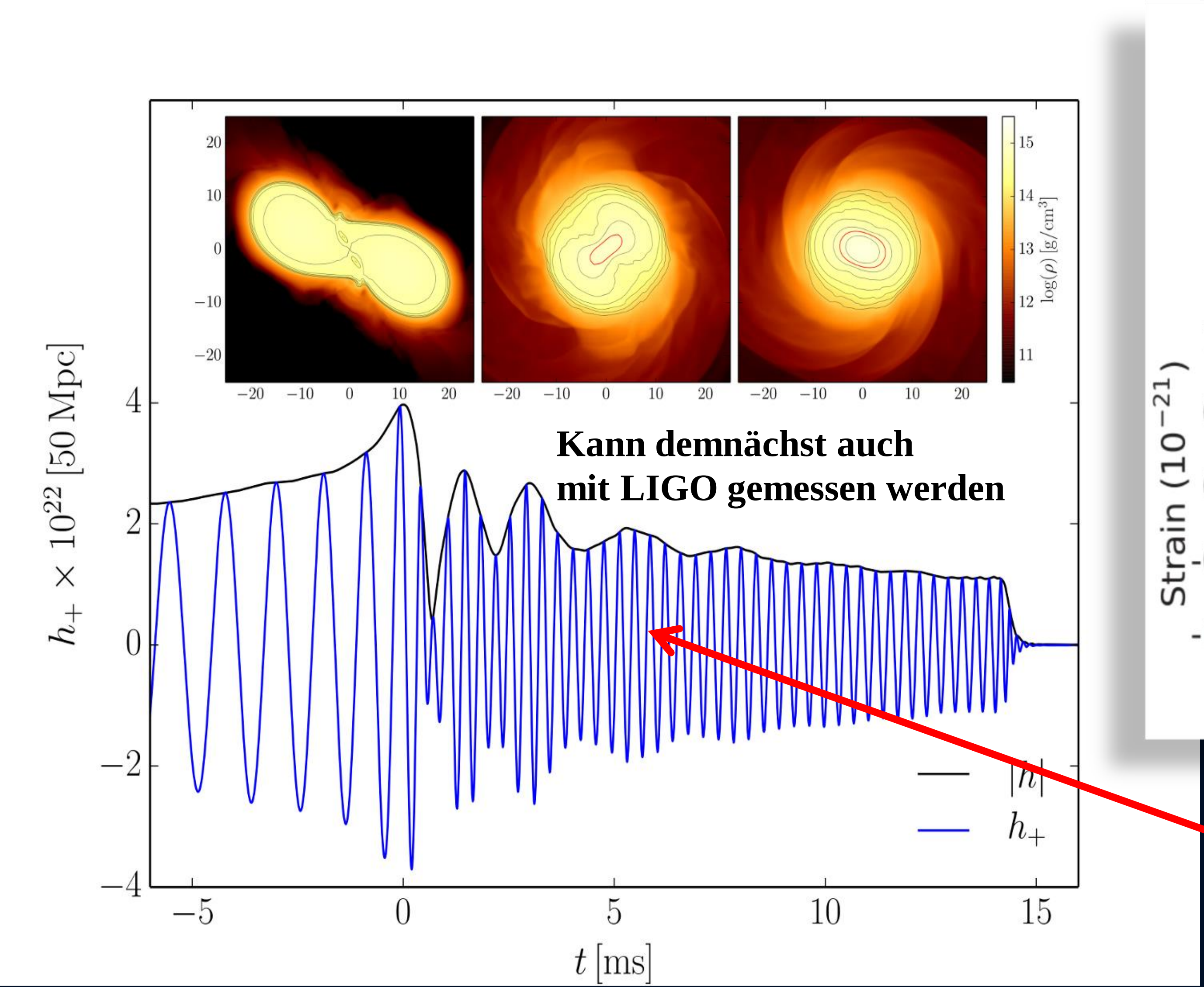

Kann demnächst auch mit LIGO gemessen werden

Kollision zweier schwarzer Löcher

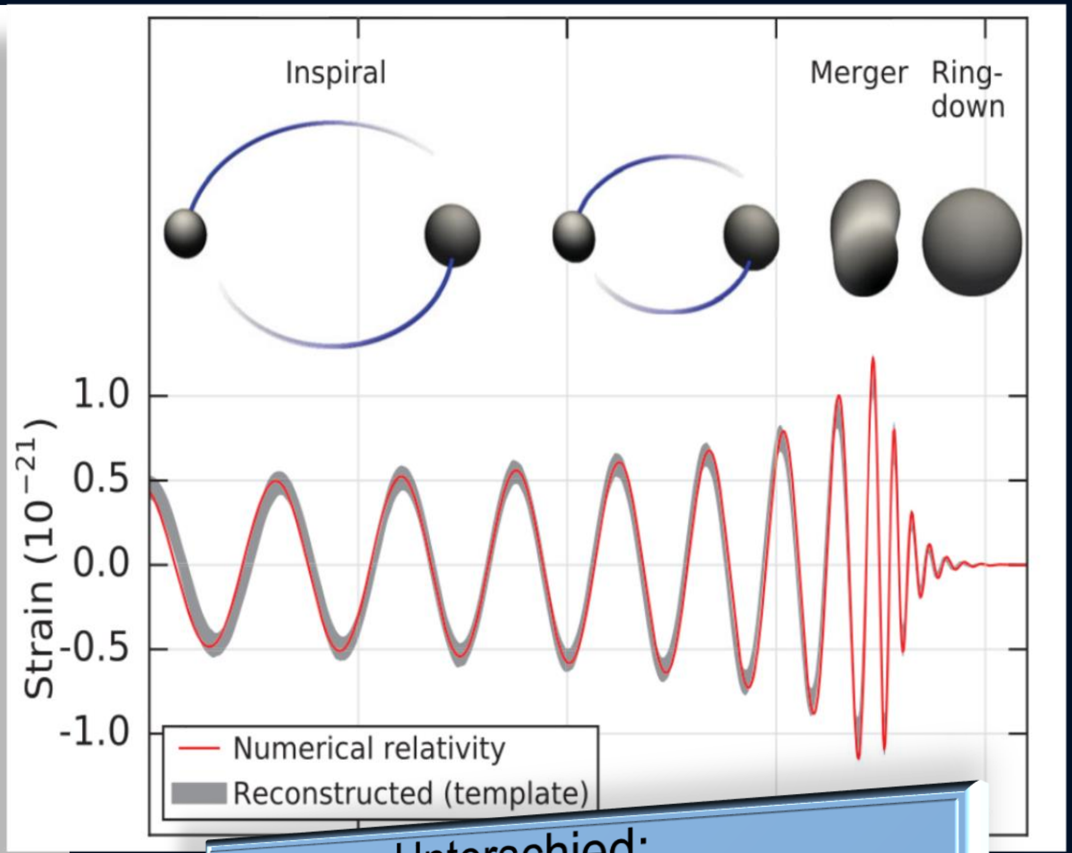

Unterschied:
Bei Neutronenstern Kollisionen gibt es meistens eine ***Post-Kollisionsphase***

Heavy-Ion Collisions vs. Neutron Star Mergers

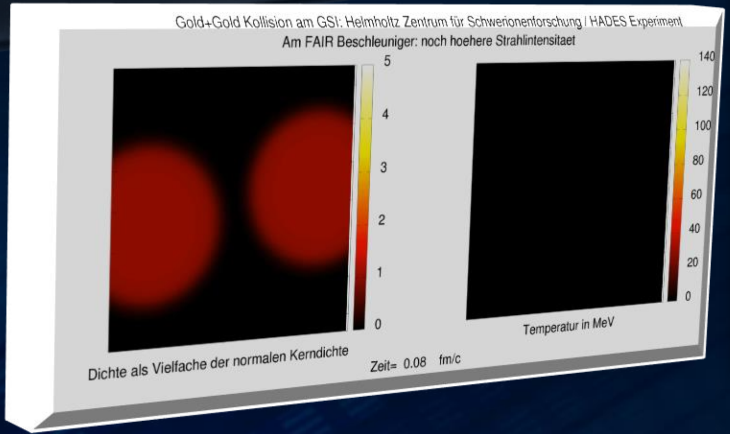

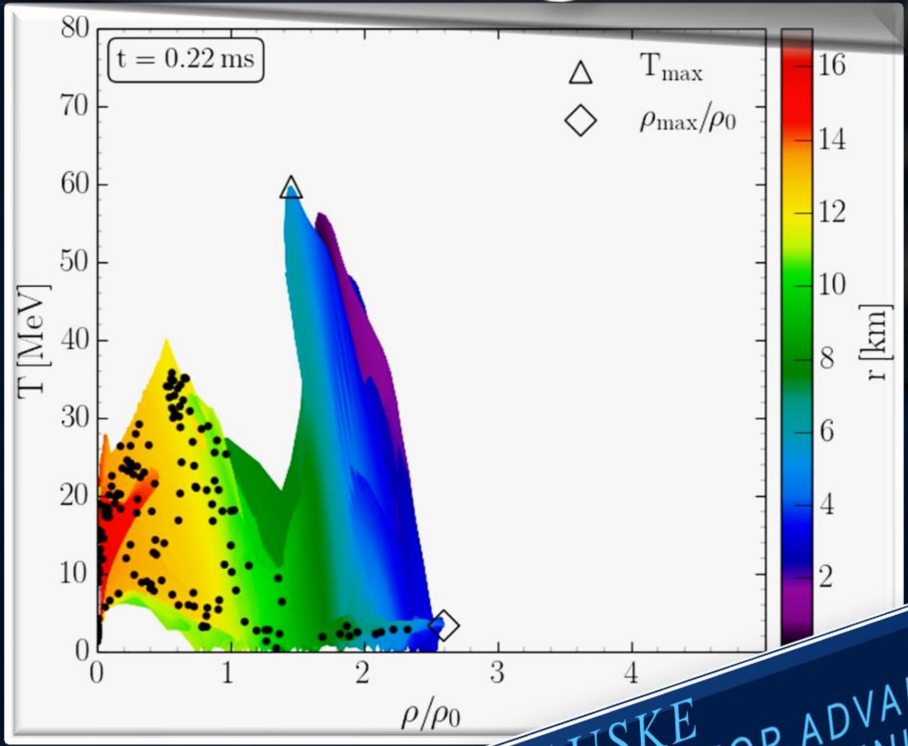

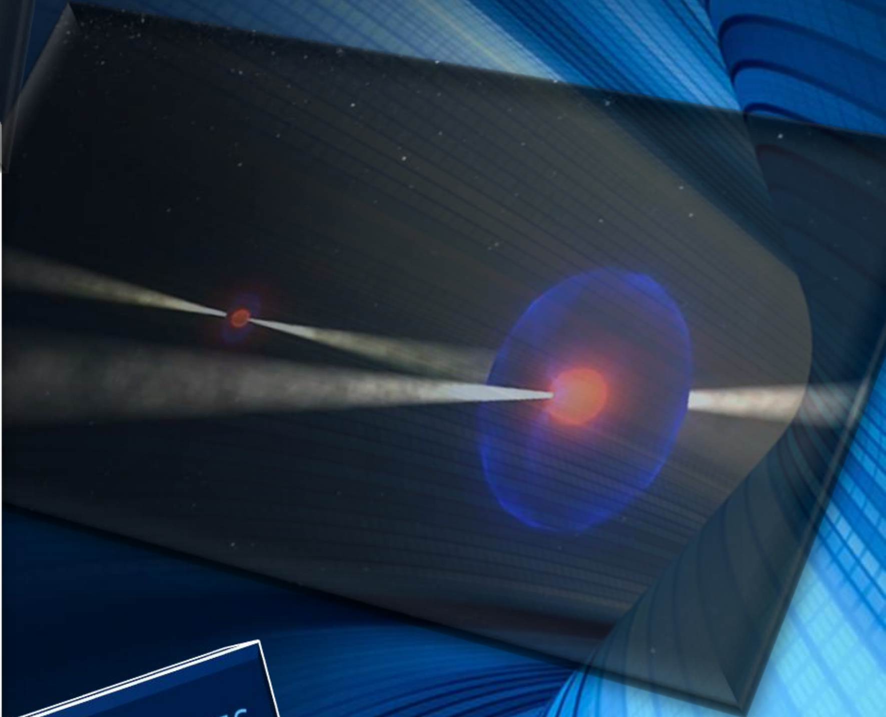

Probing dense baryonic matter with hadrons

Status and Perspective

Comparison between different transport models and similarities to neutron star mergers

MATTHIAS HANAUSKE
FRANKFURT INSTITUTE FOR ADVANCED STUDIES
JOHANN WOLFGANG GOETHE UNIVERSITÄT
INSTITUT FÜR THEORETISCHE PHYSIK
ARBEITSGRUPPE RELATIVISTISCHE ASTROPHYSIK
D-60438 FRANKFURT AM MAIN

VORTRAG AN DER GSI

DARMSTADT, 13 FEBRUARY 2019